PROCESSING AND CHARACTERIZATION OF POLYETHYLENE VITRIMERS

BY

MARIA CAMILA MONTOYA OSPINA

A DISSERTATION SUBMITTED IN PARTIAL FULFILLMENT OF THE REQUIREMENTS FOR THE DEGREE OF

DOCTOR OF PHILOSOPHY

(MECHANICAL ENGINEERING)

AT THE

UNIVERSITY OF WISCONSIN - MADISON

2023

Date of final oral examination: May 5th, 2023

The dissertation is approved by the following members of the Final Oral Examination Committee:

Tim A. Osswald, Professor, Mechanical Engineering

Lih-Sheng Turng, Professor, Mechanical Engineering

Alejandro Roldán-Alzate, Associate Professor, Mechanical Engineering

Pavana Prabhakar, Associate Professor, Civil and Environmental Engineering

Lianyi Chen, Associate Professor, Mechanical Engineering

To my abuelitos, Amparo y Pompilio. This is for you.

To my parents, this could not have been possible without you.

Abstract

Polyethylene (PE) is one of the most used commodity plastics worldwide. PE is versatile, lightweight, tough, easy to process, and exhibits excellent chemical resistance. Some of the limitations of this material are its lower strength, poor dimensional stability at elevated temperature, and strong creep behavior. Cross-linked PE (XLPE) offers an improvement to these limitations with the sacrifice of not being recyclable due to its permanent cross-links. A new class of materials, called vitrimers, combines the properties of thermoplastics and thermosets: they behave like traditional cross-linked materials at service temperature while being re-moldable and recyclable like thermoplastics when heated. Vitrimers consist of chemically cross-linked networks that engage in thermoactivated associative exchange reactions. These exchange reactions can impart malleability, healing, and recyclability properties to thermosets. While significant focus has been placed on the development of vitrimer chemistry, there is little understanding on how to process at scale. This research aims to enable industrial applications of polyethylene vitrimers by defining the relationships between processability, recyclability, and final part properties.

In this dissertation, a one-step protocol to prepare PE vitrimer-like materials with disulfide exchange bonds via reactive blending is presented. The cross-linking reaction of maleic anhydride-grafted-polyethylene (PE-MAH) and 4,4' – dithiodianiline (DTA) is conducted in the melt state. The final rheological, thermal and mechanical properties of PE vitrimers (PE-V) are investigated. The disulfide exchange reactions enable re-processing of PE-V and the mechanical and rheological properties remain constant after two processing cycles. It is demonstrated that PE-V can be processed using single screw extrusion processes without the need to modify the standard equipment. The formation of cross-links in PE-V decreases the degree of crystallinity of the material which leads to a decrease in stiffness. However, PE-V exhibits higher thermal stability,

higher dimensional stability above melting temperature, and lower shrinkage compared to PE. The improvement in these properties allows the use of PE-V in material extrusion additive manufacturing (ME-AM) to reduce mechanical anisotropy and improve dimensional accuracy.

Acknowledgments

First, I want to express my appreciation to my mentor and academic guide, Professor Tim Osswald. You have been a constant source of inspiration and motivation for me. Your technical expertise has been influential in my research work, and you have imparted invaluable life advice that has been crucial in my personal growth. I will forever be grateful for you taking me into your research group and for being my professional and personal match-maker.

I would like to express my sincere gratitude to my dissertation committee members: Prof. Lih-

Sheng Turng, Prof. Alejandro Roldán-Alzate, Prof. Pavana Prabhakar, and Prof. Lianyi Chen, for generously dedicating their time and providing me with their valuable feedback and suggestions. I want to thank the students that made this research possible: Victor Bulat, Katherine Koets, Amy Lossen, Mark Ordner, Xiao Tan, Hannah Walker, and Jiachen Zeng. In addition, I want to thank my colleagues at the Polymer Engineering Center for providing me with a supportive environment that facilitated my professional growth and encouraged collaborations. Thank you, Dr. Tom Mulholland, for teaching me both how to use the processing equipment and how to fix it.

I would like to thank SABIC for sponsoring this project and in particular, Dr. Henk Verhoogt, for your contributions and mentorship. Our discussions and brainstorming sessions have been instrumental in shaping my understanding of the topic and refining my research. Your dedication to the project and willingness to offer your support and guidance is so greatly appreciated.

Finally, I would like to express my appreciation to my husband and family. Alec, thank you for your constant and unconditional support, which has helped me overcome the different challenges throughout this journey, and for correcting all my in's and on's.

Gracias a mis padres y hermanos por el apoyo a lo largo de estos años. Mamá, gracias por todos los sacrificios que has hecho para que yo pueda estar aquí hoy.

Table of Contents

Abstract	i
Acknowledgements	iii
Table of Contents	iv
List of Figures	vii
List of Tables	X
List of Abbreviations	xi
List of Symbols	xiii
1. Introduction	1
1.1 Polyethylene	1
1.2 Progress in Cross-Linked Materials	4
1.3 Vitrimers	5
1.4 Motivation and Objectives	10
2. Processing and Rheological Behavior of Cross-Linked Polyethylene Containing	
Disulfide Bonds	11
2.1 Introduction	11
2.2 Materials and Methods	14
2.2.1 Materials	14
2.2.2 Synthesis of Polyethylene Vitrimers	14
2.2.3 Fourier-Transform Infrared Measurement	16
2.2.4 Thermal Properties: Differential Scanning Calorimetry	16
2.2.5 Determination of Swelling Ratio and Gel Content	17
2.2.6 Rheology	17
2.2.7 Dynamic Mechanical Analysis	18
2.2.8 Ultimate Tensile Testing	19
2.3 Results	19
2.3.1 Torque Rheometer Curves	19
2.3.2 FTIR Analysis	21

2.3.3 Thermal Properties: Differential Scanning Calorimetry	24
2.3.4 Gel Content	25
2.3.5 Rheological Properties	26
2.3.6 Thermo-Mechanical Properties	31
2.3.7 Re-Processing	34
2.4 Conclusions	35
3. Effect of Cross-linking on the Mechanical Properties, Degree of Crystallinity and Thermal Stability of Polyethylene Vitrimers	. 37
3.1 Introduction	37
3.2 Materials and Methods	40
3.2.1 Materials and Sample Preparation	40
3.2.2 Differential Scanning Calorimetry	41
3.2.3 Polarized Optical Microscopy	42
3.2.4 Thermogravimetric Analysis	42
3.2.5 Ultimate Tensile Testing	42
3.2.6 Creep	42
3.2.7 Dynamic Mechanical Analysis	43
3.3 Results	43
3.3.1 Differential Scanning Calorimetry Analysis	44
3.3.2 Optical Microscopy Analysis of Crystallization	46
3.3.3 Thermogravimetric Analysis	47
3.3.4 Ultimate Tensile Properties	48
3.3.5 Correlation Between Yield Strength and Crystallinity	51
3.3.6 Viscoelastic Properties	53
3.3.7 Creep	54
3.4 Conclusions	57
4. Material Extrusion Additive Manufacturing with Polyethylene Vitrimers	. 58
4.1 Introduction	58
4.2 Materials and Methods	62

	Appendix	94
	References	85
	8.3 Publications	84
	8.2 Recommendations for Future Work	82
	8.1 Contributions	81
5.	Summary	81
	4.4 Conclusions	80
	4.3.5 Microstructures	78
	4.3.4 Mechanical Properties	75
	4.3.3 Shrinkage	74
	4.3.2 Printing Challenges	70
	4.3.1 Assessment of Processability in Screw-Assisted AM	66
	4.3 Results	66
	4.2.5 Annealing Procedure	66
	4.2.4 Characterization	65
	4.2.3 Shrinkage Evaluation	65
	4.2.2 Material Extrusion Additive Manufacturing and Geometric Design	63
	4.2.1 Materials	62

List of Figures

1.1	Schematic of two types of CANs: dissociative and associative	5
1.2	Angell fragility plot showing the viscosity as a function of temperature of three vitrimers scaled with T_g (epoxy-anhydride, epoxy-acid and vinylogous urethane).	6
1.3	$\label{eq:Viscoelastic behavior of vitrimers.} \textbf{(A) Viscoelastic behavior of vitrimers for $T_g < T_v$ and \textbf{(B) Viscoelastic behavior of vitrimers for $T_g > T_v$.} \\$	7
1.4	Summary of relevant properties of vitrimers: (A) relaxation time of vitrimers containing dual dynamic covalent exchange reaction, (B) environmental stress cracking performance of PS vitrimer, (C) dimensional stability at 250 °C of PBT vitrimers, (D) increased healing performance of epoxidized natural rubber (ENR) with dynamic cross-links (red) in comparison to permanent cross-links (in blue), (E) improved processability of ENR with dynamic cross-links in comparison to ENR with permanent cross-links, and (F) Improved creep performance of PE vitrimers at 80 °C.	9
2.1	Chemical structures of LLDPE-MAH, DTA and LLDPE-V. The side group, R, is an ethyl group.	15
2.2	Flow behavior of cross-linked LLDPE using various degrees of MAH functionality and MAH:DTA molar ratio (control temperature: 160 °C, 50 rpm). Torque is shown with solid lines and melt temperature with dashed lines.	20
2.3	Reactive blending of LLDPE-V1.2 at 160 °C and 50 rpm after: (A) 5 minutes of the addition of DTA and (B) 12 minutes of the addition of DTA	21
2.4	FTIR spectral curves. (A) cross-linker (DTA), thermoplastic precursor (LLDPE), functionalized polymer (LLDPE-MAH0.6) and vitrimer (LLDPE-V0.6), (B) four vitrimers with different initial MAH content (0.15, 0.3, 0.6 and 1.2 wt.%)	23
2.5	MAH conversion after reactive blending measured with FTIR using the IR signal at 1789 cm ⁻¹ .	24
2.6	DSC heating curves of (A) precursors and (B) vitrimers (second heating ramp, 10 K/min).	25
2.7	SAOS measurements - 190 °C. (A) complex viscosity of LLDPE and four grades of LLDPE-MAH and (B) complex viscosity of LLDPE vitrimers. Circles and triangles represent the experimental data, and the lines represent the Cross model fit	27
2.8	SAOS measurements - 190 °C. Storage (G') and loss (G'') modulus of LLDPE vitrimers.	29

2.9	Stress relaxation of LLDPE, LLDPE-MAH0.6 and LLDPE-V0.6 at 190 °C under 5% strain: (A) log-log scale and (B) normalized semi-log scale	31
2.10	Storage modulus as a function of temperature for LLDPE and four grades of LLDPE vitrimers with various cross-linking densities (10 Hz, 0.1% strain)	32
2.11	Dimensional stability at 190 °C and varying heating time. (A) LLDPE, (B) LLDPE-V0.15, (C) LLDPE-V0.3, (D) LLDPE-V0.6, and (E) LLDPE-V1.2	33
2.12	Complex viscosity of LLDPE-V0.6 virgin and LLDPE-V0.6 re-processed (190°C).	34
2.13	Mechanical properties of LLDPE-V0.6 virgin and LLDPE-V0.6 re-processed: (A) yield strength and (B) displacement at break.	35
3.1	Graphical representation of the mixing protocol used to produce PE-V. The side group, R, can be a hydrogen or an alkyl group.	4]
3.2	DSC scans from second heating/cooling ramp at 10 K/min: (A) heating of LLDPE MAH, (B) heating of LLDPE-V, (C) cooling of LLDPE-MAH, and (D) cooling of LLDPE-V.	45
3.3	Polarized optical microscopy images (20x magnification) after 2 minutes of isothermal crystallization at 110 °C: (A) LLDPE, (B) LLDPE-MAH0.6, and (C) LLDPE-V0.6.	46
3.4	TGA measurements obtained at 10 K/min in oxygen atmosphere: (A) LLDPE, LLDPE-MAH0.3, LLDPE-V0.3, (B) LLDPE, LLDPE-MAH0.6, and LLDPE-V0.6, and (C) LLDPE, LLDPE-MAH1.2, LLDPE-V1.2.	48
3.5	Representative stress-displacement curves of LLDPE, LLDPE-MAH, and LLDPE-V with varying grafting and cross-linking level (23 °C, 50 mm/min).	5(
3.6	Reprocessing and mechanical characterization of LLDPE-V0.6: (A) Diagram showing the reprocessing cycle, and (B) yield strength after three processing cycles.	51
3.7	Relationship between yield strength and degree of crystallinity of LLDPE and HDPE systems.	52
3.8	Viscoelastic properties as a function of frequency of LLDPE and LLDPE-V materials: (A) complex modulus and (B) $\tan \delta$.	54
3.9	Creep experiments at 50 °C and 5 MPa of HDPE and HDPE-V(0.6): (A) strain vs time in linear scale, and (B) creep compliance vs time in semi-log scale	55
3.10	Comparison of degree of crystallinity of HDPE and HDPE-V0.6	56
4.1	Graphical representation of the protocol used to produce HDPE-V using ME-AM.	63

4.2	Material Extrusion Additive Manufacturing (ME-AM) and Geometric Design (A) Schematic of screw-assisted ME-AM; (B) sample geometry used for microstructure characterization; (C) specimens used for viscoelastic characterization (H: 3 mm).	64
4.3	DSC heating and cooling curves (10 °C/min in nitrogen)	68
4.4	Complex viscosity, $ \eta^* $, as a function of frequency of HDPE and HDPE-V (220 °C).	69
4.5	Square plates (60 mm × 60 mm × 3 mm) produced (A) without brims and (B) with brims. (C) Melt fracture observed in HDPE-V.	71
4.6	Dynamic moduli as a function of frequency for HDPE (black lines) and HDPE-V (red lines) at 220 °C. Storage modulus (G') is represented by the solid lines and viscous modulus (G") is represented by the dashed lines	72
4.7	Print speed and multiplier optimization for HDPE-V to reduce melt fracture. (A) Speed: 800 mm/min; multiplier: 1×. (B) Speed: 500 mm/min; multiplier: 1×. (C) Speed: 500 mm/min; multiplier: 1.2×.	73
4.8	DMA frequency sweeps of compression-molded (CM) samples and 3D-printed specimens with loading parallel to the bead orientation (0°) and perpendicular to the bead orientation (90°): (A) HDPE, and (B) HDPE-V.	76
4.9	DMA frequency sweeps of compression-molded (CM) samples and 3D-printed specimens with loading parallel to the bead orientation (0°) and perpendicular to the bead orientation (90°) after an annealing process.	77
4.10	Visual demonstration of the annealing process: (A) before placing the parts in the oven, and (B) after 10 min in the oven at 150 °C.	78
4.11	SEM imaging of the samples shown in Figure 2B: (A–C) 3D-printed samples normal to the print direction (X-Z view in Figure 2B), and (D–F) 3D-printed samples parallel to the print direction (Y-Z view in Figure 2B).	79

List of Tables

1.1	Molecular structure and physical properties of HDPE and LLDPE	1
1.2	Comparison between cross-linking processes used in XLPE	3
2.1	Vitrimer materials prepared in the internal batch mixer.	15
2.2	Swelling and gel content of vitrimers.	26
2.3	Zero-shear viscosity of LLDPE and LLDPE-MAH estimated with three models.	28
2.4	Storage modulus at 180 °C and cross-linking density of the vitrimers studied	33
3.1	Characteristic properties of materials used in this study.	40
3.2	Cross-linking density of LLDPE and HDPE vitrimer based materials obtained from DMTA characterization (See appendix A.3).	44
3.3	Summary of thermal and mechanical properties of LLDPE, LLDPE-MAH and LLDPE-V.	49
4.1	Characteristic properties of the materials used in this study.	62
4.2	Printing parameters of HDPE and HDPE-V	67
4.3	Shrinkage perpendicular (S_w) and parallel (S_l) to the print orientation in the plates shown in Figure 4.2.	75

List of Abbreviations

Abbreviation Meaning

AM Additive manufacturing

CANs Covalent adaptable networks

DMA Dynamic Mechanical Analysis

DMTA Dynamic mechanical thermal analysis

DSC Differential scanning calorimetry

DTA 4,4' – dithiodianiline

ENR Epoxidized natural rubber

FTIR Fourier transform infrared

HDPE High-density polyethylene

HDPE-GMA Glycidyl methacrylate-grafted-high-density polyethylene

HDPE-MAH Maleic-anhydride-grafted high-density polyethylene

HDPE-V High-density polyethylene vitrimer

LDPE Low density polyethylene

LLDPE Linear low-density polyethylene

LLDPE-MAH Maleic anhydride-grafted-linear low-density polyethylene

LLDPE-V Linear low-density polyethylene vitrimer

MAH Maleic anhydride

ME Material extrusion

ME-AM Material extrusion additive manufacturing

MFI Melt flow index

PBT Polybutylene terephthalate

PC Polycarbonate

PCL Polycaprolactone

PE Polyethylene

PE-MAH Maleic anhydride-grafted-polyethylene

PET Polyethylene terephthalate

PE-V Polyethylene vitrimer

PLA Polylactic acid

PMMA Polymethyl methacrylate

PP Polypropylene

PS Polystyrene

PTMEG Polytetrahydrofuran

SAOS Small-amplitude oscillatory shear

SEBS Styrene-ethylene-butylene-styrene

SEM Scanning electron microscopy

SLS Selective laser sintering

TBD Triazobicyclodecene

TGA Thermogravimetric analysis

UHMWPE Ultra-high molecular weight polyethylene

UV Ultraviolet

Wt.% Weight percentage

XLPE Cross-linked polyethylene

List of Symbols

Greek letter symbols

Symbol	Unit	Description	
γ	[1/s]	Shear rate	
ΔH_m	[J/g]	Measured melting enthalpy	
ΔH_{m^0}	[J/g]	Theoretical melting enthalpy of 100% crystalline polymer	
ΔL_b	[mm]	Displacement at break	
$\varepsilon(t)$	[-]	Creep strain	
η	[Pa·s]	Viscosity	
$ \eta^* $	[Pa·s]	Complex viscosity	
η_0	[Pa·s]	Zero-shear viscosity	
λ	[s]	Time constant	
ν	[mol/cm ³]	Cross-linking density	
σ_b	[MPa]	Stress at break	
σ_0	[MPa]	Creep stress	
$\sigma_{\mathcal{y}}$	[MPa]	Yield stress	
χ_c	[%]	Degree of crystallinity	

Latin letter symbols

Symbol	Unit	Description
а	[-]	Dimensionless parameter in Adams-Crane model
E^*	[MPa]	Tensile complex modulus

E'	[MPa]	Tensile storage modulus
$E^{\prime\prime}$	[MPa]	Tensile loss modulus
G'	[Pa]	Shear storage modulus
$G^{\prime\prime}$	[Pa]	Shear loss modulus
G(t)	[Pa]	Relaxation modulus
G_0	[Pa]	Stress relaxation initial modulus
i	[-]	Imaginary unit
J(t)	[1/MPa]	Creep compliance
K	[-]	Density ratio of polymer to solvent at immersion temperature
L_m	[mm]	Measured dimensions parallel to bead orientation
L_o	[mm]	Original dimensions parallel to bead orientation (from CAD design)
n	[-]	Power law index
R	[J/mol·K]	Universal gas constant
S_l	[%]	Shrinkage parallel to bead orientation
S_w	[%]	Shrinkage perpendicular to bead orientation
$tan\delta$	[-]	Tangent of delta
T	[K]	Absolute temperature in the rubbery region
T		
T_c	[°C]	Crystallization temperature
T_{g}	[°C]	Crystallization temperature Glass transition temperature
T_g	[°C]	Glass transition temperature

T_v	[°C]	Topology freezing temperature
W_{s}	[g]	Initial weight of specimen
W_g	[g]	Weight of swollen gel after immersion period
W_d	[g]	Weight of dried gel
W_{α}	[mm]	Original dimensions perpendicular to bead orientation

1. Introduction

1.1. Polyethylene

Polyethylene (PE) is one of the most widely used commodity plastics by volume and it is frequently used in packaging, construction and electrical industry. Some examples include plastic bags, plastic bottles and films, tubes and wire insulation. The vast range of applications is attributed to the different chemical structures of PE. The difference in the chemical structure refers to variations in the branches which modifies the nature of the material. The mechanical and thermal properties of PE depend significantly on the type of branching and density. Table 1.1 summarizes relevant properties of two types of PE with very distinct properties and applications: high-density polyethylene and linear low-density polyethylene [1], [2].

Table 1.1. Molecular structure and physical properties of HDPE and LLDPE [1], [2].

	1 7 1 1	2 3, 2 3
Property	HDPE	LLDPE
Molecular structure	V. C.	WE'NG
Density [g/cm ³]	0.94-0.97	0.90-0.94
Degree of crystallinity [%]	55-77	22-55
Tensile modulus [MPa]	1068-1378	262-896
Tensile yield strength [MPa]	17-31	7-19
Melting temperature [°C]	125-132	100-125
Applications	Household containers and tubes	High performance bags and films

PE is versatile, lightweight, tough, easy to process, and exhibits excellent chemical resistance and low coefficient of friction [1], [3]. Some of the limitations of this material are its lower strength, poor dimensional stability at high temperature, and strong creep behavior. Crosslinked PE (XLPE) offers an improvement to these properties with the sacrifice of not being recyclable due to its cross-linked network [4]. Cross-linked polyethylene (XLPE) consists of PE that has been chemically modified to form covalent bonds linking adjacent chains. The presence of the cross-links creates a gel like network of interconnected chains which is insoluble but can be swollen by several organic solvents. Cross-links can hinder crystallization by restricting movement of chains required to arrange into crystallites [2]. Therefore, the density of XLPE is usually lower than that of PE. Furthermore, the cross-links reduce the melt index and elongation at break, while improving impact resistance, environmental stress cracking, creep and abrasion resistance [5].

Several methods have been developed throughout the years to permanently cross-link polyethylene. These methods can be divided into physical and chemical cross-linking [5]. Physical cross-linking of PE was first demonstrated by Dole in 1948 [6]. In this method, cross-linking is obtained by a free radical mechanism generated in the polymer chain by using high energy radiation. These radiations include electron beam, gamma rays and ultraviolet radiation [4], [5], [7]. Chemical cross-linking is a method in which chemicals or initiators are used to generate free radicals. In the early 1960s, the first chemical cross-linking of PE was conducted by the decomposition of various organic peroxides [6]. In the early 1970s another method of chemically cross-linking PE was developed that involves grafting of silane [8]. A third type of chemical cross-linking method has been reported in literature using azo compounds (molecules containing -N=N-groups) as initiators [7]. This method is less commonly used due to the higher temperature

requirements (240 - 270 ° C) and low cross-linking efficiency. Table 1.2 summarizes the most common methods used to produce XLPE and relevant characteristics of the process.

Table 1.2. Comparison between cross-linking processes used in XLPE [5].

Characteristics	Physical cross-linking	Chemical cross-linking	
	Radiation	Peroxide	Silane
Number of steps	1	1	2
Cross-linking mechanism	Free radical	Free radical	Grafting
Curing time	Very low	Low	Very high
Curing temperature [° C]	Room temperature	150-160	80-90
Gel content [%]	>60	>75	>65
Equipment cost	High	Medium	Low
Degree of cross-linking	Varies with thickness	Constant through thickness	Varies with residence time

Usually, compounding and shaping operations of XLPE products are done under controlled temperature to prevent premature cross-linking. It is critical that the cross-linking agent remains inactive at processing temperature. For this reason, the peroxide cross-linking continues to be the most common choice to produce XLPE. However, this process produces volatiles and hazardous byproducts. An alternate cross-linking approach has been used in the last decade. This consists of incorporating functional comonomers or pendant groups which can react on-demand to cross-link the polymer. Some examples include polyethylene copolymers that feature epoxy functional groups as part of a glycidyl methacrylate comonomer [9] and blends of statistical ethylene-glycidyl copolymer methacrylate/ethylene-acrylic acid copolymer [10].

1.2. Progress in Cross-Linked Materials

Cross-linked materials were first introduced in 1839 with the discovery of vulcanization by Charles Goodyear. It was found that this process significantly enhanced the properties of natural rubber [1]. However, this process reduced the recyclability of the material and healing properties. Starting in the late 1980s, research in supramolecular chemistry, pioneered by Jean-Marie Lehn, grew at a very fast pace. Supramolecular chemistry consists of chemical systems based on molecular components held together by non-covalent intermolecular forces [11], [12]. These forces include hydrogen bonding, hydrophobic forces, π - π interactions and metal-ligand bonds [13]. Because these bonds are non-covalent, materials can be remelted, which increases the recyclability and healing ability of materials. However, the mechanical performance is decreased due to their weaker bond energies (1-5 kcal/mol) compared to covalent bond energy (50-150 kcal/mol) [11], [12], [14]–[16]. In the early 2000s, a special type of covalent bond was developed which can dissociate and reassociate under an external stimulus. This type of bond is called a dynamic covalent bond [17].

The networks containing such dynamic covalent bonds are referred to in the literature as covalent adaptable networks (CANs). Supramolecular networks use non-covalent interactions to form a cross-link, while CANs make use of reactive covalent bonds. CANs can be divided into sub-groups: dissociative and associated, as depicted in Figure 1.1. In dissociative CANs, cross-links dissociate when an external stimulus, such as heat or ultraviolet (UV) light, is applied and then reform when the stimulus is removed. During the dissociation step the network integrity is compromised. An example of dissociative dynamic bond is the Diels-Alder reaction developed by Wudl et al. in 2002 [17]. For associative CANs, which were first shown by Bowman et al. in 2005, bond exchange only occurs after a new cross-link is formed [18]. Therefore, the network integrity

remains intact due to the constant cross-link density. It was not until 2011, that Leibler and coworkers coined the term *vitrimers* to describe associative CANs [19].

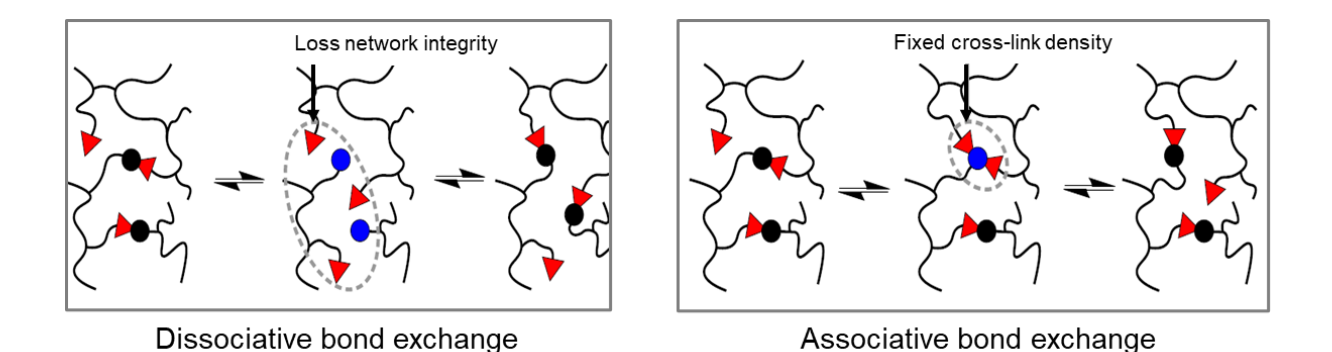


Figure 1.1. Schematic of two types of CANs: dissociative and associative [20].

1.3. Vitrimers

Vitrimers were introduced as a new classification of polymeric materials in 2011 by Leibler et al. [19]. The cross-linked network contains covalently bonded chains that can change its topology via exchange reactions. When heated, vitrimers can flow due to thermally triggered bond shuffling mechanisms. Moreover, covalent bonds only detach when a new bond is formed, maintaining a fixed cross-linking density. If the temperature of the system is increased, the viscosity is controlled by the chemical exchange reactions. It has been demonstrated that the viscosity gradually decreases following the Arrhenius law as observed in typical inorganic silica materials [19]. This behavior is demonstrated in Figure 1.2 with the Angell fragility plot. Figure 1.2 displays the viscosity as a function of temperature scaled with the glass transition temperature (T_g) of three vitrimers (epoxy-anhydride, epoxy-acid, and vinylogous urethanes). In this example, the viscosity dependency with temperature is very different than for polystyrene (PS). The latter is characterized with a narrow transition temperature and therefore a very fast decrease in the

viscosity near T_g . On the other hand, vitrimers show an Arrhenius-like dependency of viscosity. This characteristic can broaden the processing temperature window [20].

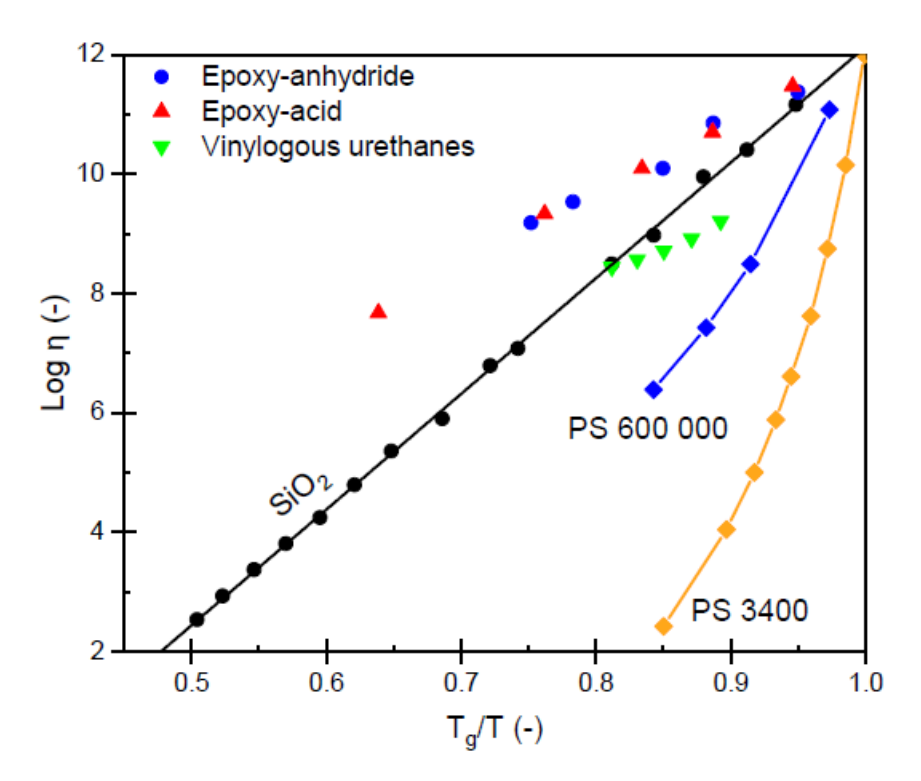


Figure 1.2. Angell fragility plot showing the viscosity as a function of temperature of three vitrimers scaled with T_g (epoxy-anhydride, epoxy-acid and vinylogous urethane) [20].

The viscoelastic behavior of vitrimers is controlled by two transition temperatures. To achieve topology rearrangements, two temperatures must be overcome: glass transition temperature (T_g) and topology freezing temperature (T_v) . In the case of semicrystalline vitrimers, melting temperature (T_m) must be exceeded. T_g and T_m are related to long range motion of polymer chains and T_v is related to the exchange reaction of the cross-links. T_v was defined as the temperature at which the viscosity reaches 10^{12} Pa·s [21]. Moreover, the position of T_v with respect to T_g (or T_m) define the viscoelastic behavior of the vitrimeric material. Two cases are presented in Figure 1.3: $T_g < T_v$ (Figure 1.3A) and $T_g > T_v$ (Figure 1.3B). For the first case, when the material

is heated above T_g , a glassy-rubber transition is observed. The material behaves as an elastomer since the exchange reactions are not active yet, impeding topology rearrangements. When the temperature reaches T_v , the exchange reactions become active, and the material presents a rubber-viscoelastic liquid transition and will start flowing with an Arrhenius viscosity dependency. For the second case, exchange reactions are limited by chain motions. Above T_g , the chain motion will begin together with the exchange reactions, leading to a rapid decrease in the viscosity. This is observed up until the diffusion is fully controlled by the exchange reactions, at which point the Arrhenius behavior is reached. It is worth mentioning that T_v belongs to the exchange reaction within the material [20], [22], [23].

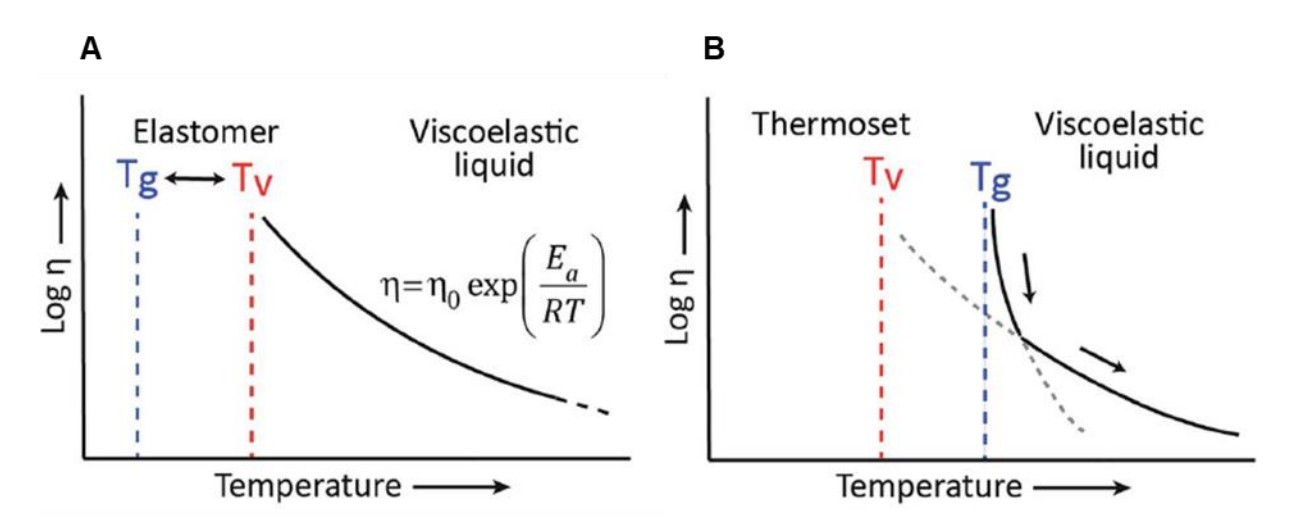


Figure 1.3. Viscoelastic behavior of vitrimers [20]. (A) Viscoelastic behavior of vitrimers for $T_g < T_v$ and (B) Viscoelastic behavior of vitrimers for $T_g > T_v$.

The vitrimer concept was first demonstrated in an epoxy network using the well-known transesterification reaction. In this case, the transesterification kinetics were controlled with a zinc acetate catalyst [19]. Other types of exchange reactions can be found in literature, including

vinylogous transamination reaction [24], [25], transcarbonation [26], trans alkylation [27] imine exchange [28], silyl ether exchange [29], [30], olefin metathesis [31], dioxaborolane metathesis [32]–[34], boronic ester transesterification [35], and disulfide metathesis [36]–[42], which can even occur in the absence of a catalyst.

Only a few of these exchange reactions have been introduced in commercial plastics. Two methods of preparing vitrimers are traditionally used. The first approach is the polymerization of multifunctional monomers to produce a network with dynamic covalent bonds. From a processing standpoint, this implies going from a solution or a melt to a gel or bulk network. The second strategy is the cross-linking of a thermoplastic. The dynamic covalent bonds can be present either in the polymer backbone, as pendant groups, or in the cross-linker. In this case, reactive extrusion can be used to turn commercial thermoplastics into vitrimers [14].

In the last five years, understanding of vitrimers has steadily increased. Efforts have been made to improve and develop suitable dynamic covalent chemistries with tunable reactivity, which has been applied to different polymers [20], [23]. Some thermoplastics that have been transformed into vitrimers are polyethylene (PE) [25], [30], [32], [43], [44], polypropylene (PP) [45], polymethyl methacrylate (PMMA) [32], polystyrene (PS) [32], polybutylene terephthalate (PBT) [46], [47] and polycarbonate (PC) [26].

Finally, a few examples showcasing improvement in control and tunability of exchange reactions and final part properties will be summarized in Figure 1.4. Chen and co-workers presented the first dual dynamic vitrimer by using a cross-linker that contained disulfide and acid for epoxy based vitrimers with triazobicyclodecene (TBD) as a catalyst. This network can simultaneously undergo disulfide metathesis and carboxylate transesterification leading to a significant decrease in the relaxation time in comparison to the single disulfide vitrimer and single

ester vitrimer (Figure 1.4A) [48]. Vitrimer preparation from elastomers and thermoplastics has proven a positive enhancement in their chemical resistance [32] (Figure 1.4B), dimensional stability (Figure 1.4C) [30], [46], healing [37] (Figure 1.4D) and the ability to be reprocessed (Figure 1.4E) [37], [38], [41], [49], [50]. An improvement on creep rate of a PE vitrimer has also been reported in the literature (Figure 1.4E) [32].

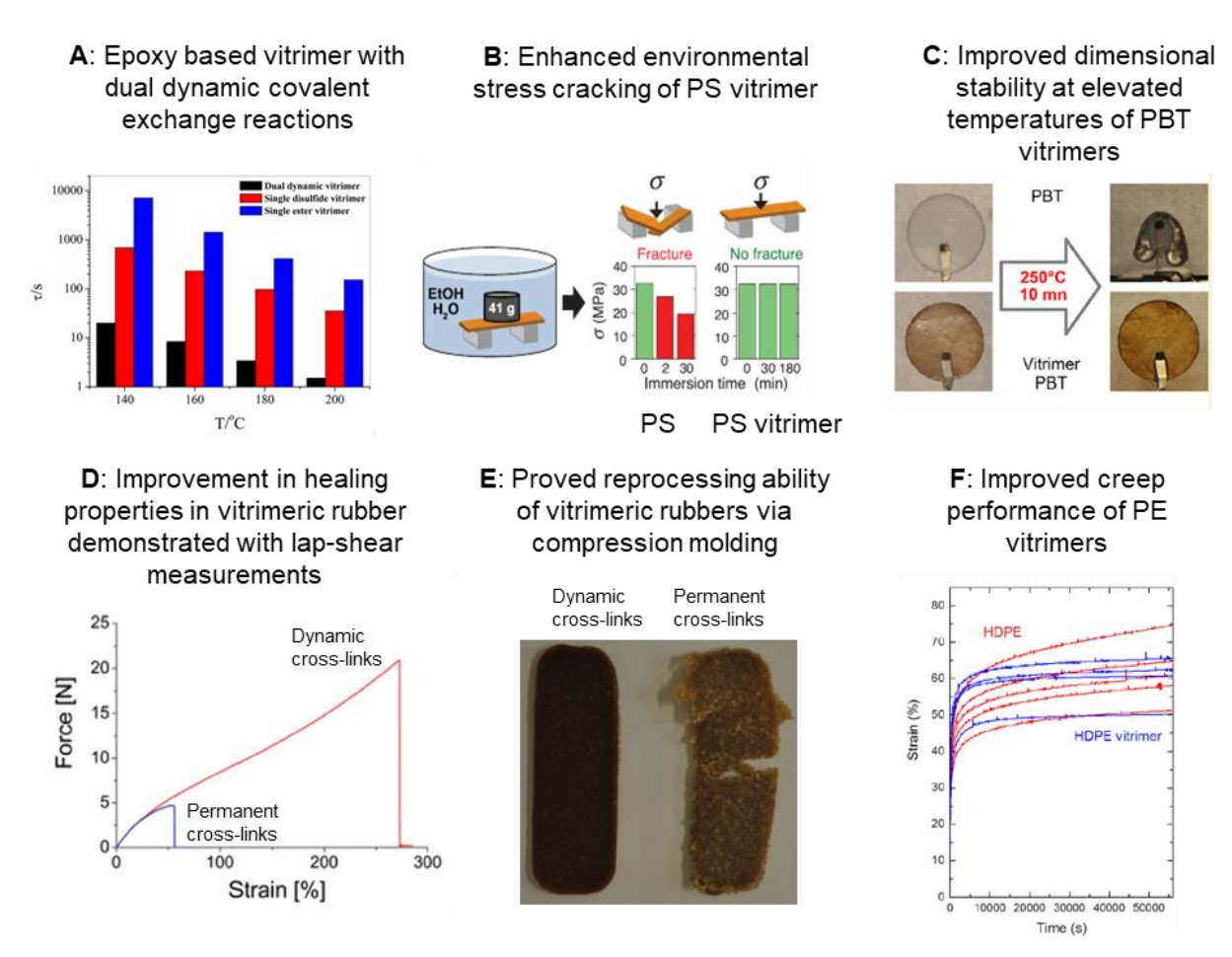


Figure 1.4. Summary of relevant properties of vitrimers: (**A**) relaxation time of vitrimers containing dual dynamic covalent exchange reactions [48], (**B**) environmental stress cracking performance of PS vitrimer [32], (**C**) dimensional stability at 250 °C of PBT vitrimers [46], (**D**) increased healing performance of epoxidized natural rubber (ENR) with dynamic cross-links (red) in comparison to permanent cross-links (in blue) [37], (**E**) improved processability of ENR with dynamic cross-links in comparison to ENR with permanent cross-links [37], and (**F**) Improved creep performance of PE vitrimers at 80 °C [32].

1.4. Motivation and Objectives

The aim of this research proposal is to enable industrial applications of polyethylene vitrimers by defining the relationships between processability, final part properties and recyclability. The three detailed research objectives of this proposal are:

Objective 1: Implement and improve existing tools to cross-link polyethylene vitrimers based on disulfide bonds and show the impact of these dynamic cross-links in the rheological properties. This is critical to understand how to process this material in secondary applications and to understand the re-processability and recycling potential.

Objective 2: Determine the implications of the dynamic cross-links and degree of cross-linking in the materials' thermal and mechanical properties. More specifically, the effect of the dynamic cross-links in crystallinity, thermal stability, short and long-term mechanical properties, and viscoelastic properties. This information will help identify suitable applications and processing techniques for polyethylene vitrimers.

Objective 3: Identify and make recommendations on secondary processing applications based on the previous rheological, thermal, and mechanical characterization conducted.

2. Processing and Rheological Behavior of Cross-Linked Polyethylene Containing Disulfide Bonds

Permanent cross-linked polyethylene (XLPE) has been used for over fifty years to improve physical properties of polyethylene (PE) such as thermal, mechanical and solvent resistance. However, the formation of non-reversible covalent bonds significantly affects the rheological properties of XLPE. These covalent cross-links cannot be easily broken and the polymer usually decomposes before melting. For this reason, re-processability and therefore recyclability is a significant problem encountered in XLPE materials. To solve the issues related to the recyclability of conventional cross-linked materials, the use of reversible and dynamic cross-links has been promoted. The following chapter shows the impact of dynamic cross-links, in the rheological properties of cross-linked polyethylene, referred to in this dissertation as polyethylene vitrimer (PE-V). This is critical to understand how to process this material in secondary applications and to understand the re-processability and recycling potential of PE-V. The intent of this chapter is to demonstrate that polyethylene vitrimer (PE-V) can be synthetized using commercially available thermoplastic PE and readily available cross-linker via melt reactive blending. This chapter is based on the research "Processing and rheological behavior of cross-linked polyethylene containing disulfide bonds" published in SPE Polymers, Volume 3, Issue 1 (2022) [51].

2.1. Introduction

Polyethylene (PE) is one of the most widely used commodity plastics by volume. PE is versatile, lightweight, tough, is easy to process, and exhibits excellent chemical resistance and low coefficient of friction [1], [3]. Some of the limitations of this material are its lower strength, poor dimensional stability at high temperature, and strong creep behavior. Cross-linked PE (XLPE)

offers these properties with the sacrifice of not being recyclable due to its permanent cross-links [4]. A new class of materials, vitrimers, combine the properties of thermoplastics and thermosets: they behave like cross-linked materials at service temperature while being recyclable due to the presence of dynamic cross-links [32].

Vitrimers are a type of covalent adaptable networks (CANs) materials and were first introduced by Leibler and co-workers in 2011 [19]. They consist of chemically cross-linked networks that engage in thermoactivated associative exchange reactions. During the exchange reactions, the network can change its topology while maintaining a constant degree of cross-linking. Regardless of a constant cross-link density, these materials can flow under the action of heat [14]. Furthermore, the exchange reactions can provide shape memory, malleability, adhesion, healing, and recyclability of thermosets [24], [36], [43], [52].

The vitrimer concept was first demonstrated in an epoxy network using the well-known transesterification reaction. In this case, the transesterification kinetics was controlled with a catalyst [19]. Other types of exchange reactions can be found in the literature including vinylogous transamination reaction [24], [25], [36], [43], [52], transcarbonation [26], trans alkylation [27], imine exchange [28], silyl ether exchange [29], [30], olefin metathesis [31], dioxaborolane metathesis [32], boronic ester transesterification [35] and disulfide metathesis [36]–[42]. Only a few of these exchange reactions have been introduced in commercial plastics. Two methods of preparing vitrimers are traditionally used. The first approach is the polymerization of multifunctional monomers to produce a network with dynamic covalent bonds. From a processing standpoint, this implies going from a solution or a melt to a gel or bulk network. The second strategy is the cross-linking of a thermoplastic. The dynamic covalent bonds can be present either

in the polymer backbone, as pendant groups, or in the cross-linker. In this case, reactive extrusion can be used to turn commercial thermoplastics into vitrimers [14].

Several studies on turning commercial PE into PE vitrimers have been conducted. Leibler and co-workers grafted maleimides bearing dioxaborolane functionalities onto HDPE and in a second step, added a bis-dioxaborolane cross-linker to prepare high density polyethylene (HDPE) vitrimers using reactive extrusion [32]. Ji et al. prepared HDPE vitrimers through reactive blending of polyethylene bearing a glycidyl methacrylate as cross-linking sites (HDPE-GMA) and an OH-terminated polycaprolactone (PCL) or polytetrahydrofuran (PTMEG) as a cross-linker [43]. Caffy and Nicolaÿ incorporated boronic ester exchange into a commercial HDPE via reactive extrusion in a single-step procedure [53]. Tellers et al. prepared reprocessable vinylogous urethane cross-linked low density polyethylene (LDPE) via a single-step reactive extrusion process [25]. More recently, Zych et al. developed dynamic cross-linked PE via reactive extrusion of hydroxyl functionalized PE and a silyl ether [30].

In this study, a vitrimer was produced using the second strategy mentioned earlier: cross-linking of a thermoplastic. The intent of this paper is to show how to prepare a PE vitrimer-like material by taking advantage of readily available and well-studied chemistries and commercially available thermoplastic to better understand processability and final part properties. This work is critical to understand how to process this material in secondary applications. For this reason, final rheological properties, thermal and thermo-mechanical properties were studied. In this case LLDPE-MAH and 4,4' – dithiodianiline (DTA) were employed via melt reactive blending in a one-step protocol. The disulfide metathesis has been shown to be a catalyst-free exchange reaction by multiple studies [36]–[42]. For this reason, this chemistry was selected for this system. LLDPE vitrimers with four

different cross-linking densities were prepared and characterized. All the samples were processable using compression molding.

2.2. Materials and Methods

2.2.1. Materials

LLDPE 430BE (4,2 g/10 min – 2,16 kg/190 °C) and LLDPE-MAH materials were supplied by SABIC. The grafting of MAH is proprietary information. The MAH concentrations used in this study are: 0.15 wt.%, 0.3 wt.%, 0.6 wt.%, and 1.2 wt.% MAH. 4,4' – dithiodianiline (DTA) supplied by Sigma Aldrich was used as a dynamic cross-linker.

2.2.2. Synthesis of Polyethylene Vitrimers

The LLDPE vitrimers were prepared in a C.W. Brabender 3-Piece mixing bowl using Banbury blades with a chamber volume of 75 cm³ and a fill factor of 0.7. The mixer was attached to an Intelli Plasti-Corder Torque Rheometer. The mixing was done using a 2-step protocol: (1) LLDPE-MAH pellets were added to the mixer and (2) after about 6 minutes, the DTA powder was added to the melt and mixed for an additional 12 minutes. Both mixing steps were done at 160 °C and 50 rpm. The reaction was monitored by measuring the torque variation over time. The chemical structures of the materials used and the produced vitrimers are shown in Figure 2.1. After mixing, samples were compressed into 2 mm sheets using a CARVER press under 0.5 tons at 190 °C for 5 minutes. The samples were cooled down under compressed air for 2 minutes. The samples needed for the characterization tests were cut from these sheets.

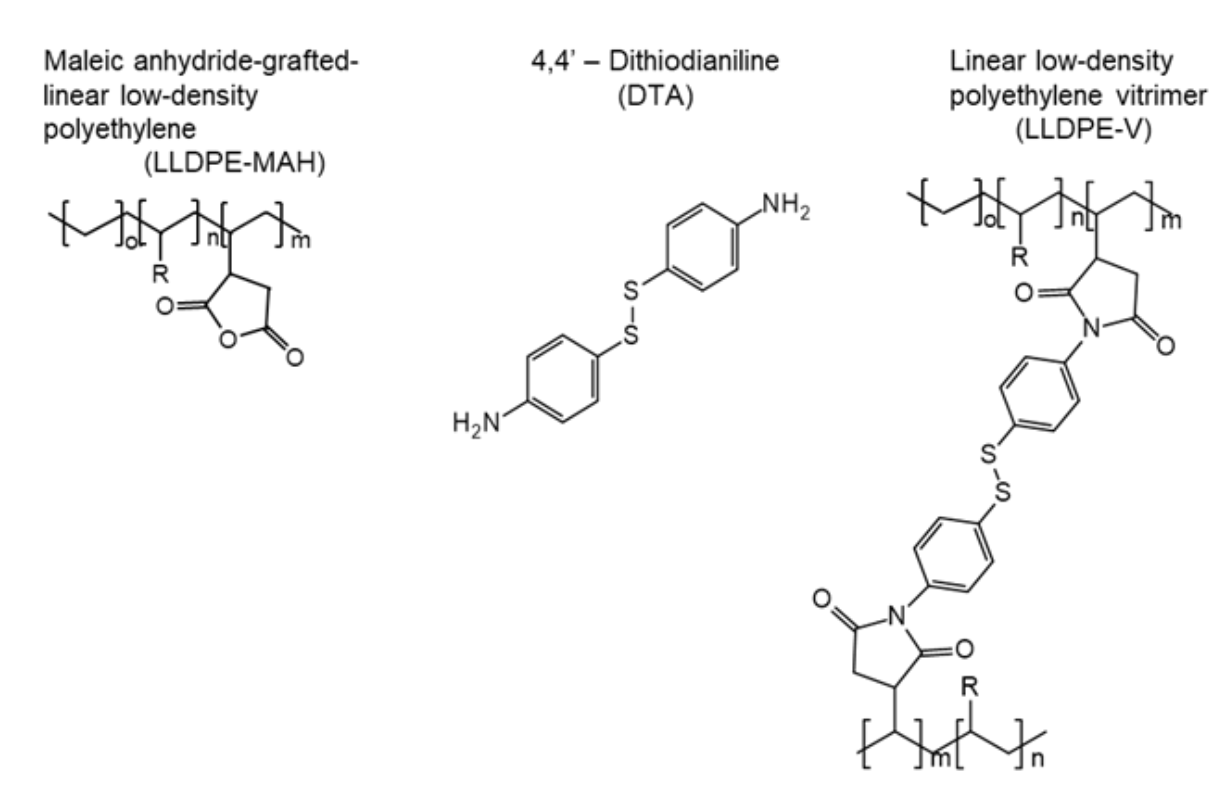


Figure 2.1. Chemical structures of LLDPE-MAH, DTA and LLDPE-V. The side group, R, is an ethyl group.

Four cross-linked materials were prepared using various degree of MAH grafting and a stoichiometric ratio of MAH to DTA [1:0.5] as summarized in Table 2.1.

Table 2.1. Vitrimer materials prepared in the internal batch mixer.

Sample identification	Initial MAH content [wt.%]	Molar ratio of MAH:DTA	
LLDPE-V0.15	0.15	1:0.5	
LLDPE-V0.3	0.3		
LLDPE-V0.6	0.6		
LLDPE- V1.2	1.2		

2.2.3. Fourier-Transform Infrared Measurement

Transmission FTIR measurements were performed using a Bruker Tensor 27 device to verify if a reaction had occurred between the MAH-group and the NH2-group of DTA. Films (250 microns) were pressed at 190 °C and 0.5 tons for 5 minutes using a CARVER press. Each measurement consisted of 32 scans in a wavenumber range of 4400-400 cm⁻¹ and a resolution of 4 cm⁻¹.

The IR signal at 1789 cm $^{-1}$ was used to quantify the wt.% of MAH in the sample using the calibration line shown in the appendix (see Figure A.1 – A.2). The MAH conversion was determined by measuring the wt.% of MAH in the samples before (LLDPE-MAH) and after the reaction (LLDPE-V) by:

Degree of conversion,
$$[\%] = \frac{\text{(Initial wt.\% MAH)} - \text{(Final wt.\% MAH)}}{\text{(Initial wt.\% MAH)}} \times 100$$
 (2.1)

2.2.4. Thermal Properties: Differential Scanning Calorimetry (DSC)

The melting and crystallization behavior of LLDPE, LLDPE-MAH and LLDPE-V were determined using a NETZSCH DSC 214 Polyma, under nitrogen atmosphere. The samples were ramped from 30 °C to 200 °C at a heating rate of 10 K/min. A linear baseline was used to measure the heat of fusion. The degree of crystallinity (χ_c) was calculated from the measured melting enthalpy (ΔH_m) using Equation 2.2.

$$\chi_c, [\%] = \frac{\Delta H_m}{\Delta H_{m^0}} \times 100$$
 (2.2)

Where ΔH_{m^0} is the theoretical melting enthalpy of 100% crystalline polyethylene (293 J/g) [54].

2.2.5. Determination of Swelling Ratio and Gel Content

The swelling ratio and gel content of LLDPE vitrimers were determined according to ASTM D2765 standard procedure [55]. A weighed specimen of approximately 250 mg was placed in a 60-mesh stainless steel wire cage. The cage was deposited in a wide-mouth glass jar (120 mL) and immersed in 30 mL of xylene. The jar was placed in an oil bath so that the level of the oil was above the level of the solvent in the jar. The temperature of the oil bath was set to 110 °C and maintained for 24 hours. After the 24-hour period, the samples were removed from the solvent and weighed in a weighing bottle (20 mL). The samples were then dried under vacuum at 100 °C for 24 hours. Finally, the dried samples were weighed. The swelling ratio and the gel content were calculated by:

Swelling ratio,
$$[-] = \left[\frac{W_g - W_d}{W_d}\right] K + 1$$
 (2.3)

Gel content,
$$[\%] = \left[\frac{W_s - W_d}{W_s}\right] \times 100$$
 (2.4)

Where W_s is the initial weight of specimen, W_g is the weight of swollen gel after immersion period, W_d is the weight of dried gel, and K is the ratio of density of polymer to that of the solvent at immersion temperature defined as 1.07 by ASTM D2765.

2.2.6. Rheology

Rheological measurements were made on a TA Instruments AR 2000ex rheometer. A 25 mm parallel steel plate fixture was used to test the materials with a gap of 2 mm. Strain sweeps were performed at a constant frequency of 1 rad/s and strains from 0.1% to 150%. The strain sweeps were used to determine the linear viscoelastic region to be explored during small-amplitude oscillatory shear (SAOS) measurements. For SAOS tests, a strain of 1% and a frequency range of

0.0628 - 628 rad/s were used. The experimental data was fitted to three rheological models to obtain the value of the zero shear viscosity as demonstrated by Shaw [56]. The models used were Cross model (Equation 2.5), Carreau model (Equation 2.6), and Adams-Crane model (Equation 2.7).

$$\eta = \frac{\eta_0}{(1+(\lambda\dot{\gamma})^{1-n})} \tag{2.5}$$

$$\eta = \frac{\eta_0}{(1+(\lambda\dot{\gamma})^2)^{(1-n)/2}} \tag{2.6}$$

$$\eta = \frac{\eta_0}{(1+(\lambda\dot{\gamma})^{\frac{1}{\alpha}})^a} \tag{2.7}$$

Where η_0 is the zero-shear viscosity, λ is a time constant, $\dot{\gamma}$ is the shear rate, n is the power law index, and a is a dimensionless parameter.

2.2.7. Dynamic Mechanical Analysis (DMA)

A DMA GABO EPLEXOR® from NETZSCH was used to measure the cross-linking density and the mechanical properties as a function of temperature of PE vitrimers. Rectangular samples $(45 \times 10 \times 3 \text{ mm})$ were used in tensile mode to perform a temperature sweep $(35 \,^{\circ}\text{C} - 220 \,^{\circ}\text{C}; 3 \,^{\circ}\text{C/min})$. All tests were performed at a constant frequency of 10 Hz and at a constant strain of 0.1%. The cross-linking density (ν) was determined using the storage modulus (E') at 180 $^{\circ}\text{C}$ by:

$$\nu = \frac{E'(T)}{3RT} \tag{2.8}$$

Where R is the universal gas constant (8.3145 J mol⁻¹ K⁻¹) and T is the absolute temperature in the rubbery region (453.15 K).

2.2.8. Ultimate Tensile Testing

The tensile tests were performed on an Instron 5967 universal testing machine with a 30 kN load cell. Type V specimens with a thickness of 2 mm according to ASTM D638 were used [57]. An extension rate of 50 mm/min was used. The small geometry of the type V specimen limited the placement of an extensometer and only the cross-head displacement was recorded. Five specimens per material were tested.

2.3. Results

2.3.1. Torque Rheometer Curves

The cross-linking process of LLDPE-V was followed using an Intelli Plasti-Corder Torque Rheometer, monitoring the torque variation as a function of time (Figure 2.2). Torque curves of LLDPE-V with four different degrees of grafting of MAH were compared using a stoichiometric molar equivalency ratio of 1:0.5 (MAH:DTA). The cross-linker (DTA) was introduced to the polymer melt by opening the feeding port in the mixer. This led to a small torque decrease before an increase was observed. This sharp increase of the torque indicates that the cross-linking reaction takes place. The maximum torque was reached within one minute for LLDPE-V0.15 and LLDPE-V0.3. In the case of LLDPE-V0.6 and LLDPE-V1.2, the maximum torque value was reached in two minutes. The feeding rate of the cross-linker into the mixer was controlled manually and was slower for LLDPE-V0.6 and LLDPE-V1.2. This could have an impact on the precise time to reach maximum torque.

The torque curves in Figure 2.2 provide additional insight valuable for determining processing trends for the materials. First, the maximum torque increases with increasing degree of MAH functionalities, indicating higher cross-link density. After the maximum torque value is reached, a

torque drop was recorded. This is less noticeable in LLDPE-V0.15. The melt temperature was monitored, and it is represented by the dashed lines in Figure 2.2. The temperature of the melt increased as soon as the DTA was introduced in the melt. The melt temperature increase recorded at the end of the process was 4 °C for LLDPE-V0.15 and LLDPE-V0.3, 14 °C for LLDPE-V0.6, and 30 °C for LLDPE-V1.2. This strong self-heating with increasing viscosity is due to viscous dissipation and led to an overall decrease of the viscosity and torque through the duration of the mixing process.

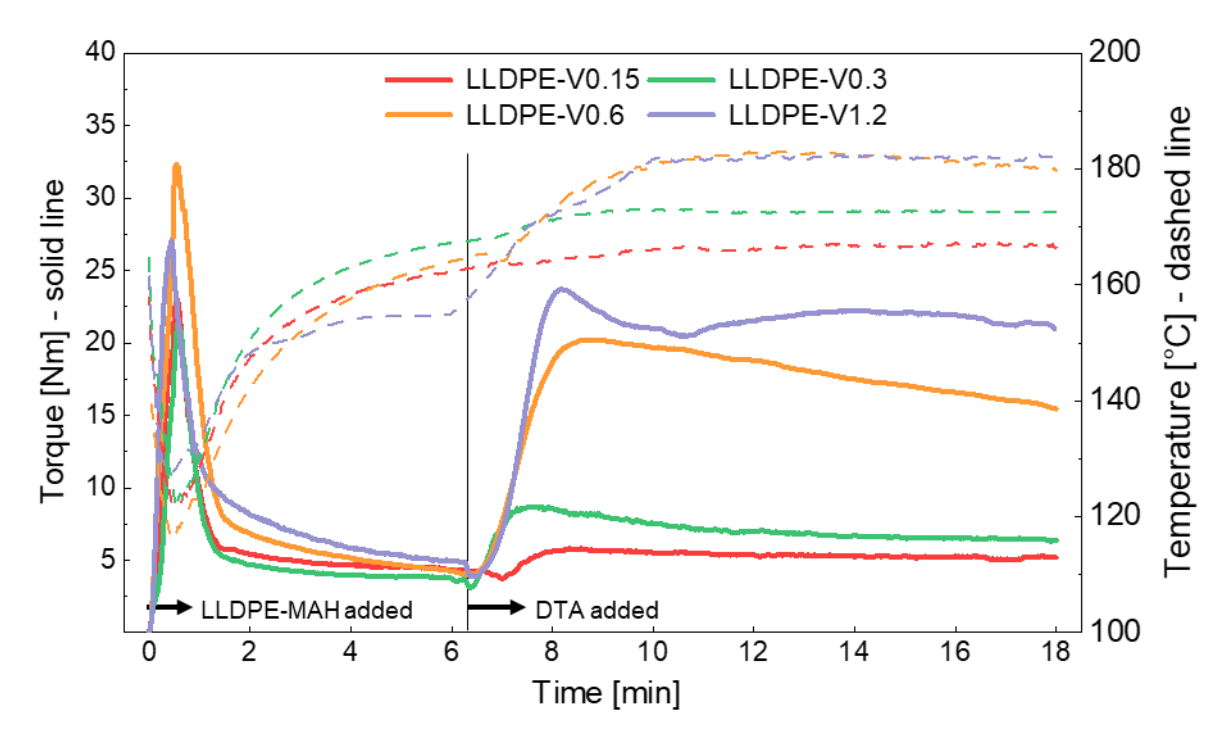


Figure 2.2. Flow behavior of cross-linked LLDPE using various degrees of MAH functionality and MAH:DTA molar ratio (control temperature: 160 °C, 50 rpm). Torque is shown with solid lines and melt temperature with dashed lines.

The reactive blending of LLDPE-V1.2 has a unique characteristic compared to the other three materials. After the DTA was added to the melt, the viscosity increased significantly, at which point the material started to grind as depicted in Figure 2.3A. After five minutes of adding the

DTA, the material started forming an elastic polymer melt and no powder was detected at the end of the process as observed in Figure 2.3B. It is possible that the cross-link content in this sample was too high for the material to be easily processable under these conditions. A consequence of this behavior is that, if reactive blending of this material were conducted in an extruder, the residence time would be significantly shorter and proper blending would not be possible.

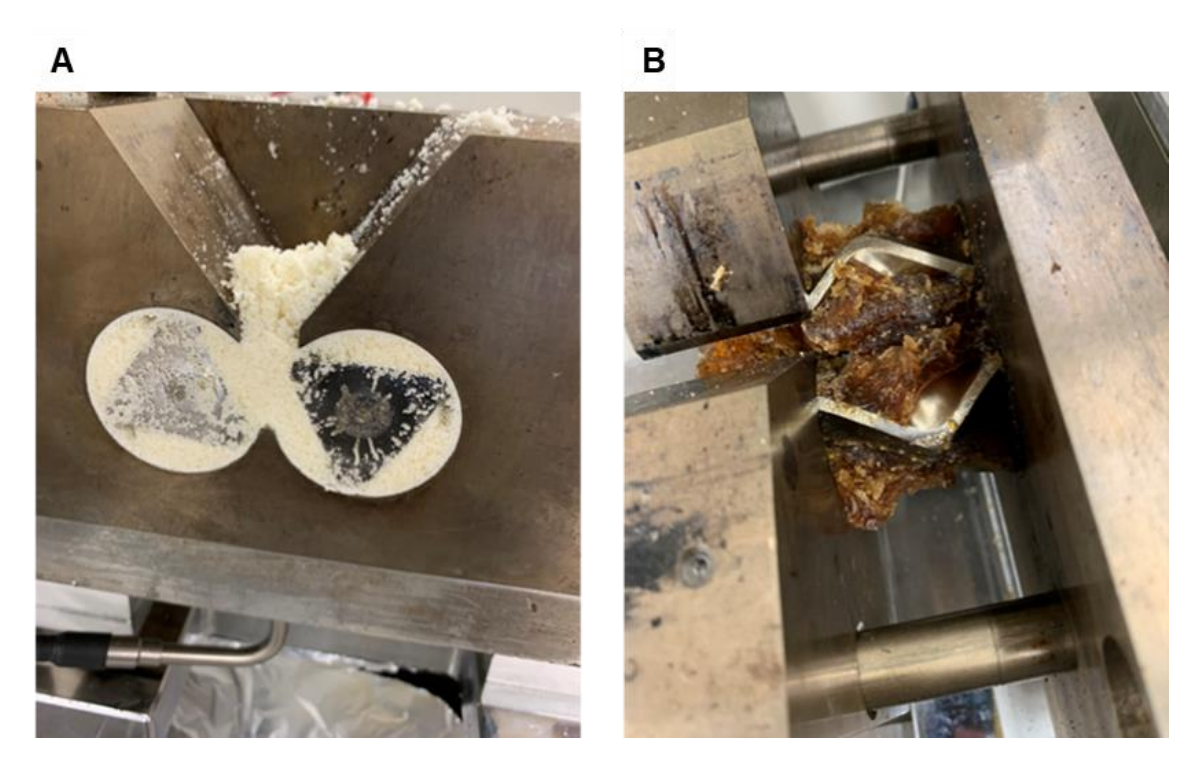


Figure 2.3. Reactive blending of LLDPE-V1.2 at 160 °C and 50 rpm after: (**A**) 5 minutes of the addition of DTA and (**B**) 12 minutes of the addition of DTA.

2.3.2. FTIR Analysis

FTIR measurements were performed to verify that the amine groups (NH₂) of the DTA reacted with the MAH of the functionalized LLDPE. Two MAH-functionalized polymer chains are linked if both NH₂-groups of DTA react with two MAH-groups of the functionalized polyolefin as shown previously in Figure 2.1. In the case where all DTA reacts, this will lead to chain extension if only

one MAH-group is present per polymer chain, and to network formation if more than two MAH-groups are present per polymer chain. FTIR-measurements were used to confirm that the reaction took place during the mixing step.

The FTIR spectrum of DTA, LLDPE, LLDPE-MAH0.6 and LLDPE-V0.6 are presented in Figure 2.4A. In the DTA spectrum, the peaks in the range of 3500-3250 cm⁻¹ corresponds to the amine group. The peak around 1789 cm⁻¹, corresponds to the signal of C=O of maleic anhydride ring. The spectrum of LLDPE-V0.6 shows a peak at 1715 cm⁻¹, characteristic of C=O of a maleimide ring, indicating that the reaction took place. The FTIR curves of the four vitrimers prepared are plotted in Figure 2.4B. The peak at 1789 cm⁻¹, corresponding to the signal of C=O of maleic anhydride ring, were present in all vitrimers. This suggests that not all the MAH groups reacted. The peak corresponding to the C=O of maleimide ring (1715 cm⁻¹) increased in intensity as the initial weight percentage of MAH increases.

The MAH conversion shown in Figure 2.5 was determined using the IR signal at 1789 cm⁻¹. Samples obtained at the end of the reactive blending process depicted in Figure 2.2 were used for these measurements. It can be observed that the MAH conversion increased as the amount of initial MAH-groups (wt.%) increased.

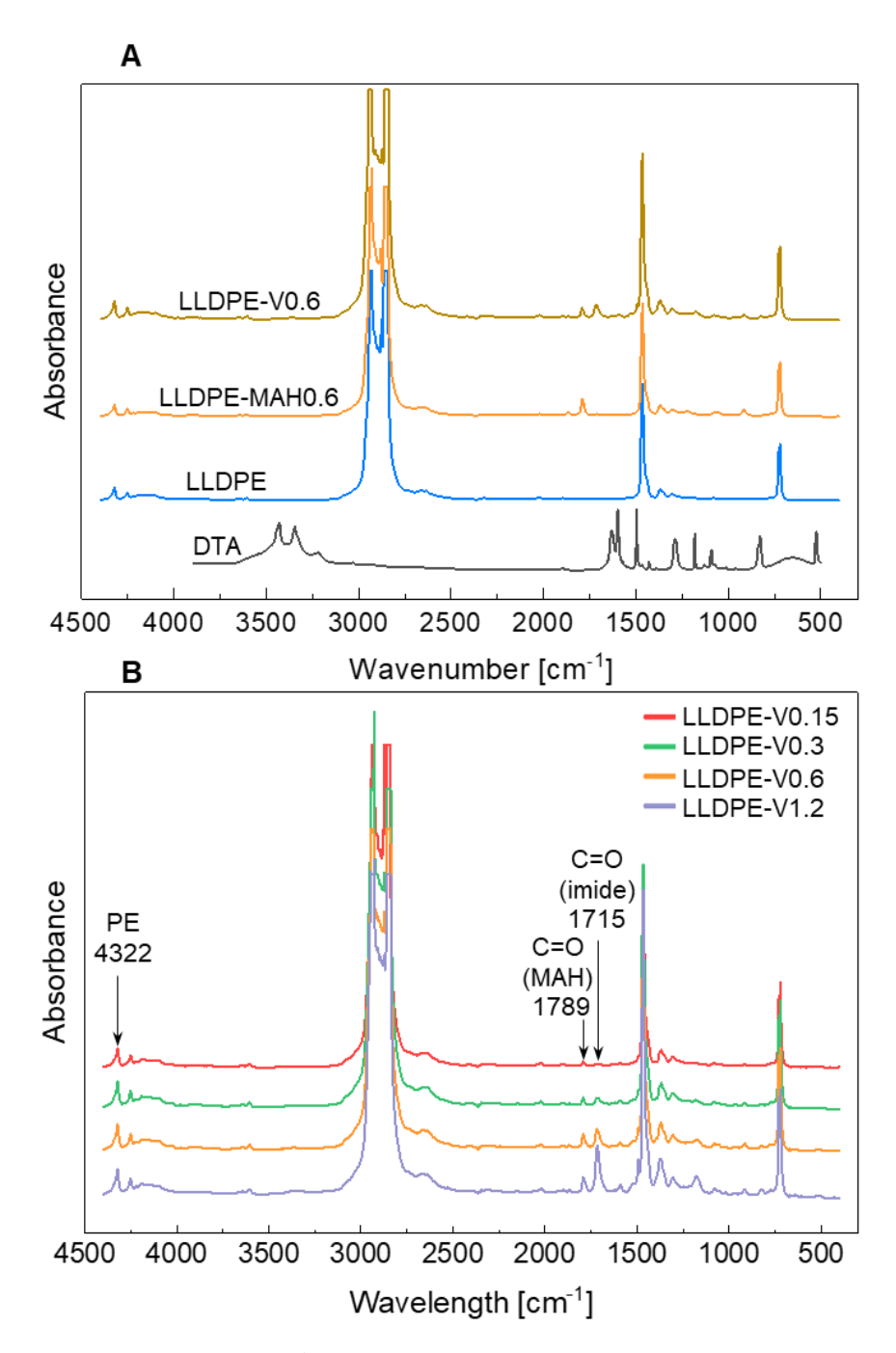


Figure 2.4. FTIR spectral curves. (**A**) cross-linker (DTA), thermoplastic precursor (LLDPE), functionalized polymer (LLDPE-MAH0.6) and vitrimer (LLDPE-V0.6), (**B**) four vitrimers with different initial MAH content (0.15, 0.3, 0.6 and 1.2 wt.%).

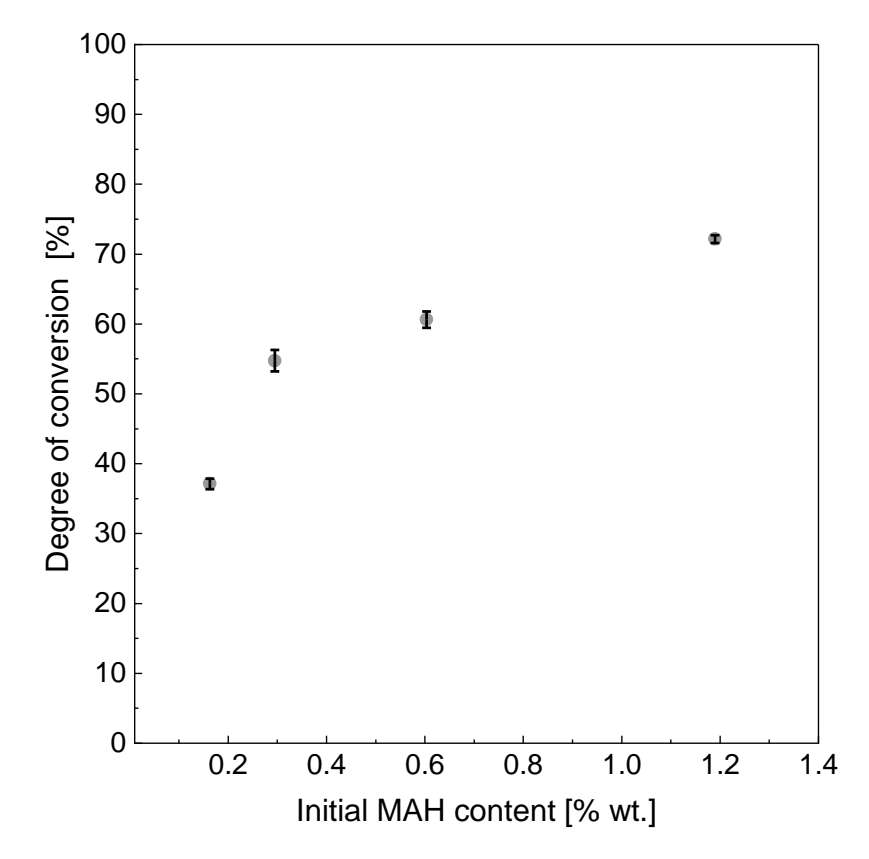


Figure 2.5. MAH conversion after reactive blending measured with FTIR using the IR signal at 1789 cm⁻¹.

2.3.3. Thermal Properties: Differential Scanning Calorimetry (DSC)

The melting temperature (T_m) and melting enthalpy (ΔH_m) were determined for LLDPE, LLDPE-MAH and LLDPE-V samples (Figure 2.6). The melting enthalpy and peak melting temperature decreased as the wt.% of MAH and cross-linking density were increased. Additionally, the melting peak was broadened. It is evidenced that the MAH groups and the formation of cross-links decrease the degree of crystallinity of the materials. This is exacerbated for the highest cross-linked system, LLDPE-V1.2. The degree of crystallinity of LLDPE was 47.5% while the degree of crystallinity of LLDPE-V1.2 was 37.9%, corresponding to a 9.6% decrease.

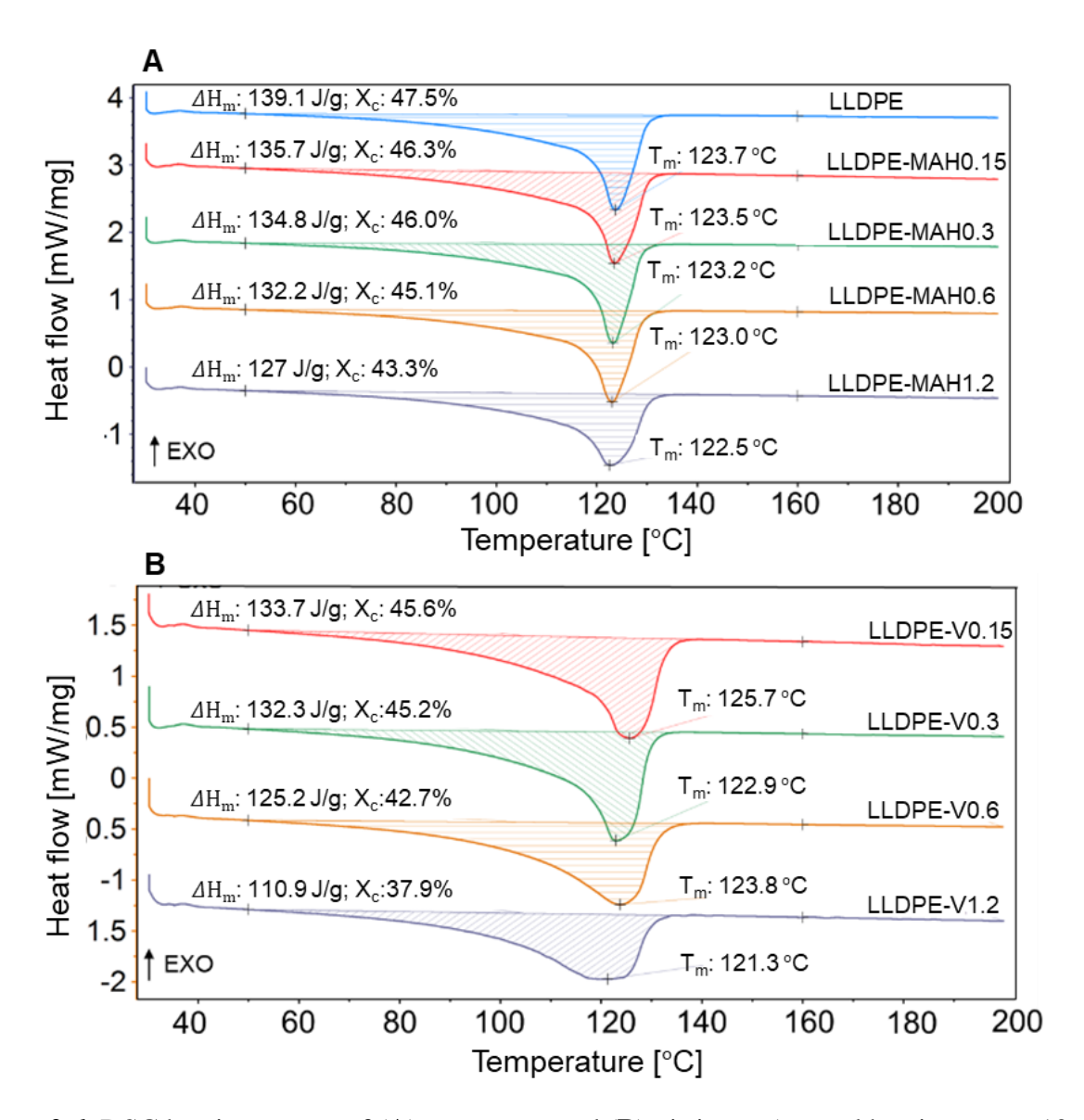


Figure 2.6. DSC heating curves of **(A)** precursors and **(B)** vitrimers (second heating ramp, 10 K/min).

2.3.4. Gel Content

After swelling in xylene at 110 °C for 24 hours, LLDPE-V0.15 and LLDPE-V0.3 completely dissolved. It is possible that a chain extension was attained instead of a network formation due to the low number of MAH-groups available. The swelling ratio and gel content of LLDPE-V0.6 and LLDPE-V1.2 are summarized in Table 2.2.

Table 2.2. Swelling and gel content of vitrimers.

Materials	Swelling ratio [-]	Gel content [%]		
LLDPE-V0.15	-	-		
LLDPE-V0.3	-	-		
LLDPE-V0.6	38.0±6.5	26.4±1.8		
LLDPE-V1.2	13.9±1.6	48.3±2.0		

2.3.5. Rheological Properties

Rheology measurements were performed to investigate the properties of LLDPE-MAH and LLDPE-V in the melt. The frequency sweeps performed at 190 °C are shown in Figure 2.7 and Figure 2.8. The data was fitted to the Cross model, with the full fitting parameters included in the appendix (Table A.1). The concentration of MAH had an impact on the rheological performance as demonstrated in the complex viscosity measurements in Figure 2.7A. All the grafted materials, LLDPE-MAH, showed lower complex viscosity values compared to the non-functionalized LLDPE above an angular frequency of 10 rad/s. This indicates that the MAH-groups act as lubricants above those frequencies. The viscosity of LLDPE-MAH1.2 at frequencies below 0.1 rad/s was twice the magnitude of LLDPE. It is believed that increasing the MAH-groups can lead to the formation of micro-phase aggregates due to their polar nature [58]. The presence of agglomerates of MAH-groups in the polyethylene matrix most likely contributes to this increasing viscosity at decreasing frequency.

The cross-linking of LLDPE-MAH resulted in a large increase in the complex viscosity at low frequencies (Figure 2.7B). The viscosity increased when the amount of MAH functionalities were increased, indicating a higher crosslink density for LLDPE-V1.2. The viscosity of LLDPE-V0.3 increased by one order of magnitude at a frequency of 0.1 rad/s compared to non-crosslinked

LLDPE. The viscosity of LLDPE-V0.6 and LLDPE-V1.2 increased by two and three orders of magnitude, respectively. However, at higher angular frequency (>100 rad/s), the viscosity of the four LLDPE vitrimers was on the same order of magnitude as LLDPE. This suggests that the materials can be processed through small strain thermoplastic processing techniques. The four vitrimers did not reach the Newtonian region within the frequency range measured. This can be an indication of relatively long relaxation times compared to the investigated times scales within the tested frequency range.

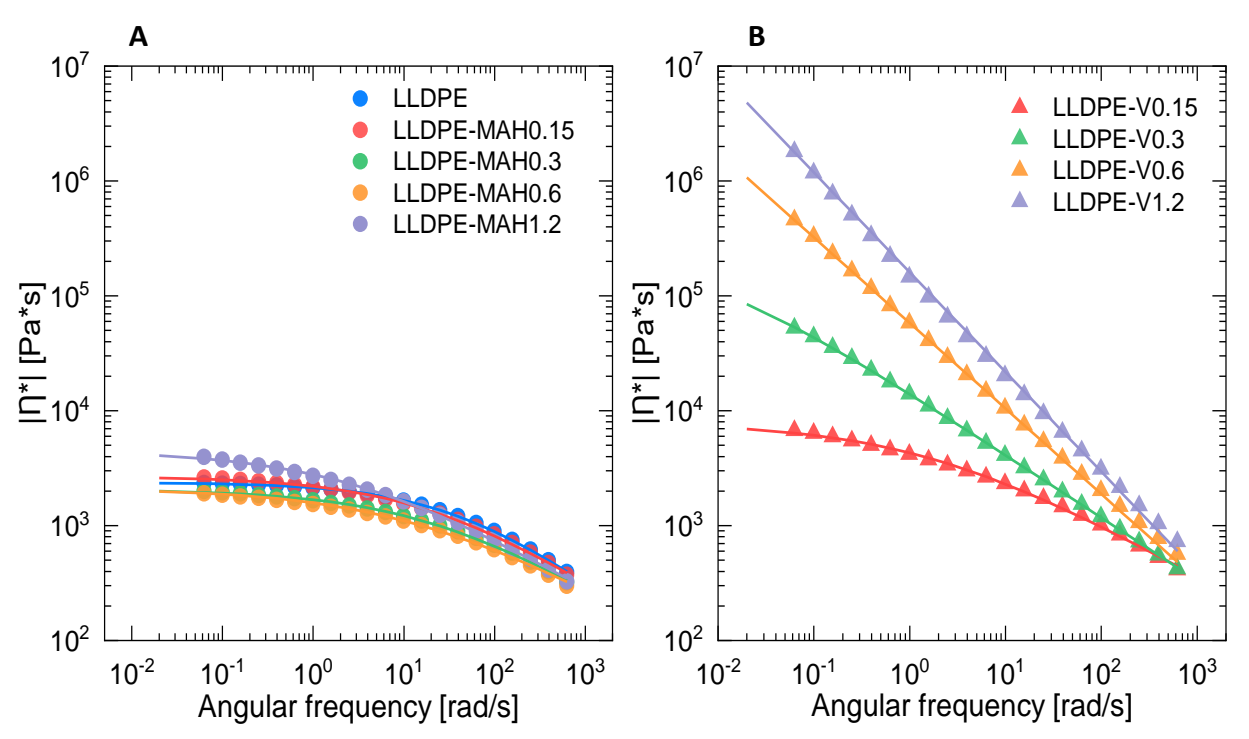


Figure 2.7. SAOS measurements - 190 °C. (**A**) complex viscosity of LLDPE and four grades of LLDPE-MAH and (**B**) complex viscosity of LLDPE vitrimers. Circles and triangles represent the experimental data, and the lines represent the Cross model fit.

The zero-shear viscosity is commonly used to describe the behavior of polymer melts and is useful for indicating the influence of molecular architecture (e.g. chain extension and cross-linking) on the flow resistance. The zero-shear viscosity of LLDPE and LLDPE-MAH grades was

determined by fitting the experimental data to the Cross, Carreau and Adams-Crane models (Table 2.3). The Carreau and Adams-Crane models were used as they have been shown to accurately bracket the zero-shear viscosity, where the Carreau model is the lower end and the Adams-Crane model is the high end [56]. The fitting parameters and correlation coefficients are included in the appendices (Table A.2 - Table A.3). The Cross and Adams-Crane had correlation coefficients above 0.99. The correlation coefficient in the Carreau model was decreased to 0.98. In all cases, the Cross model was contained within this bracket. The bracketing range is narrower for materials that are reaching the Newtonian region. The Newtonian region is not reached in LLDPE-MAH1.2. Therefore, the bracketing range increases dramatically. A wider frequency range is needed to accurately estimate the zero-shear viscosity of the vitrimers. However, this was not possible due to limitations in the equipment and the data is not reported.

Table 2.3. Zero-shear viscosity of LLDPE and LLDPE-MAH estimated with three models.

Materials	Zero shear viscosity, η_0 [Pa*s]					
Materials	Carreau	Cross	Adams-Crane			
LLDPE	2174.22	2365.13	2469.75			
LLDPE-MAH0.15	2351.54	2666.92	2922.66			
LLDPE-MAH0.3	1803.48	2052.32	2250.02			
LLDPE-MAH0.6	1708.21	1975.66	2210.39			

The storage (G') and loss (G'') modulus of LLDPE vitrimers are given in Figure 2.8. For the vitrimers with the lowest amount of MAH functionalities, LLDPE-V0.15 and LLDPE-V0.3, a cross-over point between G' and G'' occurred at 298 rad/s and 12 rad/s, respectively. Furthermore, LLDPE-V0.3, displayed similar values and power law dependences for G' and G'': $G' \sim G'' \sim \omega^{0.51}$.

This behavior is characteristic of a critical gel as demonstrated by Chambon and Winter [59]. The storage modulus was higher than the loss modulus for LLDPE-V0.6 and LLDPE-V1.2 and no cross-over point was observed in the frequency range tested. This behavior is characteristic of cross-linked materials. Based on rheological measurements, LLDPE-V1.2 had the highest cross-link density as it had the largest storage modulus. Finally, the storage and loss modulus were less affected by the angular frequency at higher cross-link density, as can be seen for LLDPE-V0.6, and especially LLDPE-V1.2.

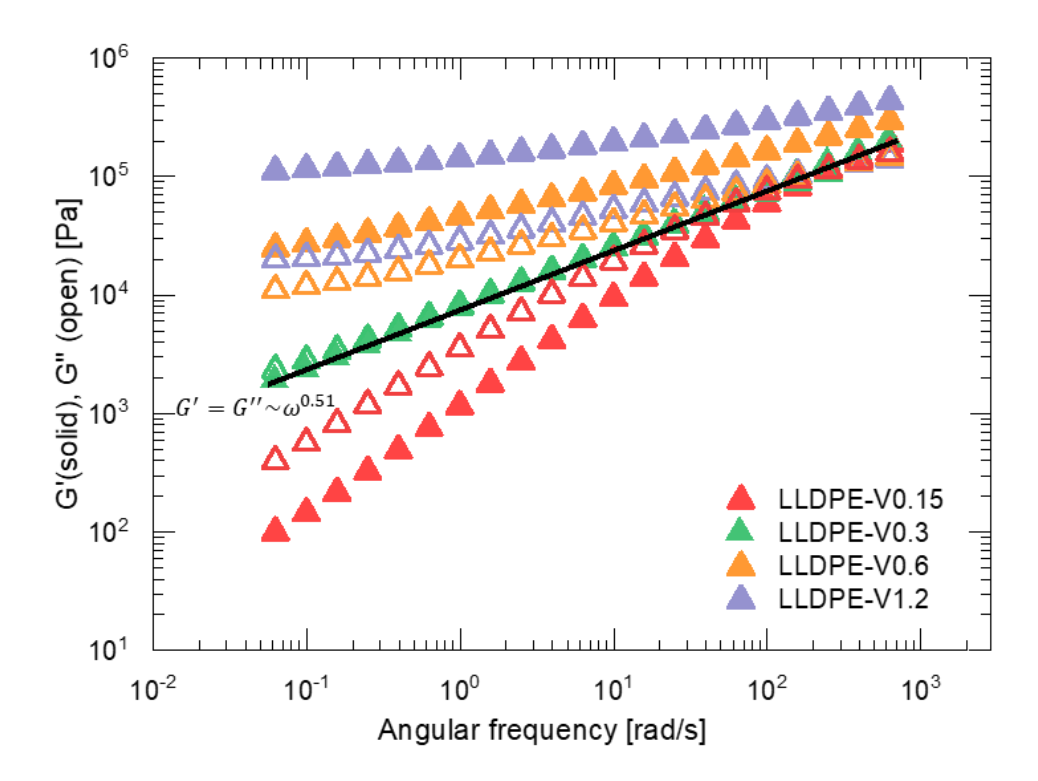


Figure 2.8. SAOS measurements - 190 °C. Storage (G') and loss (G'') modulus of LLDPE vitrimers.

The shear stress relaxation of LLDPE, LLDPE-MAH0.6, and LLDPE-V0.6 was measured by applying a strain of 5% and monitoring the relaxation modulus, G(t), over time at 190 °C (Figure 2.9A). The curves are plotted in a non-normalized way on logarithmic axes, since G(t) involves

various relaxation modes that occur at different time scales and temperature [34]. The relaxation rate of LLDPE-V0.6 is lower compared to LLDPE and LLDPE-MAH0.6. The normalized curves are plotted in Figure 2.9B for comparison purposes. The initial modulus, G_0 , measured at 0.05 seconds was 1.0×10^4 Pa, 5.7×10^3 Pa and 1.1×10^5 Pa for LLDPE, LLDPE-MAH0.6 and LLDPE-V0.6, respectively.

The relaxation of polyethylene vitrimers is complex and still not fully understood. Different relaxation modes might include topological defects (trapped loops), Rouse relaxation, disentanglement, reptation and dynamic cross-linking [34]. The relaxation time was determined when the relaxation modulus, G(t), reached 5% of the initial modulus. The 5% cut-off point was chosen to minimize the amount of noise induced by reaching a low-resolution region of the instrument as seen in the 0.01 - 0.1 Pa region. LLDPE and LLDPE-MAH0.6 behaved like a viscoelastic liquid with a relaxation time of 0.34 seconds and 0.60 seconds, respectively. The MAH groups have an effect in the relaxation behavior of LLDPE, delaying the relaxation time by 0.3 seconds. This reinforces the hypothesis that MAH-groups form micro-phase aggregates due to their polar nature [58]. LLDPE-V0.6 had a relaxation time of 283 seconds and was not able to completely relax in the time range measured. After three hours, LLDPE-V0.6 has 0.9% residual stress. Topological constraints in the system can hinder a full relaxation of stress as previously proposed by Ricarte et al [34]. Furthermore, LLDPE-V0.6 does not follow a single exponential decay. This result is in agreement with what Ricarte et al., and Maaz et al. reported for polyethylene vitrimers undergoing dioxaborolane metathesis [34], [44]. Stress relaxation is not adequate to show the reversibility of disulfide bonds in these materials. The relaxation of this material is complex and multiple relaxation modes are involved. A more suitable demonstration of the reversibility of the S-S bonds are healing or lap shear experiments as published by Imbernon et al. [37] and Zheng

et al. [39]. Regardless, LDPE-V0.6 was able to be processed twice in the internal mixer and compression molded into plates clearly showing that it is processable.

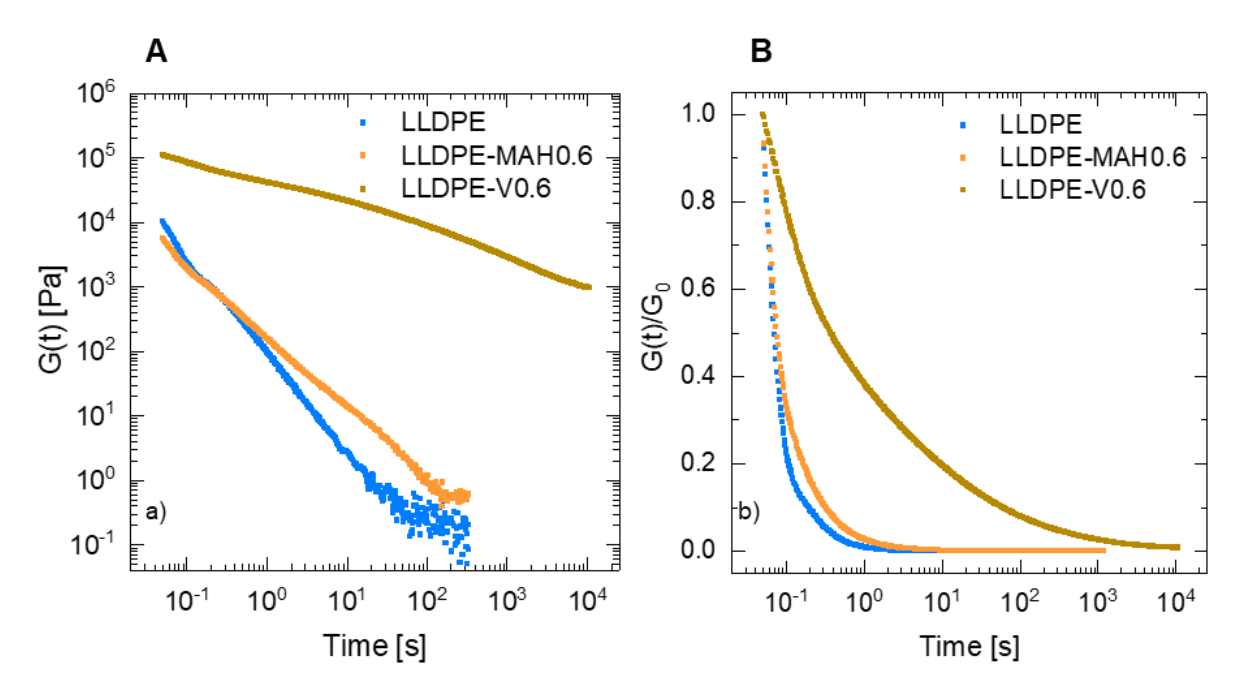


Figure 2.9. Stress relaxation of LLDPE, LLDPE-MAH0.6 and LLDPE-V0.6 at 190 °C under 5% strain: (**A**) log-log scale and (**B**) normalized semi-log scale.

2.3.6. Thermo-Mechanical Properties

DMA measurements were used to determine mechanical properties as a function of temperature (Figure 2.10). The storage modulus (E') at 35 °C decreased as the cross-linking density increased. The E' of LLDPE, LLDPE-V0.15, LLDPE-V0.3, LLDPE-V0.6 and LDPE-V1.2 was 550 MPa, 499 MPa, 493 MPa, 439 MPa, and 333 MPa, respectively. This drop in modulus is a consequence of the decrease in degree of crystallinity as discussed in Section 2.3.3. The measurement of pristine LLDPE and LLDPE-V0.15 stopped at 128 °C when it reached the melting point and an abrupt decrease of the storage modulus (E') was observed. These samples flowed under their own weight, leading to the rupture of the sample. LLDPE-V0.3, LLDPE-V0.6 and LLDPE-V1.2 retained a

modulus above melting temperature, however, the LLDPE-V0.3 sample failed at 200 °C. The rubbery plateau was directly proportional to the MAH content in the vitrimer.

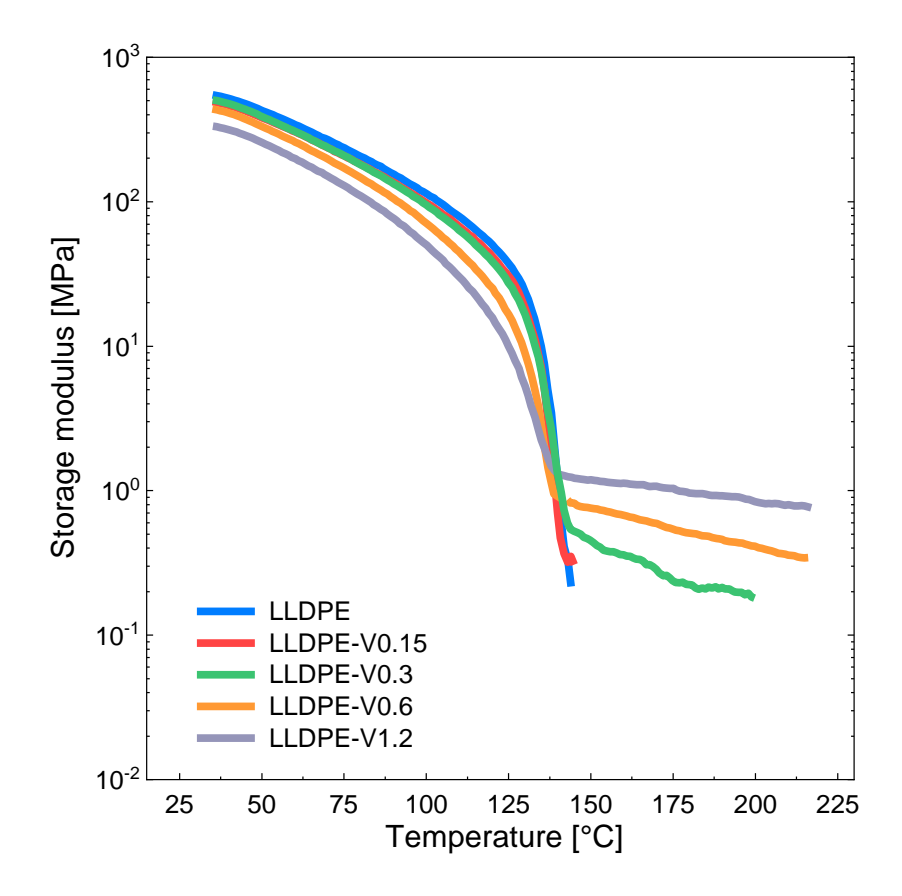


Figure 2.10. Storage modulus as a function of temperature for LLDPE and four grades of LLDPE vitrimers with various cross-linking densities (10 Hz, 0.1% strain).

The cross-linking density was determined for LLDPE-V0.3, LLDPE-V0.6, and LLDPE-V1.2 using the E' value at 180 °C as shown in Table 2.4. The cross-linking density of LLDPE-V0.15 was not calculated since a rubbery plateau was not observed. Furthermore, it was determined in Section 3.4 that most likely a chain extension was attained instead of a network formation for this system.

Table 2.4. Storage modulus at 180 °C and cross-linking density of the vitrimers studied.

Material	E' at 180 °C [MPa]	Cross-linking density, $\nu \times 10^{-5}$ [mol/cm 3]			
LLDPE-V0.15	-	-			
LLDPE-V0.3	0.21	1.86			
LLDPE-V0.6	0.51	4.51			
LLDPE-V1.2	0.96	8.50			

As an additional visual demonstration of this behavior, circular discs of these same materials were heated in an oven at 190 °C as depicted in Figure 2.11. The LLDPE disc starts collapsing after two minutes and fully collapsed after five minutes. LLDPE-V0.15 started collapsing after five minutes, however, after 20 minutes there was still a strand holding the material together. The three remaining vitrimers did not collapse after 20 minutes. The formed cross-links clearly prevented the material from fully collapsing. This improved property is critical for processes such as blow molding, film blowing, foaming, and thermoforming.

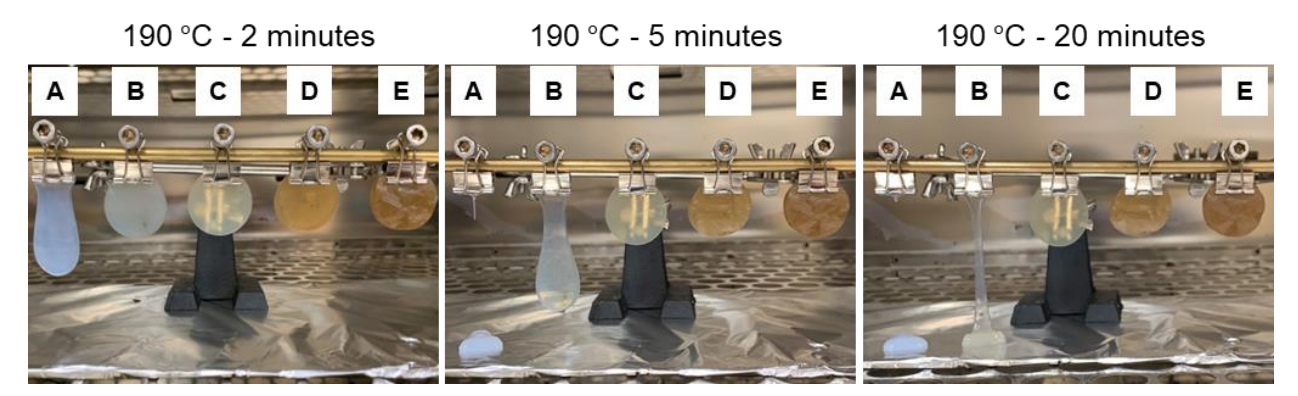


Figure 2.11. Dimensional stability at 190 °C and varying heating time. (**A**) LLDPE, (**B**) LLDPE-V0.15, (**C**) LLDPE-V0.3, (**D**) LLDPE-V0.6, and (**E**) LLDPE-V1.2.

2.3.7. Re-Processing

To demonstrate the re-processing ability of these materials, LLDPE-V0.6 was processed twice in the 3-Piece mixing bowl using the same conditions described in Section 2.2.2. The rheological and mechanical properties of the virgin and re-processed material were measured, and the results are summarized in Figure 2.12 and Figure 2.13. The viscosity of the virgin and the re-processed material is comparable over the entire frequency range (Figure 2.12). This indicates that the cross-linking density is retained after a second processing cycle in the mixing bowl.

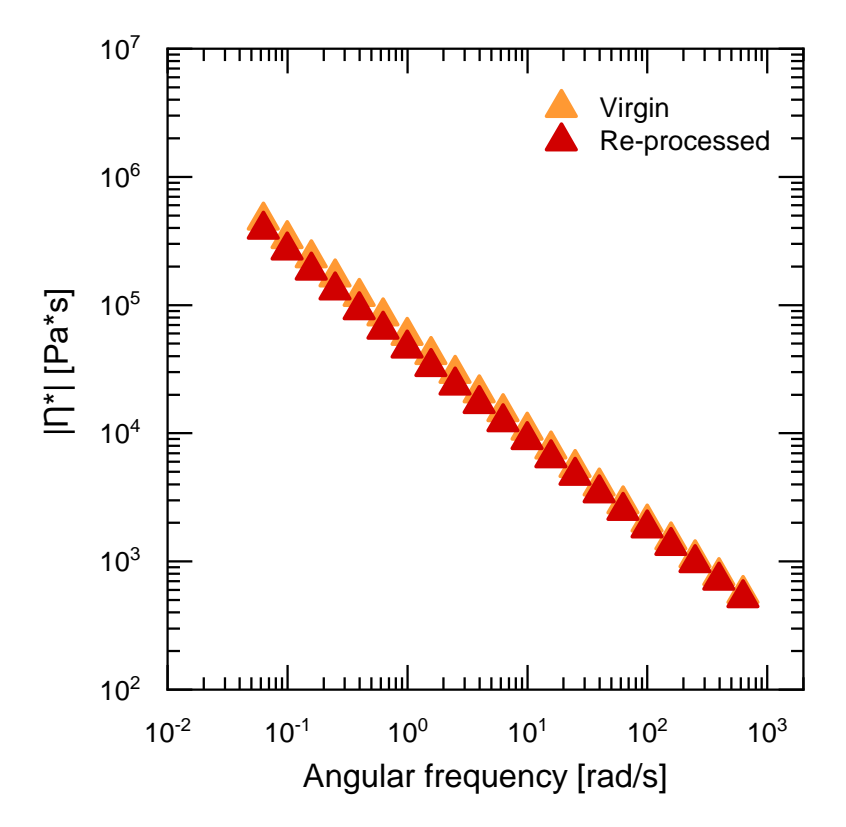


Figure 2.12. Complex viscosity of LLDPE-V0.6 virgin and LLDPE-V0.6 re-processed (190°C).

Finally, the tensile properties of LLDPE, virgin and re-processed LLDPE-V0.6 were measured (Figure 2.13). The yield stress slightly decreased after cross-linking and after re-processing. The yield stress of LLDPE was 14.2 ± 0.2 MPa, while the yield stress of the virgin vitrimer and the re-

processed vitrimer was 13.2 ± 0.2 MPa and 12.8 ± 0.2 MPa, respectively. It was expected that the cross-links would stiffen the materials. However, as shown in Section 2.3.3, the cross-links decreased the degree of crystallinity of the materials which explains the decreased in yield stress. The displacement at break of the virgin and re-processed vitrimer decreased from 201.1 ± 26.0 mm (LLDPE) to 80.2 ± 15.7 mm, 81.1 ± 17.7 mm, respectively. This behavior is characteristic of cross-linked materials.

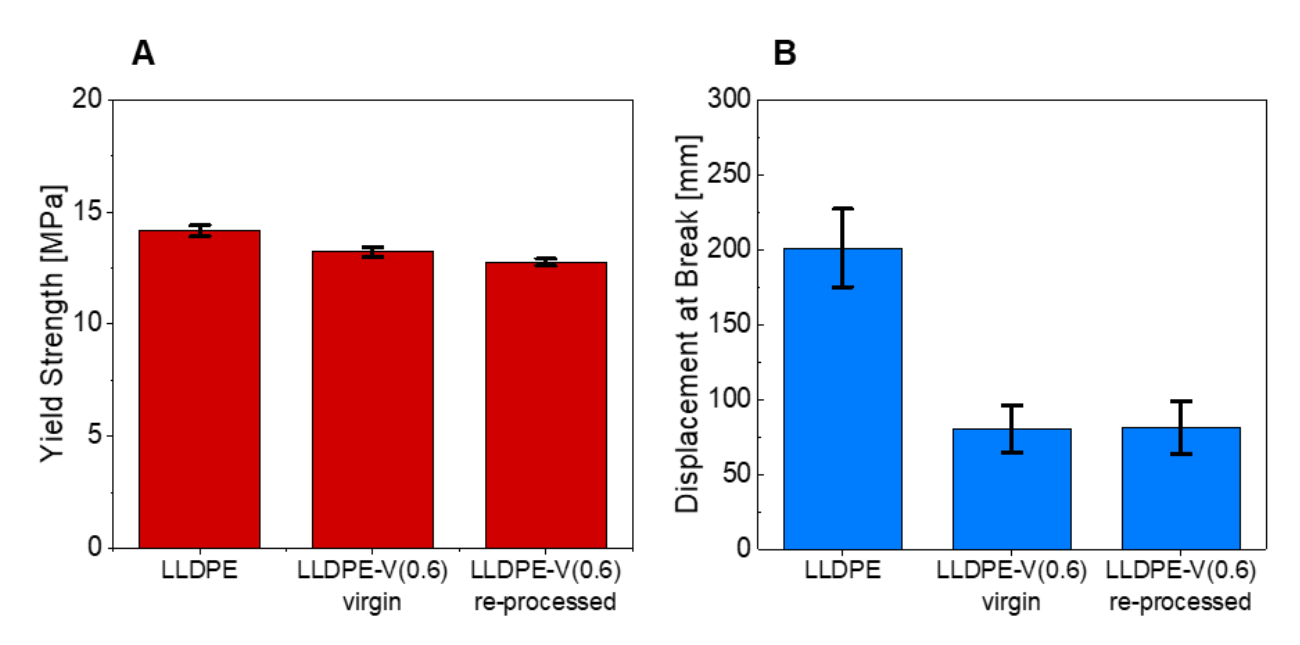


Figure 2.13. Mechanical properties of LLDPE-V0.6 virgin and LLDPE-V0.6 re-processed: (**A**) yield strength and (**B**) displacement at break. Error bars are calculated from the standard deviation of 5 replicates.

2.4. Conclusions

Dynamic cross-linked LLDPE were obtained by cross-linking LLDPE-MAH with a disulfidecontaining diamine via reactive blending. The exchange reaction occurs due to the presence of disulfide bonds in the cross-linker. The presence of formed cross-links is demonstrated with torque curves, swelling experiments, frequency and temperature sweeps. The FTIR measurements of the vitrimer-like materials shows the appearance of a characteristic peak of C=O of a maleimide indicating that the reaction took place. The torque experiments revealed a sharp increase in torque as the cross-linking reaction took place. The maximum torque is reached in one minute for LLDPE-V0.15 and LLDPE-V0.3 and in two minutes for LLDPE-V0.6 and LLDPE-V1.2. The last two materials possessed a very elastic performance at 190 °C, as G' was larger than G'' in the frequency range investigated. The complex viscosity of vitrimers at low frequencies (0.1 rad/s) increased up to three orders of magnitude compared to the thermoplastic LLDPE. However, at frequencies larger than 100 rad/s the magnitude of the complex viscosity of thermoplastic LLDPE and the vitrimer is in the same order of magnitude. The relaxation of LLDPE-V0.6 in the melt was hindered by the formation of cross-links and topological constraints in the system hindered a full relaxation of stress. The time to release 95% of the applied stress of LLDPE, LLDPE-MAH0.6, and LLDPE-V0.6 was 0.34 seconds, 0.60 seconds and 283 seconds, respectively. The MAH-groups and the formation of cross-links in the materials led to a decrease in the degree of crystallinity. The increased dimensional stability at elevated temperatures of the vitrimers is a very promising property for processes such as film blowing, blow molding, foaming and thermoforming which will be evaluated in future research. Finally, the re-processing ability was demonstrated with LLDPE-V0.6 via internal mixing and the rheological and mechanical properties were retained.

3. Effect of Cross-linking on the Mechanical Properties, Degree of Crystallinity and Thermal Stability of Polyethylene Vitrimers

The intent of this chapter is to better understand thermal and mechanical properties of PE vitrimers with varying cross-linking density. More specifically, the effect of the dynamic cross-links in crystallinity, thermal stability, short and long-term mechanical properties, and viscoelastic properties. In the context of this dissertation, the information found in this chapter is used to identify suitable applications and processing that will be discussed in chapter 4. This chapter is based on the research "Effect of cross-linking on the mechanical properties, degree of crystallinity and thermal stability of polyethylene vitrimers" published in *SPE Polymer Engineering and Science*, Volume 62, Issue 12 (2022) [60].

3.1. Introduction

Polyethylene (PE) is presently the most-used commodity plastic by volume and it is frequently used in consumer goods, construction and electrical industry [1], [3]. Some examples include plastic bags, bottles, films, tubes and wire insulation. Cross-linked polyethylene (XLPE) consists of PE that has been either physically or chemically cross-linked to form permanent covalent bonds linking adjacent chains [61]. The presence of the cross-links leads to enhanced properties which give it an advantage in performance. Some common applications of XLPE include pipes and insulation for high voltage cables [2], [4]. However, the permanent covalent bonds lead to inferior processability which makes recycling and reusing of XLPE more difficult compared to PE [5], [61], [62].

Usually, compounding and shaping operations of XLPE products are done under controlled temperature to prevent premature cross-linking. It is critical that the cross-linking agent remains inactive at processing temperature, which is why peroxide cross-linking continues to be the most common choice to produce XLPE [5], [6], [63]. However, this process produces volatiles and hazardous byproducts. To bypass this, an alternate cross-linking approach has been used in the last decade. This consists of incorporating functional comonomers or pendant groups which can react on-demand to cross-link the polymer without hazardous byproducts [9], [10]. This approach has gained more interest after the concept of vitrimer was introduced in 2011 [19].

Vitrimers consist of a cross-linked network that contains dynamic covalently bonded chains that can change its topology via exchange reactions [19]. Vitrimers have promising properties which includes creep resistance, shape memory, weldability, and healing properties [14]. Unlike XLPE, PE vitrimers (PE-V) could improve the performance of traditional PE without the sacrifice of reprocessing and recycling. Various researchers have been able to successfully transform polyethylene into polyethylene vitrimers using reactive melt extrusion as an alternative process of traditional peroxide cross-linking used in XLPEs [30], [32], [43], [44], [64].

This new class of material, vitrimer, opens the possibility to transform commodity thermoplastic to high performance materials [32]. The relative low cost of PE makes it the most used plastic globally and a large component of the plastic waste stream [65]. In 2019, it was reported that PE represented 38% of the global plastic demand which translates into 100 million tons [66]. To industrially transform commodity thermoplastic into vitrimers the chemistry of vitrimers has to make them processable like traditional thermoplastic without considerable impact on production speed or without the need to change current processing equipment [32], [45]. Therefore, the majority of research around thermoplastic vitrimers have focused on improving and

developing dynamic covalent chemistries with tunable reactivity [14]. However, there are still gaps to be filled to fully understand the implications of the dynamic cross-links and cross-linking density in the final part properties, specifically in thermal and mechanical properties.

The intent of this paper is to better understand final part properties of PE vitrimer-like materials that were obtained by taking advantage of readily available and well-studied chemistries and commercially available cross-linker and thermoplastic. To achieve this, the structure of PE was altered by grafting maleic anhydride (MAH) and the MAH-grafted polyethylene (PE-MAH) material was blended with 4,4' – dithiodianiline (DTA) in the melt state to form polyethylene vitrimer (PE-V). MAH was chosen as a grafting agent as it has been proven by previous studies that MAH has low reactivity towards itself and it grafts onto the polymer [67]-[69]. PE-MAH was used to promote the cross-linking reaction between the carbonyl group of the MAH-group and the amine groups of DTA. The cross-linker agent, DTA, contains sulfur-sulfur bonds that can undergo disulfide metathesis. The disulfide metathesis has been shown to be a catalyst-free exchange reaction by multiple studies in the area of vitrimers and it has been proven that this chemistry provides healing, weldability and malleability properties to cross-linked materials [36]— [39], [41], [42]. For this reason, this cross-linker was selected for this system. The material properties of interest in this study include mechanical, viscoelastic, crystallinity and thermal stability. This work is a continuation of a recent publication that focused on processing and rheological behavior of linear low density polyethylene (LLDPE-V) [51].

3.2. Materials and Methods

3.2.1. Materials and Sample Preparation

LLDPE 430BE [Melt flow index (MFI) = 4.2 g/10 min at 190 °C with 2.16 kg], HDPE F04660 [MFI = 0.7 g/10 min at 190 °C with 2.16 kg] and MAH-grafted PE's based on this LLDPE and HDPE were supplied by SABIC. The concentrations of MAH used in this study ranged from 0.15 -1.2 wt.%. The dynamic cross-linker used throughout this study was 4,4' – dithiodianiline (DTA) and was purchased from Sigma Aldrich. A summary of relevant material properties are given in Table 3.1.

Table 3.1. Characteristic properties of materials used in this study.

Material	Melting Temperature, [°C]	Density, [g/cm ³]	Molecular Weight, [g/mol]		
HDPE F04660	134	0.961	-		
LLDPE 430BE	124	0.930	-		
DTA	77	-	248.37		

Vitrimers were produced by cross-linking PE-MAH with DTA via melt reactive blending as shown in a previous study [51]. This was performed in a 3-piece internal batch mixer from C.W. Brabender with Banbury blades. The mixing steps were done at 50 rpm and 160 °C for LLDPE-MAH and 190 °C for HDPE-MAH. The mixer was attached to an Intelli Plasti-Corder which measured the variation of the torque exerted by the screws on the polymer melt. A graphical representation of the mixing protocol used to produce PE-V is shown in Figure 3.1. Plates were compression molded at 190 °C for 10 minutes under a load of 0.5 tons and specimens required for characterization were punched from these plates. All samples in this manuscript are designated by

the weight percent of grafting and cross-linking. For example, LLDPE-MAH0.3 is an LLDPE grafted with 0.3 wt% MAH and LLDPE-V0.3 is a LLDPE-MAH0.3 crosslinked with DTA under stoichiometric ratio of MAH:DTA of 1:0.5.

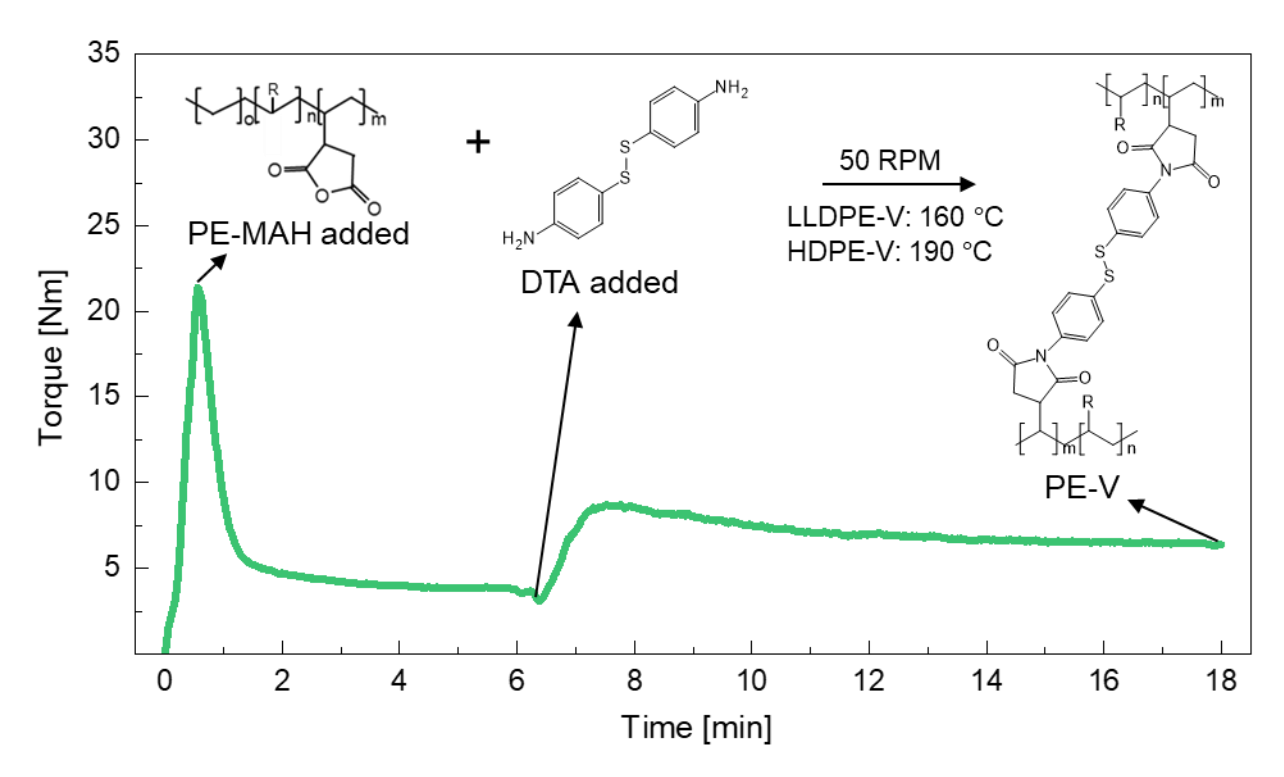


Figure 3.1. Graphical representation of the mixing protocol used to produce PE-V. The side group, R, can be a hydrogen or an alkyl group.

3.2.2. Differential Scanning Calorimetry

Differential scanning calorimetry (DSC) experiments were performed with a 214 Polyma DSC (NETZSCH). Samples of 10 mg +/- 0.5 mg were extracted from compression molded plates. Samples were placed in aluminum DSC pans with a pierced lid. Measurements were conducted at a heating rate of 10 °C/min with a starting temperature of 30 °C and end temperature of 200 °C in a nitrogen atmosphere. Two heating cycles were performed - the first to erase the thermal history and the second to measure the melting and crystallization properties. The heat of fusion was

determined using a linear baseline. The degree of crystallinity (χ_c) was calculated from the ratio of the measured melting enthalpy (ΔH_m) and the theoretical melting enthalpy (ΔH_{m^0}) of 100% crystalline polyethylene (293 J/g) [54].

3.3.3. Polarized Optical Microscopy

Polarized optical microscopy was conducted with an Olympus BX3 – URA microscope equipped with a 20× objective and a Linkam THMS600 hot-stage. 250-micron films were heated between a glass slide and cover slip to 190 °C and held for 2 minutes. The samples were quenched to an isothermal temperature corresponding to the peak crystallization temperature of LLDPE (110 °C).

3.3.4. Thermogravimetric Analysis

Thermogravimetric analysis (TGA) was conducted with a NETZSCH TGA 209 F1 Libra. A small sample (10 mg +/- 0.5 mg) placed in an alumina pan was ramped from 25 °C to 600 °C at a heating rate of 10 °C /min under oxygen atmosphere.

3.3.5. Ultimate Tensile Testing

An Instron 5967 universal testing machine was used to perform ultimate tensile testing. The device was equipped with a 30 kN load cell. Tests were performed according to ASTM D638 standard. Type V specimens with a thickness of 2 mm were loaded with an extension rate of 50 mm/min [57]. The small geometry of the specimens did not allow for placement of an extensioneter, so only the crosshead displacement was recorded.

3.3.6. Creep

Tensile creep resistance tests were performed under a constant stress of 5 MPa at 50 °C using the DMA GABO EPLEXOR® from NETZSCH. After 5 min of equilibration at 50 °C, samples

were subjected to a constant stress of 5 MPa, which was maintained for 15 hours. The tensile creep compliance, I(t), was determined by:

$$J(t) = \frac{\varepsilon(t)}{\sigma_0} \tag{3.1}$$

Where $\varepsilon(t)$ is the strain recorded and σ_0 is the constant stress applied (5 MPa).

3.3.7. Dynamic Mechanical Analysis

Dynamic Mechanical Analysis (DMA) tests were conducted using the tensile configuration of the GABO EPLEXOR® (NETZSCH) DMA at room temperature. Rectangular specimens produced via compression with dimensions of 45 mm x 10 mm x 3 mm were used to conduct strain sweeps and frequency sweeps. Strain sweeps were conducted on all samples at 10 Hz from strains of $10^{-3}\% - 10^{-1}\%$ to identify the range of linear viscoelastic behavior. Then, frequency sweeps were conducted using the linear viscoelastic dynamic strain percentage of 0.05% as the strain amplitude.

3.3. Results

The following sections present the thermal and mechanical results of this research until this date. Materials with varying cross-linking density were studied. The cross-linking density was determined using dynamic mechanical thermal analysis (DMTA) as described in the appendix section (A.3). The cross-linking density values are summarized in Table 3.2. The results presented in most of this paper will be focused on LLDPE-V. However, results for HDPE-V will be shown in Section 3.3.5 and Section 3.3.7.

Table 3.2. Cross-linking density of LLDPE and HDPE vitrimer based materials obtained from DMTA characterization (See appendix A.3).

Material	Cross-linking density, $\nu \times 10^{-5}$ [mol/cm 3]				
LLDPE-V0.3	1.86				
LLDPE-V0.6	4.51				
LLDPE-V1.2	8.50				
HDPE-V0.3	3.54				
HDPE-V0.6	6.02				
HDPE-V1.2	9.12				

3.3.1. Differential Scanning Calorimetry Analysis

The melting and crystallization behavior of LLDPE based materials was studied. Figure 3.2 shows the melting enthalpy (ΔH_m), the degree of crystallinity (χ_c), the peak melting temperature (T_m) and the peak crystallization temperature (T_c) of LLDPE, LLDPE-MAH and LLDPE-V. It is observed that the degree of crystallinity decreased as the wt.% of MAH and cross-linking density was increased as displayed in Figure 3.2A and Figure 3.2B, respectively. The melting and crystallization peak was significantly broadened for the LLDPE-V materials suggesting differences in the crystallite size distribution. Increasing grafting content and cross-linking density led to a small decrease in the melting temperature. However, it was noticed that LLDPE-V materials had an increase on the melting temperature of 2 °C over their precursors, LLDPE-MAH. This fact can be explained by the increase in molecular weight due to the cross-linking.

The cooling graphs in Figure 3.2C and Figure 3.2D reveals a peak around 65 °C corresponding to the small fraction of LLDPE with high branching degree that is unable to crystallize with the major component around 110 °C. The peak at 65 °C is present at the same intensity on LLDPE-MAH and LLDPE-V, indicating that the MAH-groups and cross-links are likely not present in the portion of LLDPE chain with high content of short chain branching [70]. MAH groups and cross-

links hindered the crystal formation and affected the lamellar thickness distribution. This effect is worsened for LLDPE-V1.2. This vitrimer led to a decrease on the degree of crystallinity of 9.5 % compared to LLDPE and was the broadest peak of all the LLDPE-MAH and LLDPE-V materials.

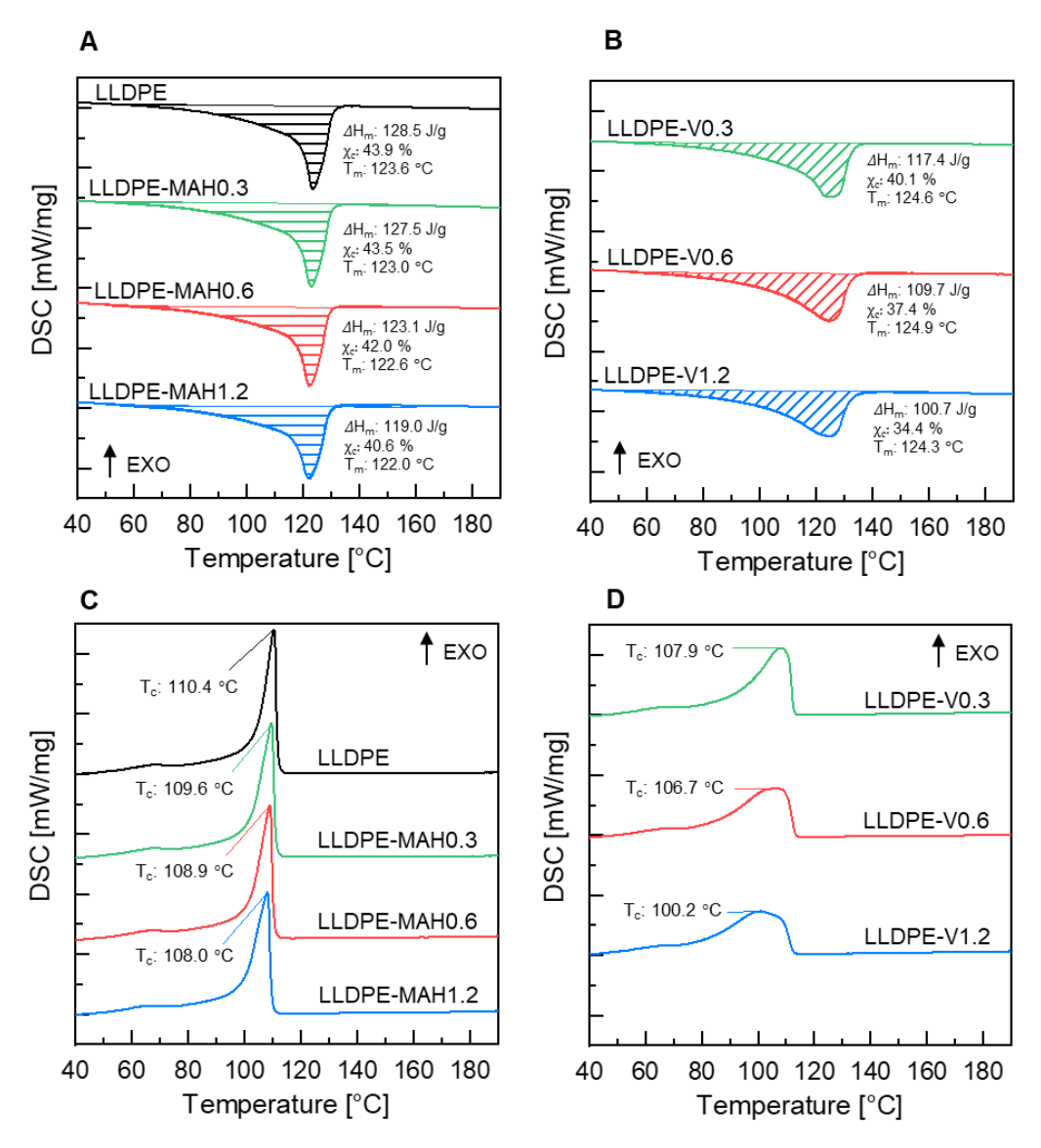


Figure 3.2. DSC scans from second heating/cooling ramp at 10 K/min: (**A**) heating of LLDPE MAH, (**B**) heating of LLDPE-V, (**C**) cooling of LLDPE-MAH, and (**D**) cooling of LLDPE-V.

3.3.2. Optical Microscopy Analysis of Crystallization

The crystal morphology of LLDPE, LLDPE-MAH0.6, and LLDPE-V0.6 was captured after two minutes of isothermal crystallization at 110 °C (Figure 3.3). Both LLDPE and LLDPE-

MAH0.6 show a Maltese Cross, an indication of spherulite growth in PE materials. The spherulites of LLDPE-MAH0.6 were not as sharp as in LLDPE, but they could still be easily distinguished. It can be noticed that the size of the crystals is smaller for LLDPE-MAH0.6 which reinforces the results obtained using DSC in Section 3.3.1. Furthermore, the cross-links seem to inhibit the growth of spherulites structure as there was no evidence of spherulites in LLDPE-V0.6. The observations in LLDPE-V0.6 are aligned with the work presented by Paajanen et al. in cross-linked polyethylene [71]. The authors demonstrated that cross-linking sites slowed down and restricted the crystallization process; the first stage of the crystallization process, the induction phase was extended, and the free growth of the crystals occurred at lower rates taking longer to complete [71].

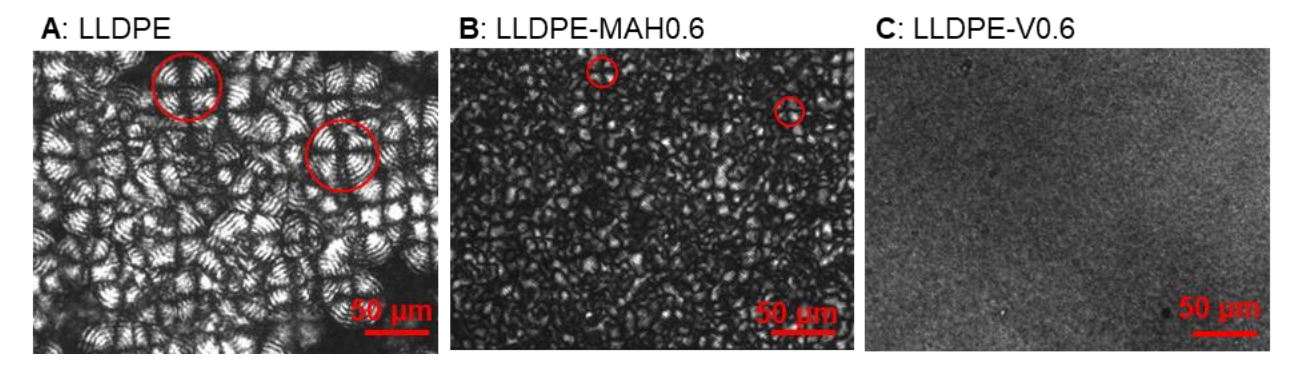


Figure 3.3. Polarized optical microscopy images (20× magnification) after 2 minutes of isothermal crystallization at 110 °C: (**A**) LLDPE, (**B**) LLDPE-MAH0.6, and (**C**) LLDPE-V0.6.

3.3.3. Thermogravimetric Analysis

Thermogravimetric experiments were conducted to gain insight into high-temperature stability of LLDPE, LLDPE-MAH, and LLDPE-V. The percentage mass loss and the mass loss rate curves are presented in Figure 3.4. Two parameters were calculated from these curves: (1) onset degradation temperature (T_o) and (2) 1st derivative peak temperature (T_p) . These parameters

denote the temperature at which the weight loss begins and indicate the point of greatest rate of change on the weight loss curve, respectively.

The results indicate that LLDPE has the lowest thermal stability with T_o of 371.2 °C and T_p of 430 °C. The MAH-grafts increased the thermal stability of LLDPE and T_o and T_p increased as the weight percentage of MAH was increased. These results are in agreement with the observations made by Huang et al [72]. The authors proposed that the degradation of PE-MAH in oxygen atmosphere is controlled by two competing factors: chain scission and cross-linking. During thermal decomposition the radical that is formed accelerates the chain scission which reduces the thermal stability. But simultaneously, the hydroxyl groups that are formed from the degradation can react with maleic anhydride groups to form a cross-linking structure which leads to an enhance thermal stability [72].

Moreover, the mass loss curves of the three vitrimers shifted to higher temperatures compared to their corresponding precursor, LLDPE-MAH. Consequently, the mass loss rate, shown in the inset graphs, was higher for these materials. Ultimately, LLDPE vitrimers show a better thermal stability and the ability to retard thermal decomposition due to the presence of cross-links and therefore an increase in the molecular weight. The material with the highest thermal stability was LLDPE-V1.2 with a T_o of 431.7 °C. This represents an increase of 60.5 °C compared to neat LLDPE.

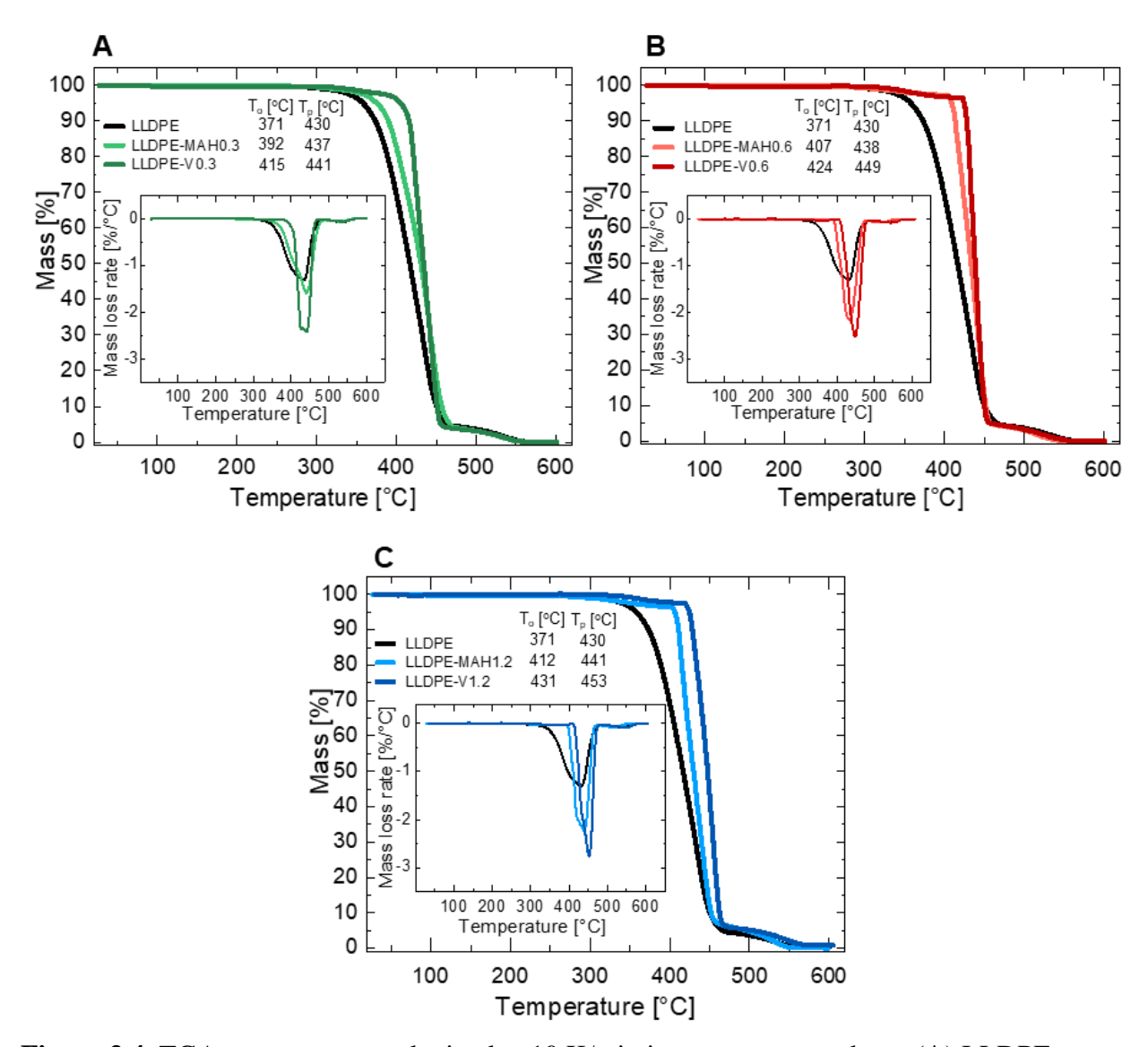


Figure 3.4. TGA measurements obtained at 10 K/min in oxygen atmosphere: (**A**) LLDPE, LLDPE-MAH0.3, LLDPE-V0.3, (**B**) LLDPE, LLDPE-MAH0.6, and LLDPE-V0.6, and (**C**) LLDPE, LLDPE-MAH1.2, LLDPE-V1.2.

3.3.4. Ultimate Tensile Properties

An assessment of ultimate tensile properties was conducted, and the results are summarized in Table 3.3. Three fundamental quantities were calculated: yield strength, stress at break, and displacement at break. It was observed that these three properties were all dependent on the MAH-grafting and cross-linking level. It was initially hypothesized that the presence of cross-links could

increase the strength of the material. Instead, it appears that the general trend is that the uniaxial tensile properties decreased for the vitrimers compared to their precursors, LLDPE-MAH and LLDPE. The yield strength and stress at break decreased as the MAH-grafting content increased and this was worsened for LLDPE vitrimers with higher cross-linking density. Furthermore, the displacement at break of the vitrimer was decreased, a feature that is characteristic of cross-linked materials. A summary of the DSC and TGA results previously discussed are also summarized in Table 3.3 for convenience to the reader.

Table 3.3. Summary of thermal and mechanical properties of LLDPE, LLDPE-MAH and LLDPE-V.

	DSC			TGA		Ultimate tensile testing			
Material	<i>T_m</i> [°C]	<i>T_c</i> [°C]	ΔH_m [J/g]	χ _c [%]	Τ _ο Τ _ο [°C] [°C	-	σ _y [MPa]	σ _b [MPa]	ΔL_b [mm]
LLDPE	123.6	110.4	128.5	43.9	371.2 432	2.7	14.9 ± 0.5	23.0 ± 0.5	184.9 ± 4.2
LLDPE-MAH0.3	123.0	109.6	127.5	43.5	392.5 437	7.1	14.6 ± 0.1	20.9 ± 0.6	187.0 ± 9.8
LLDPE-MAH0.6	122.6	108.9	123.1	42.0	407.8 436	5.5	14.3 ± 0.4	19.4 ± 0.4	169.7 ± 6.0
LLDPE-MAH1.2	122.0	108.0	119.0	40.6	412.3 441	1.4	13.5 ± 0.4	19.4 ± 0.8	152.9 ± 10.1
LLDPE-V0.3	124.6	107.9	117.4	40.1	415.1 441	1.7	14.3 ± 0.1	19.6 ± 1.3	135.8 ± 9.1
LLDPE-V0.6	124.9	106.7	109.7	37.4	424.3 449	9.0	13.3 ± 0.2	17.5 ± 0.8	98.9 ± 4.7
LLDPE-V1.2	124.3	100.2	100.7	34.4	431.7 453	3.8	11.5 ± 1.3	16.9 ± 0.8	87.1 ± 4.8

Representative stress-displacement curves from the materials are included in Figure 3.5 to show the deformation behavior. LLDPE-V materials display a reduced stress-strain curve (solid lines) compared to its precursors, LLDPE-MAH (dashed lines). The decrease in yield strength and stress at break can be explained by the decrease in crystallinity. The reduction of displacement at break

can be explained by the decrease in chain mobility due to the presence of cross-links. Strain hardening was evidenced in all the samples. Furthermore, the strain hardening modulus increased as the cross-linking density increased, which aligns with the observations made by Melick [73]. The strain hardening modulus is defined as the slope of the stress-strain curve after the yield point of the material. This parameter could not be quantified because strain values were not recorded. As mentioned earlier, the small geometry of the specimen limited the placement of an extensometer and only the crosshead displacement was recorded.

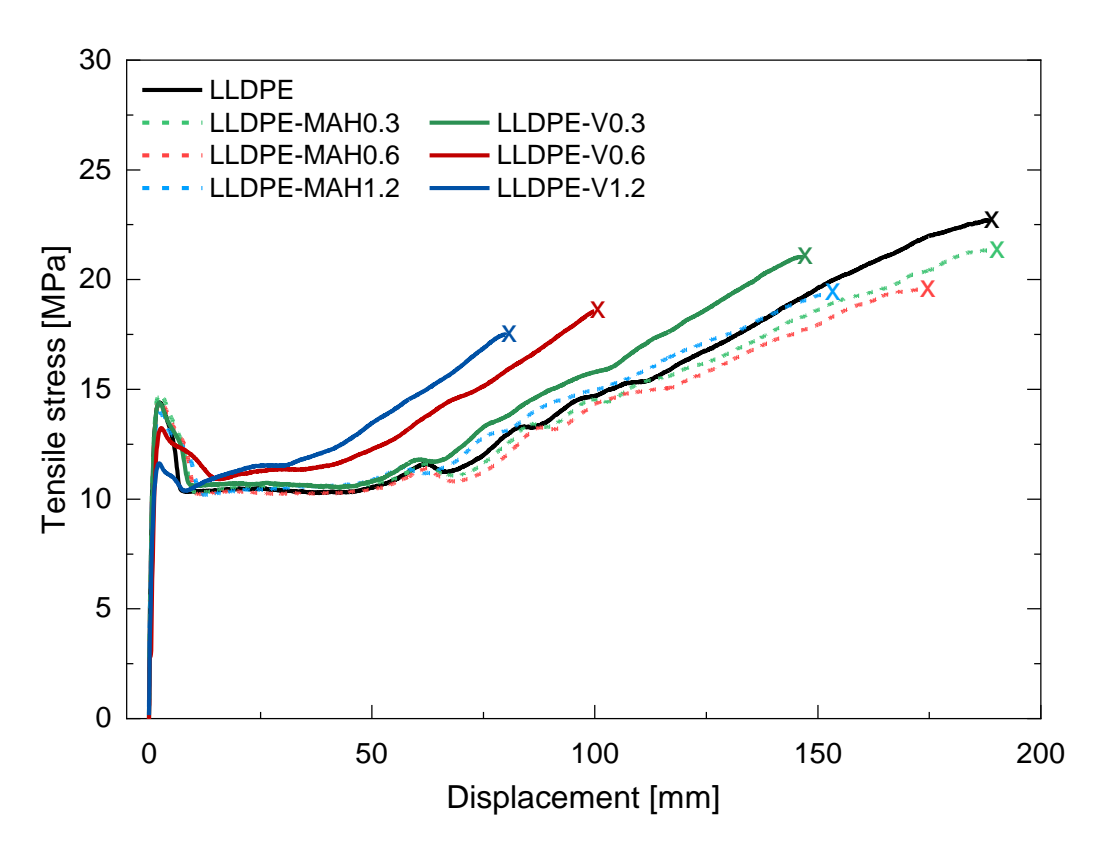


Figure 3.5. Representative stress-displacement curves of LLDPE, LLDPE-MAH, and LLDPE-V with varying grafting and cross-linking level (23 °C, 50 mm/min).

In our previous work, it was demonstrated that PE vitrimer could be reprocessed in an internal batch mixer [51]. It this study, the impact of multiple reprocessing cycles in the mechanical

properties was quantified. Figure 3.6A depicts the three steps taken: (1) an internal batch mixer was used to prepare the vitrimer, (2) tensile test specimens were compression molded and tested, and (3) the material was grinded and remelted in the internal batch mixer. This process was repeated three times. The yield strength marginally declines after the second reprocessing cycle. However, this property remained constant after the third reprocessing cycle as observed in Figure 3.6B. This demonstrates that the material retains its mechanical integrity after three processing cycles and therefore the recovery of the initial cross-link density showing the robustness of the dynamic cross-linker.

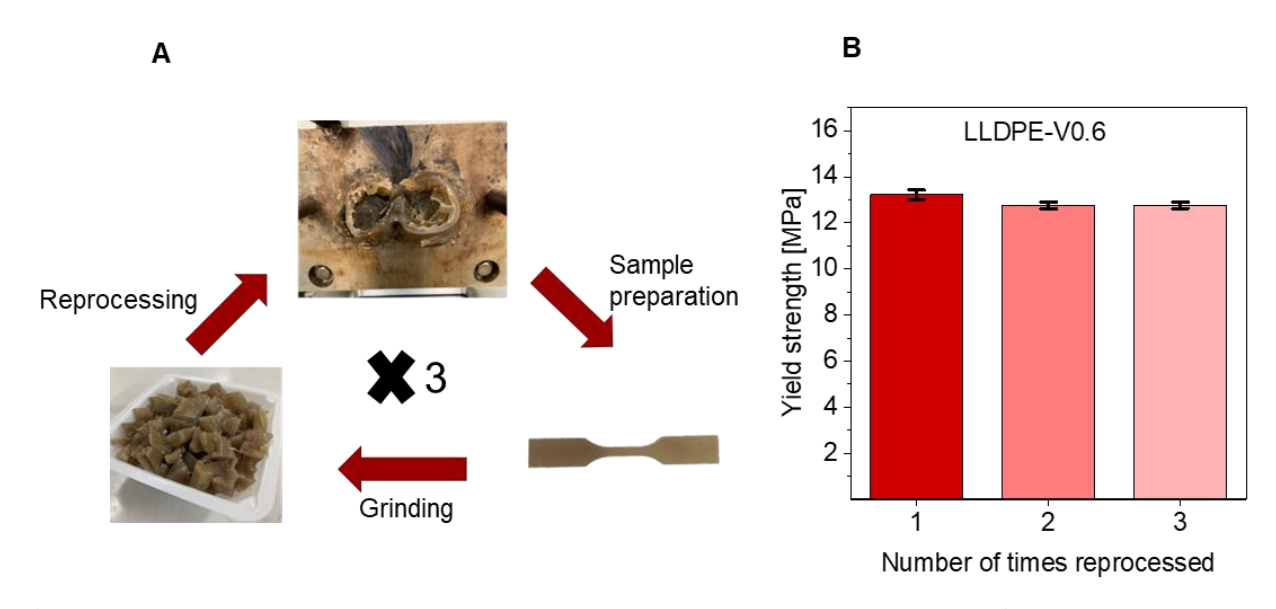


Figure 3.6. Reprocessing and mechanical characterization of LLDPE-V0.6: (**A**) Diagram showing the reprocessing cycle, and (**B**) yield strength after three processing cycles. Error bars are calculated from the standard deviation of 5 replicates.

3.3.5. Correlation Between Yield Strength and Crystallinity

A correlation between degree of crystallinity and yield strength of PE materials presented in this work was attained. To expand the range of degree of crystallinity, the mechanical and thermal properties of HDPE, HDPE-MAH and HDPE-V materials were also determined. For all the samples, the yield strength was plotted as a function of degree of crystallinity in Figure 3.7. It was noted that the yield strength of the material decreased as the MAH grafting and cross-linking density was increased. This behavior was directly proportional to the degree of crystallinity measured in the material. The MAH grafts and cross-linking disrupted the crystals formation and the crystallites size which are responsible for the decrease in yield strength in PE materials. Finally, it was found that the yield strength and degree of crystallinity follow a linear relationship with a slope of 0.35×. This model is beneficial to predict the yield strength of PE vitrimers based on degree of crystallinity values or vice-versa.

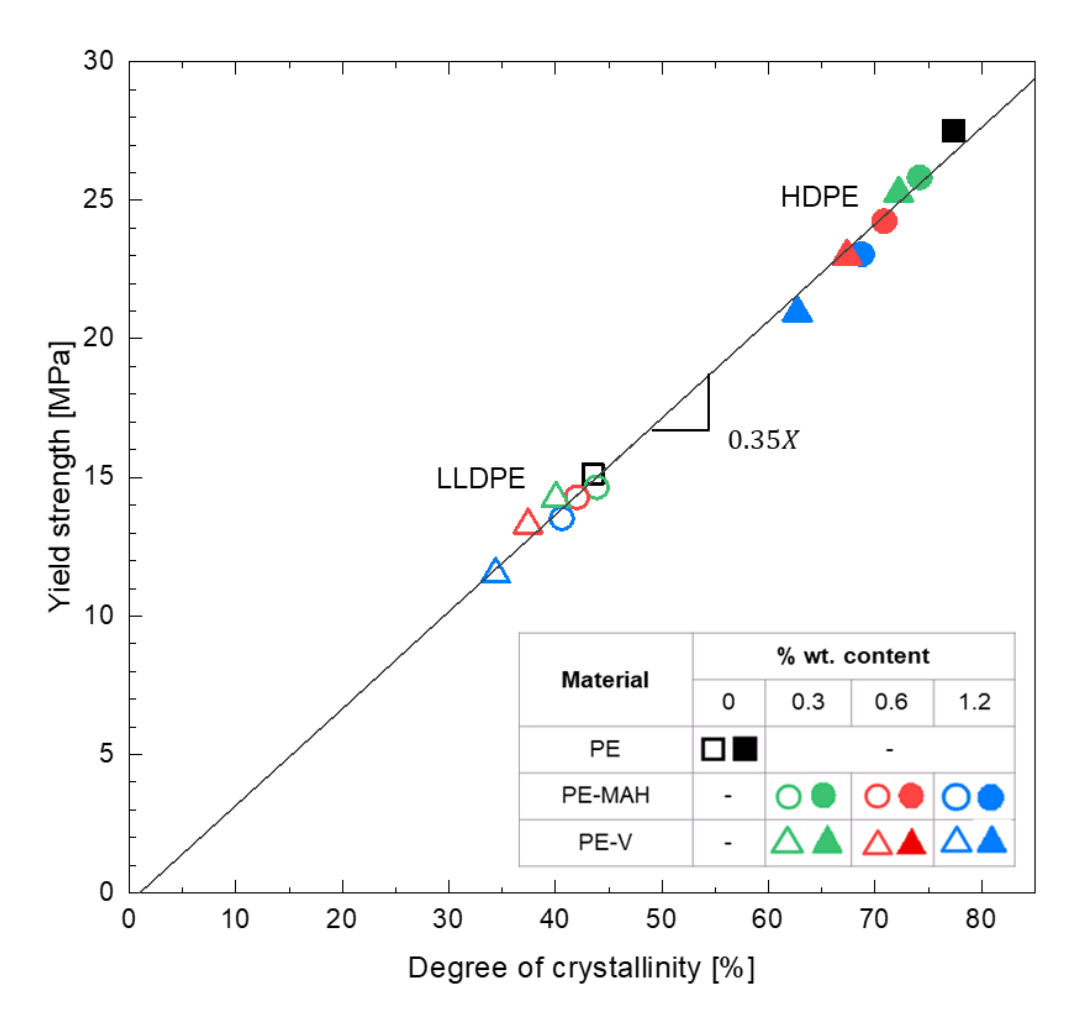


Figure 3.7. Relationship between yield strength and degree of crystallinity of LLDPE and HDPE systems.

3.3.6. Viscoelastic Properties

Dynamic mechanical analysis (DMA) was employed to determine the frequency dependent stiffness and damping behavior of PE vitrimers at room temperature. Figure 3.8 displays the results obtained for complex modulus and $\tan \delta$. The complex modulus (E^*) involves two components: the storage (E') and loss moduli (E''). The former refers to the stiffness of the materials while the latter describes the damping or viscoelastic behavior of the material. E^* is the sum of E' and E'' and E'' and E'' as shown in Equation 3.2 and Equation 3.3.

$$E^* = E' + iE'' (3.2)$$

$$\tan\delta = \frac{E''}{E'} \tag{3.3}$$

Where i is the imaginary unit.

In all materials, the complex modulus increases with increasing frequency while $tan\delta$ decreases with increasing frequency. This behavior is typical of polymers in the glassy regime [74]. It is also clear that the modulus decreases as the cross-linking density increases. As previously discussed, the cross-linking sites are hindering the crystallites formation, and this is translated into a decrease in the modulus. In this system, two competing mechanisms play a role in the mechanical properties: crystallinity and cross-linking. The decrease on the degree of crystallinity is more dominant compared to the effect that the cross-link sites have. However, the decrease in stiffness in LLDPE vitrimers, led to materials with higher $tan\delta$ values compared to LLDPE, which makes them a suitable candidate for damping applications at room temperature. For reference, typical $tan\delta$ values for PE materials at 1 Hz fall in the range of 0.05 - 0.12 at room temperature [75]. The

introduction of cross-links increased the $\tan\delta$ of LLDPE by 10% at low frequencies (0.5 – 1 Hz) and by 20% at high frequencies (50 – 100 Hz) as observed in LLDPE-V1.2 material.

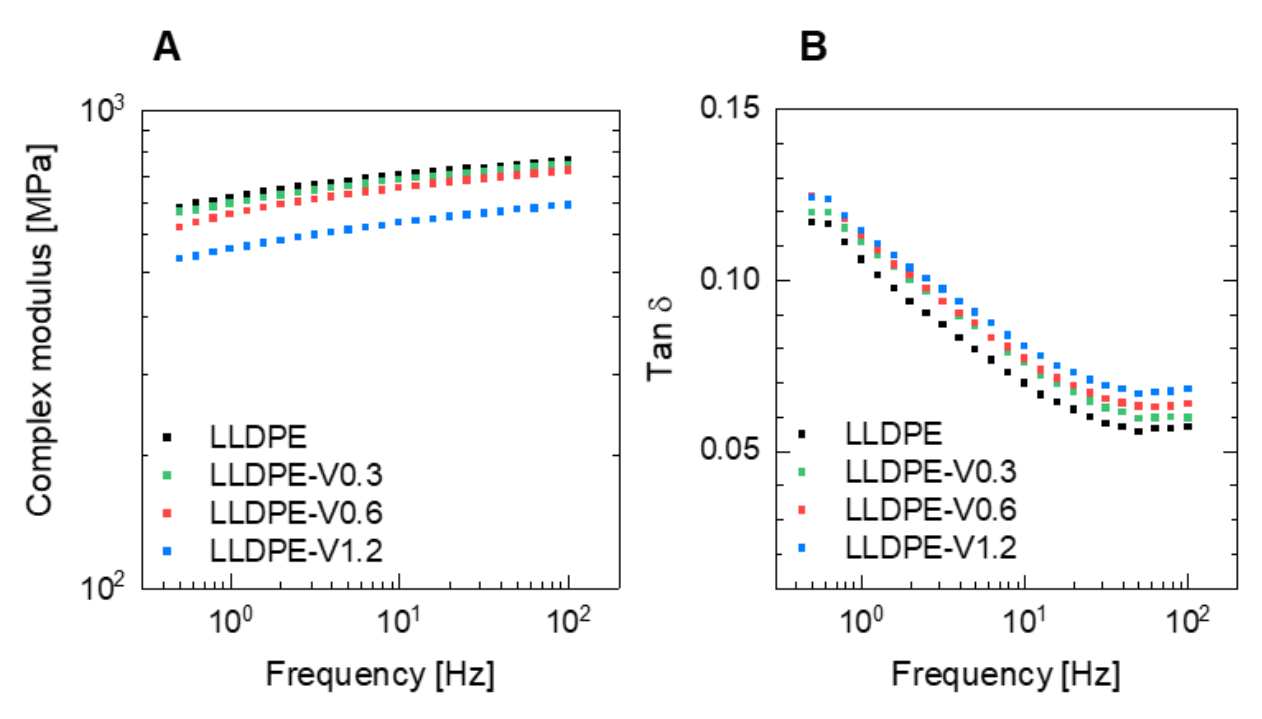


Figure 3.8. Viscoelastic properties as a function of frequency of LLDPE and LLDPE-V materials: (**A**) complex modulus and (**B**) $tan\delta$.

3.3.7. Creep

HDPE and HDPE-V0.6 were subjected to creep measurement to evaluate the time-dependent deformation. Figure 3.9A displays the strain percentage with respect to time in a linear scale. The creep compliance determined with Equation 3.1 is presented in a semi log scale in Figure 3.9B. HDPE-V0.6 had a higher initial deformation compared to HDPE and the rate of creep in the secondary regime (after 10⁴ seconds) was identical in both materials. This behavior can be related once again to the decrease in the crystallinity as demonstrated in Figure 3.10.

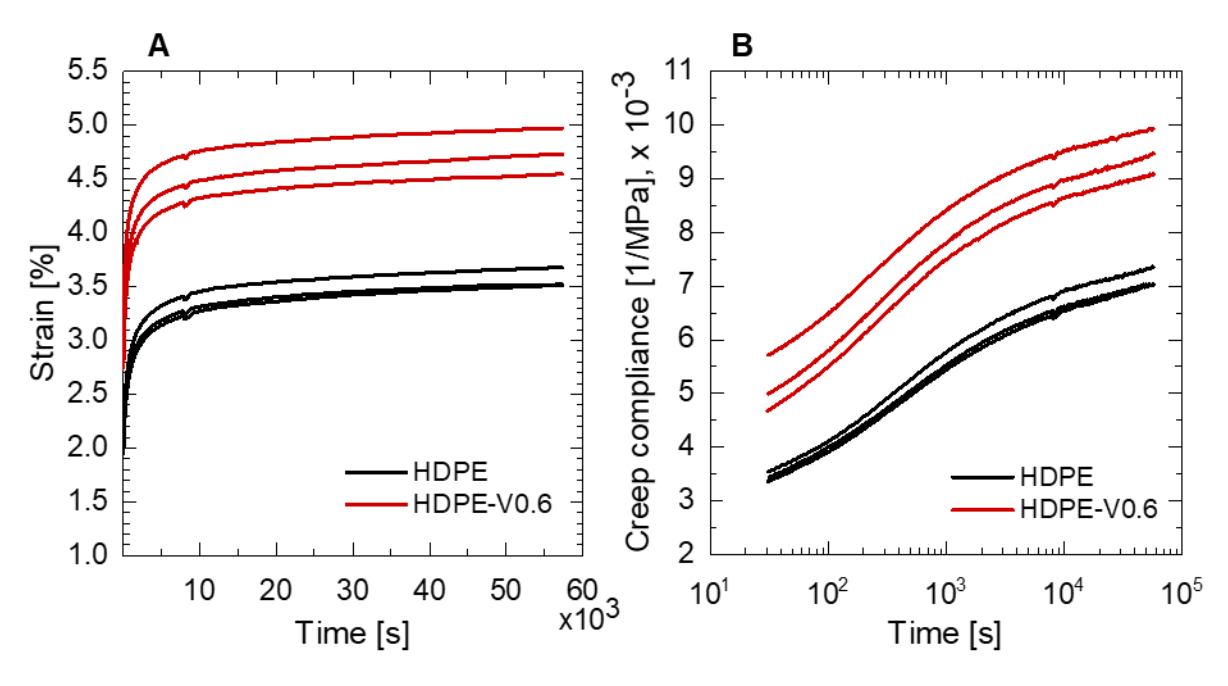


Figure 3.9. Creep experiments at 50 °C and 5 MPa of HDPE and HDPE-V0.6: (**A**) strain vs time in linear scale, and (**B**) creep compliance vs time in semi-log scale.

The creep results presented in Figure 3.9 contradict with other results reported in the literature for other PE vitrimers with different chemistries. For example, Rottger et al. reported an enhancement in the creep rate at 80 °C for HDPE vitrimers [32]. The authors also reported a decrease in the degree of crystallinity of their vitrimers with respect to the neat HDPE. The contradicting results could stem from the difference in sample preparation. Rottger et al. manufactured their creep specimens using injection molding technique while this study uses compression molding. Manufacturing techniques may influence the mechanical response of HDPE, such as creep performance. This can be attributed to different molecular morphologies through the thickness of the final product. During injection molding, the high shear stresses could have caused alignment of the molecular chains and these alignments can vary with molecular weight. For example, Maeda and co-workers demonstrated that polypropylene (PP) resins with higher molecular weight yield to a thicker characteristic skin layer structure compared to the one

obtained with a lower molecular weight PP [76]. Therefore, it is possible that the processing technique played a significant role in molecular orientation of HDPE vitrimers and in consequence in the long-term mechanical properties.

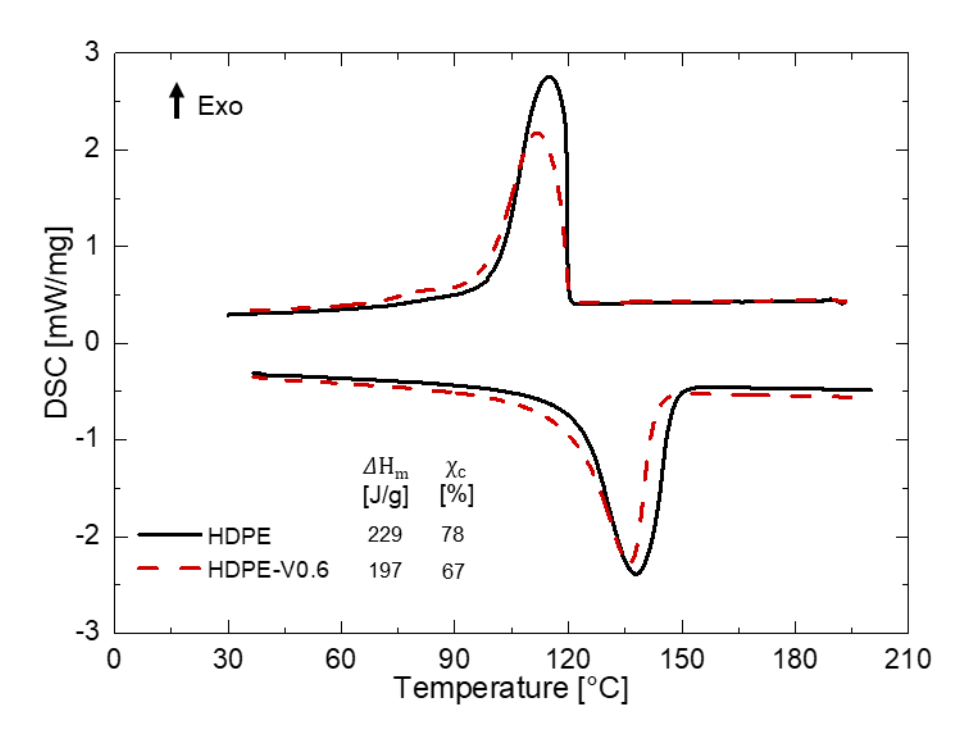


Figure 3.10. Comparison of degree of crystallinity of HDPE and HDPE-V0.6.

Ultimately, the dynamic cross-links in PE-V led to more flexible materials. The mechanical performance of PE-V is not suitable for application where an increase in stiffness of PE is required. However, the results presented in this work only represent the mechanical performance of PE manufactured via compression molding. The trends could possibly change if samples are manufactured using injection molding. This was outside the scope of the current project but should continue to be investigated.

3.4. Conclusions

Polyethylene vitrimers were obtained via reactive melt blending of PE-MAH and DTA. This process was conducted in a single step protocol allowing for a fast process without the need to use toxic solvents. It was determined that the presence of cross-links in PE vitrimers had a significant impact in the thermal and mechanical properties of the material. The yield strength of PE vitrimers decreases linearly in relation to the degree of crystallinity. PE vitrimers led to materials with higher $\tan\delta$ values compared to PE, which makes them a suitable candidate for damping applications. Furthermore, the stiffness and damping properties could be tuned by adjusting the cross-linking density. The degradation study revealed that PE vitrimers have higher thermal stability compared to PE which was observed from an increase in the onset degradation temperature. PE vitrimers could enable applications that require flexible and damping behavior and in polymer processes that could benefit from lower levels of crystallinity. The latter is particularly of interest in 3D printing of semicrystalline materials where shrinking and warpage is a challenge. Ultimately, it was proven that reprocessing of polyethylene vitrimer was possible without considerable impact in mechanical properties.

4. Material Extrusion Additive Manufacturing with Polyethylene Vitrimers

Polyethylene (PE) is one of the most widely used polymers in conventional polymer manufacturing processes. However, it remains a challenge to use PE in extrusion-based additive manufacturing (AM). Some of the challenges that this material presents include low self-adhesion and shrinkage during the printing process. These two issues lead to higher mechanical anisotropy when compared to other materials, along with poor dimensional accuracy and warpage. This chapter presents an approach to overcome these issues by utilizing two key properties of polyethylene vitrimer (PE-V) found in the previous chapter. Chapter 3 suggested that the dynamic cross-links in PE-V increased the dimensional stability at elevated temperature and reduced the degree of crystallinity. The former enabled a thermal treatment that promotes interlayer chain diffusion which improves mechanical anisotropy, while the latter reduced shrinkage of 3D printed parts. This chapter is based on the research "Material Extrusion Additive Manufacturing with Polyethylene Vitrimers" published in *Polymers*, Volume 15, Issue 6 (2023) [77].

4.1. Introduction

Additive manufacturing (AM) is an advanced manufacturing technique that allows the fabrication of customized 3D objects with high geometric complexity that cannot be achieved with other processing techniques. The process consists of building the part in a layer-by-layer manner [78]. For several decades, AM has mainly been used for aesthetic and functional prototyping due to its cost-effectiveness and rapid prototyping. However, as innovative materials and AM methods are being developed, new applications are emerging in the field [79]–[81]. In general, these

applications are shifting from prototypes to functional products [82], [83]. Material extrusion (ME) is the most widely used AM technique, due to its low cost of fabrication and the availability of low-cost printers [80]. Material extrusion additive manufacturing (ME-AM) uses a relatively small number of working parts in the printing hardware, making it more user-friendly, and generally uses thermoplastics, which can reduce cost and allow for more freedom in material selection [81]. In ME-AM, the polymer is heated above the melting temperature for semicrystalline materials (and above the glass transition temperature for amorphous materials) and is dispensed through a nozzle. Once the polymer exits the nozzle, the viscosity sharply increases as it cools down to form a permanently bonded structure and retain the desired shape [80], [84].

One significant limitation encountered by structures fabricated via ME-AM for functional applications is the decreased mechanical properties caused by anisotropy [85], [86]. This is due to the weak bonds formed between layers during the printing process. Several studies have focused on improving the mechanical properties of printed parts via ME. Efforts have been made to understand the weld formation in ME-AM from the perspective of polymer interdiffusion [87]. Other works focusing on reducing the anisotropic properties of the 3D-printed parts include infrared preheating in polyphenylene sulfide parts [88], crosslink formation between layers in polylactic acid (PLA) parts [89], implementing thermoplastic supramolecular interactions in polyethylene terephthalate/phenylacetylene [90], and introducing Diels-Alder reactions based on furan-maleimide [91]. Low dimensional accuracy is another challenge in ME-AM and is related to warping, shrinkage, and delamination during the printing process [92]-[96]. These issues are exacerbated when 3D printing with semicrystalline materials. Common approaches to improve dimensional accuracy in ME-AM include increasing bed adhesion, reducing the degree of crystallinity, and optimizing the processing parameters [97].

Introducing novel materials in the ME-AM process, such as vitrimers, is a promising approach to tackle these challenges [98]. Vitrimers are a new class of covalent adaptable network (CAN) materials introduced by Leibler and co-workers in 2011 [19]. They consist of chemically crosslinked networks that engage in thermoactivated associative exchange reactions. During the exchange reactions, the network can change its topology while maintaining a constant degree of crosslinking [32]. Due to this constant degree of crosslinking, the structural integrity of the part is minimally affected when heat is applied. Furthermore, the dynamic crosslinking can provide shape memory, malleability, adhesion, and healing, unlike permanently crosslinked networks such as thermosets [24], [32], [52].

Vitrimers prepared from commercial or recycled thermoplastics can be utilized in ME-AM [99]. An excellent candidate thermoplastic to be transformed into a vitrimer is polyethylene (PE). PE is commonly used in a wide range of industrial and consumer applications due to its affordability, ease of processability, and high chemical resistance [2]. Nevertheless, PE has exhibited significant challenges in ME-AM processes; therefore, filaments for 3D printing are not widely available [96]. Due to its semicrystalline nature, PE tends to shrink during the filament manufacturing process, leading to low diametric consistency [100]. Additionally, PE has low adhesion to traditional metal and glass beds and tends to warp [101].

This study explores the printability of high-density polyethylene vitrimer (HDPE-V) using ME-AM as an approach to reduce mechanical anisotropy and improve dimensional accuracy. HDPE and HDPE-V pellets were used as the feedstock instead of a filament, due to the challenges that filament production of HDPE presents [100], [102]. The crosslinking reaction that produced the HDPE-V presented in this study was obtained from the reaction between maleic -anhydride-grafted high-density polyethylene (HDPE-MAH) and a diamine crosslinker—4,4'-dithiodianiline

(DTA). The concentration of MAH was 0.3 wt.%, and a molar ratio of 1:0.5 (MAH:DTA) was used. The reaction was conducted via a single-step process in a screw-assisted 3D printer at 220 °C. Pellet-fed screw-assisted 3D printers are increasingly being used to bypass the need for filaments, reducing the associated cost of filament production, while also increasing the deposition rate and expanding the range of 3D-printing materials [103]. For example, modified 3D printers have enabled the use of recycled polymer flakes from polyethylene terephthalate (PET) water bottles [104], polymer composites that are too brittle to be spooled into filaments [105], and recycled selective laser sintering (SLS) powder [106].

In a previous study, it was shown that vitrimers prepared from HDPE (HDPE-V) significantly affect the properties of the material in the melt and solid states [60]. In the melt state, the crosslinks in HDPE-V were responsible for its superior dimensional stability at elevated temperatures, due to the presence of a rubbery plateau compared to un-crosslinked HDPE. In the solid state, it was observed that the crosslinks hindered the crystallization of the material. The objective of this study was to apply these findings to demonstrate that HDPE-V is a promising material for ME-AM. This research shows that shrinkage and mechanical anisotropy were decreased when using HDPE-V in an ME-AM process compared to HDPE. The reduced degree of crystallinity in HDPE-V played a role in the reduced shrinkage of the parts. An improvement in mechanical anisotropy was observed in HDPE-V, and this was achieved via a thermal post-processing step. The annealing step was only possible because of the enhanced dimensional stability of HDPE-V at elevated temperatures.

4.2. Materials and Methods

4.2.1. Materials

High-density polyethylene (HDPE) F04660 (MFI = 0.7 g/10 min at 190 °C with 2.16 kg) and maleic-anhydride-grafted high-density polyethylene (HDPE-MAH) were supplied by SABIC. The grafting process of MAH is proprietary information. The MAH concentration used in this study was 0.3 wt.% The crosslinker used to produce the HDPE vitrimer (HDPE-V)—4,4′-dithiodianiline (DTA)—was purchased from Tokyo Chemical Industry. A summary of the relevant material properties provided by the suppliers is given in Table 4.1.

Table 4.1. Characteristic properties of the materials used in this study.

Material	Melting Temperature [°C]	Density [g/cm ³]	Molecular Weight [g/mol]
HDPE F04660	134	0.961	-
DTA	77	-	248.37

HDPE-V was obtained from the reaction of HDPE-MAH and the diamine crosslinker containing disulfide bonds—4,4′ dithiodianiline (DTA)—as described in a previous work [60]. The concentration of MAH was 0.3 wt.%, and a molar ratio of 1:0.5 (MAH:DTA) was used. The HDPE-V feedstock for the 3D printer was prepared by dissolving the crosslinker powder (DTA) in acetone, and HDPE-MAH pellets were coated in this solution at room temperature. The solution was constantly stirred for 24 h to ensure evenly coated pellets. After this period, the acetone evaporated, and the pellets were fully dried. This dry blend was then introduced to the (pellet-fed) screw-assisted 3D printer, where the reaction took place in the melt state to form HDPE-V. This procedure is summarized in Figure 4.1.

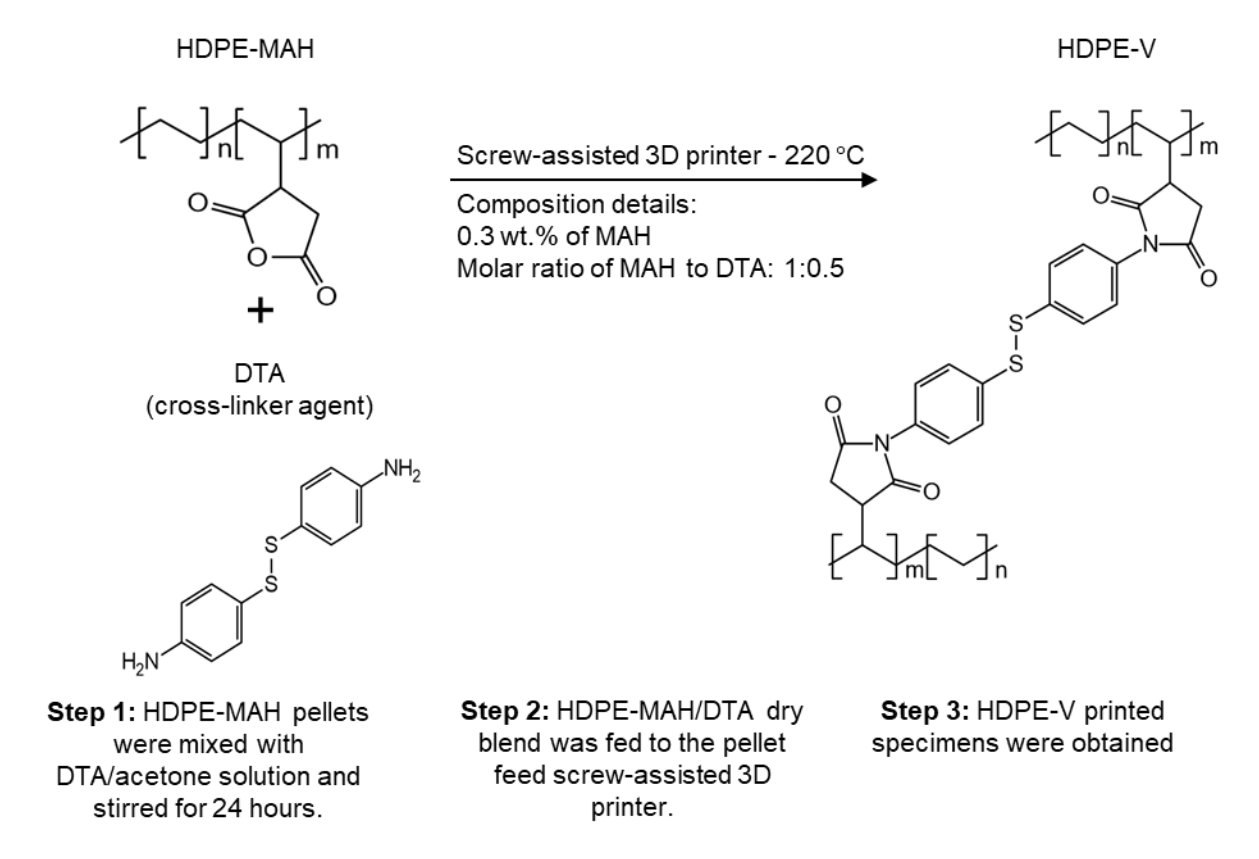


Figure 4.1. Graphical representation of the protocol used to produce HDPE-V using ME-AM.

4.2.2. Material Extrusion Additive Manufacturing and Geometric Design

A screw-assisted 3D printer was used to produce all test specimens. The machine used in this study was a Cosine AM1 with a pellet-fed extruder attachment. This configuration allows the extrusion of materials without the need to manufacture filaments as the feedstock. The pellets were fed through a hopper and then transported and melted through the heated single screw. The material was pushed through the nozzle and deposited layer-by-layer on a polypropylene (PP) substrate, as depicted in Figure 4.2A. PP was used as a substrate, as it has been proven to improve bed adhesion and, therefore, reduce delamination [102].

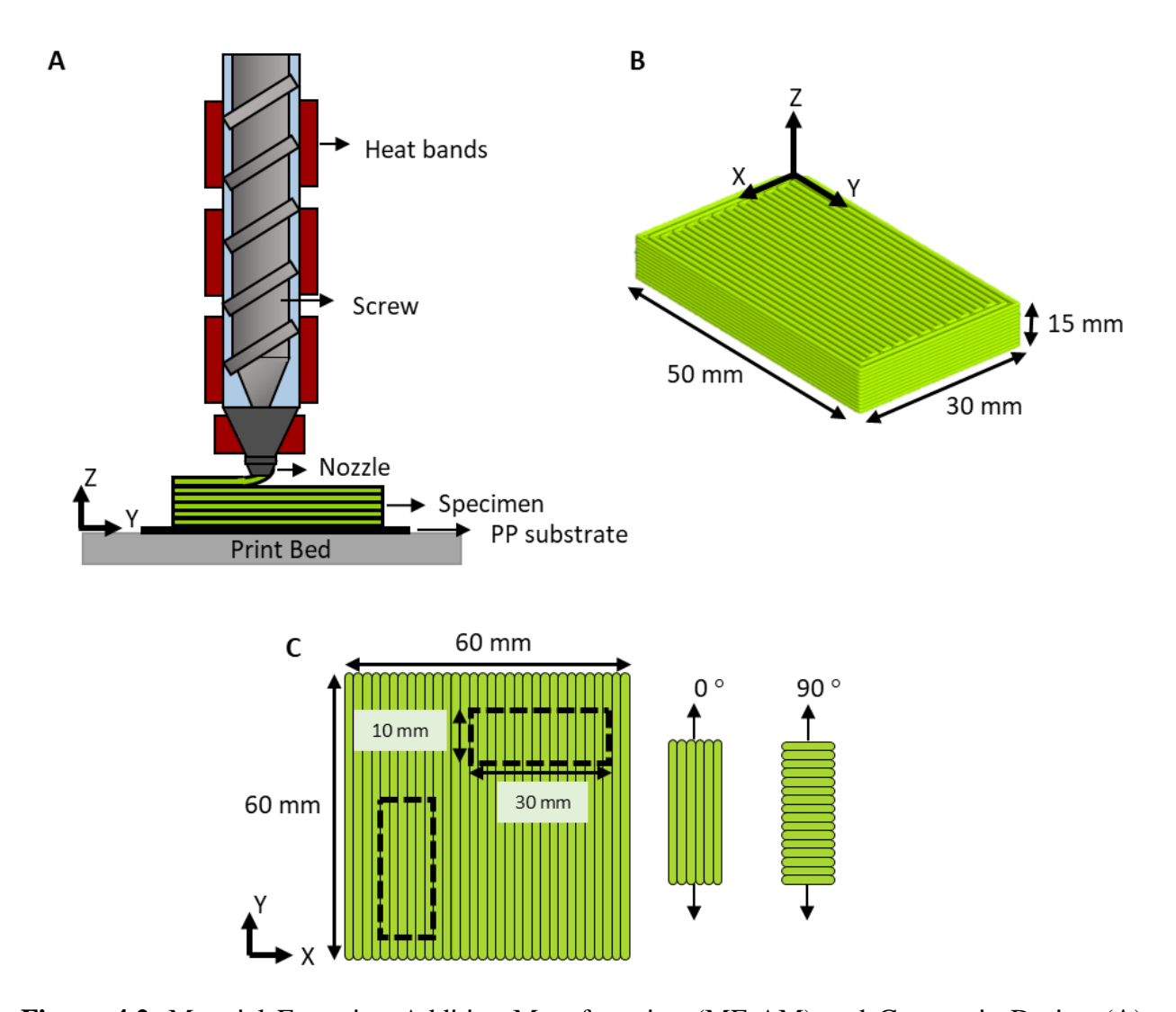


Figure 4.2. Material Extrusion Additive Manufacturing (ME-AM) and Geometric Design (**A**) Schematic of screw-assisted ME-AM; (**B**) sample geometry used for microstructure characterization; (**C**) specimens used for viscoelastic characterization (H: 3 mm).

Rectangular specimens used for examining the microstructure were produced with dimensions of H: 15 mm × W: 30 mm × L: 50 mm, as shown in Figure 4.2B. Square plates (H: 3 mm × W: 60 mm × L: 60 mm) were also produced to evaluate shrinkage, thermal, rheological, and viscoelastic properties. Smaller rectangular specimens (10 mm × 30 mm) were punched from the square plates, as depicted in Figure 4.2C, to evaluate the viscoelastic behavior of the parts with varying bead orientation.

The specimens shown in Figure 4.2B and Figure 4.2C were generated through computer-aided design using SOLIDWORKS 2021 and were translated into G-Code using Simplify 3D software (Version 4.1.2).

4.2.3. Shrinkage Evaluation

Shrinkage perpendicular to bead orientation and parallel to bead orientation was measured by comparing the original dimensions in the X-Y plane of the specimens shown in Figure 4.2C (60 mm \times 60 mm) to the final dimensions of the printed specimens. The final dimensions were measured after 48 h of printing. Equation (4.1) refers to the shrinkage perpendicular to bead orientation (S_w), while Equation (4.2) refers to the shrinkage parallel to bead orientation (S_l) [107].

$$S_w = \frac{W_o - W_m}{W_o} \times 100 \tag{4.1}$$

$$S_l = \frac{L_o - L_m}{L_o} \times 100 \tag{4.2}$$

Where,

 W_o = original dimensions (from CAD) perpendicular to bead orientation;

 W_m = measured dimensions perpendicular to bead orientation;

 L_o = original dimensions (from CAD) parallel to bead orientation;

 L_m = measured dimensions parallel to bead orientation.

4.2.4. Characterization

Differential scanning calorimetry (DSC) experiments were performed with a NETZSCH 214 Polyma DSC. Two heating cycles were conducted in the range of 30–200 °C at a heating rate of 10 °C/min in a nitrogen atmosphere. The melting and crystallization properties were determined from the second heating and cooling cycle. The degree of crystallinity (χ_c) was calculated from

the ratio of the measured melting enthalpy (ΔH_m) and the theoretical melting enthalpy of 100% crystalline polyethylene (293 J/g) [54].

Rheological tests were conducted using a TA Instruments AR 2000 ex rheometer. A 25 mm parallel steel plate fixture was used with a 1.85 mm gap. Frequency sweeps were performed over a range of 0.01 to 100 rad/s at 220 °C and 0.1% strain.

Dynamic mechanical analysis (DMA) measurements were conducted in a NETZSCH Explexor 500 N DMA. Frequency sweeps were performed at room temperature in tension within the linear viscoelastic regime, using a dynamic strain of 0.03% and a frequency range of 0.5–100 Hz.

Scanning electron microscopy (SEM) was used to identify voids in the 3D-printed specimens. The 3D-printed samples were examined using a Hitachi S3400 Variable-Pressure Scanning Electron Microscope at 15 kV and 30 Pa.

4.2.5. Annealing Procedure

A post-processing treatment was conducted with the purpose of reducing mechanical anisotropy by improving chain diffusion between layers. The 3D-printed specimens used in DMA testing were heat-treated for 10 minutes at 150 °C in an oven under normal atmospheric conditions. A prototype was printed and annealed to visually demonstrate the dimensional stability of the parts during the heat treatment process.

4.3. Results

4.3.1. Assessment of Processability in Screw-Assisted AM

Differential scanning calorimetry was utilized to determine the melting temperature, crystallization temperature, and heat of fusion of the materials to be printed. The results from the second heating and cooling cycle are shown in Figure 4.3. The melting temperature of HDPE and

HDPE-V was 138.0 °C and 136.8 °C, respectively. The crystallization temperature of HDPE and HDPE-V was 114.7 °C and 112.5 °C, respectively. Since the difference in both transition temperatures was small (<2.2 °C), the temperature profile of the printing process was chosen to be the same for both materials, as summarized in Table 4.2. The heat of fusion of HDPE-V was decreased by 16.1 J/g compared to HDPE. The heat of fusion was used to determine the degree of crystallinity of the samples: 77.9% (HDPE) and 72.4% (HDPE-V). Lower crystallinity can be beneficial for 3D-printing processes, as it can reduce the shrinkage of samples and improve their dimensional accuracy [95], [101].

Table 4.2. Printing parameters of HDPE and HDPE-V.

Parameters	Value		
Nozzle diameter	1 mm		
Extruder temperature	220 °C		
Nozzle temperature	220 °C		
Bed temperature	60 °C		
Printing speed	500 mm/min		
Extrusion multiplier	1.2		
Layer height	0.6 mm		
Infill percentage	100%		
First layer setting	Height 50%; speed 60%		
Brim	5 layers		
Substrate	PP sheet		

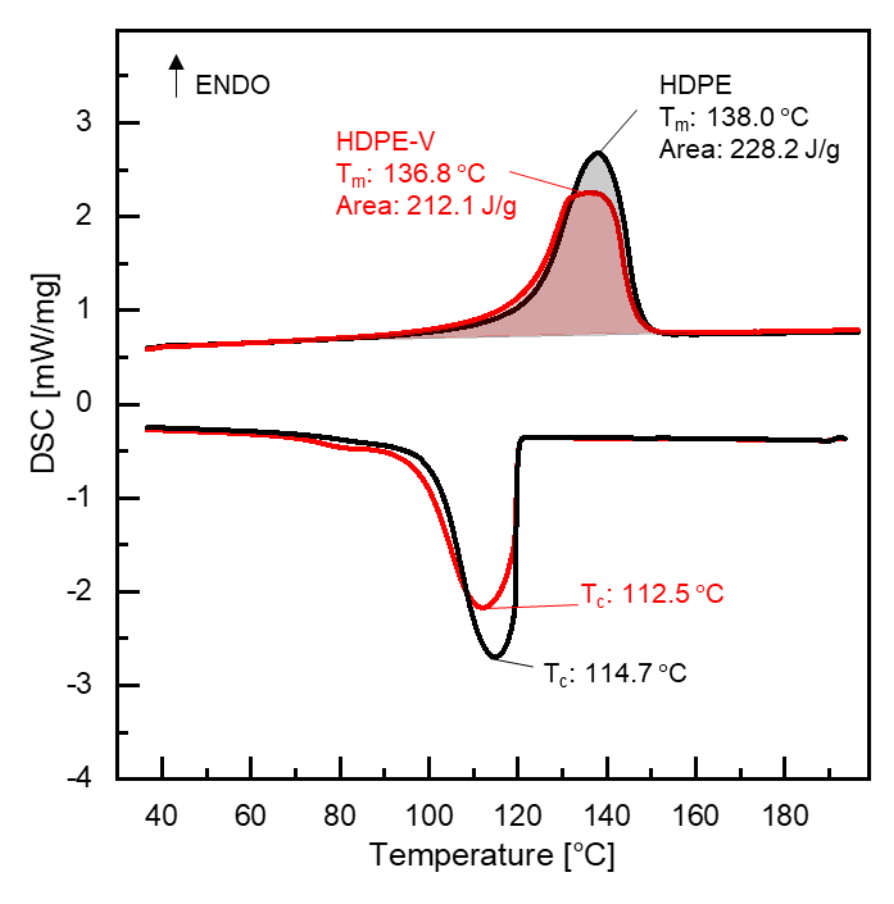


Figure 4.3. DSC heating and cooling curves (10 K/min in nitrogen).

The rheological behavior of HPDE and HDPE-V was studied to assess the processability of the materials and tune the parameters in the screw-assisted 3D printer. The measurements were conducted in a parallel-plate rheometer within the linear viscoelastic regime at 220 °C. This temperature was chosen because it is well above the melting temperature of both materials and falls within the range of typical temperatures used for 3D printing of PE [96]. HDPE-V shows higher complex viscosity $|\eta^*|$ at low frequency (0.01–10 rad/s) compared to HDPE (Figure 4.4). The high viscosity seen at the lower end of the frequency range tested was due to the presence of the characteristic crosslinked network of the vitrimer. However, in the range of 10–100 rad/s, the complex viscosity values of HDPE and HDPE-V are very comparable. Since the typical shear rate

experienced in screw-assisted 3D printing is usually higher than 10 s⁻¹, it can be concluded that both materials in this study can be processed at the same temperature [84], [91].

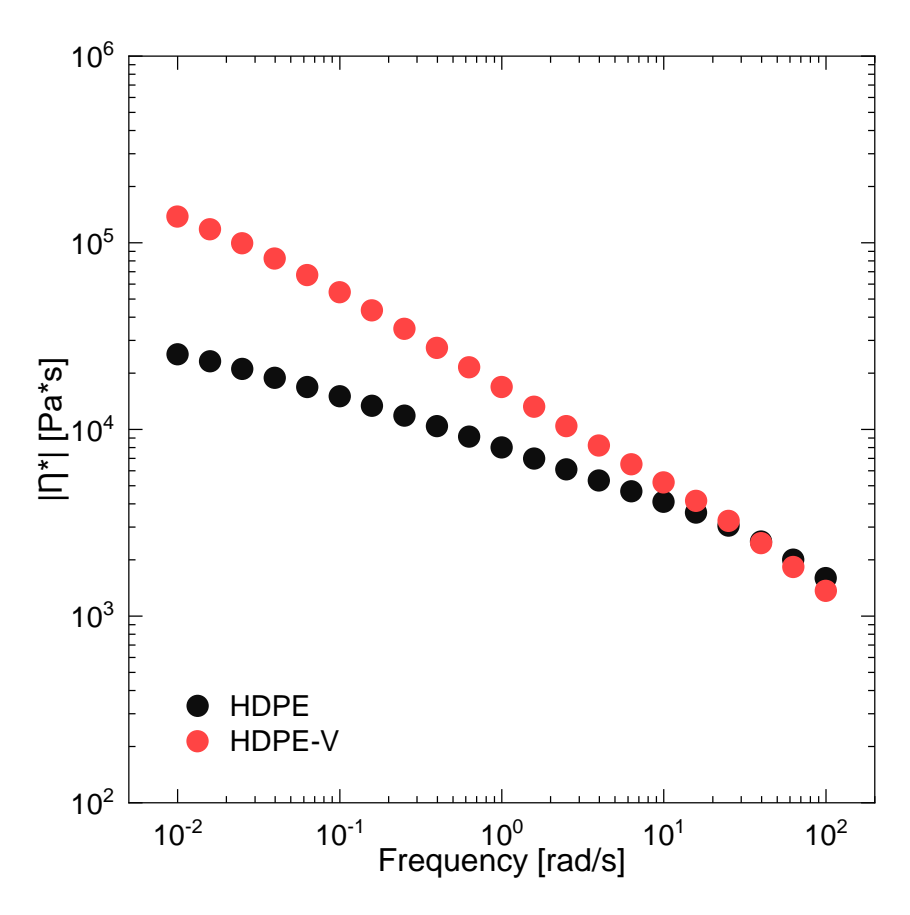


Figure 4.4. Complex viscosity, $|\eta^*|$, as a function of frequency of HDPE and HDPE-V (220 °C).

Figure 4 also reveals the shear-thinning behavior of both polymers. The extent of shear thinning was estimated by fitting the data in Figure 4.4 to the power-law model (Equation (4.3)), where K is the consistency index and n is the power-law index. Low values of n indicate a stronger shear-thinning behavior. The calculated values of n of HDPE and HDPE-V were 0.59 and 0.41, respectively. Therefore, the vitrimer has a higher shear-thinning dependency, which is usually desirable in extrusion-based 3D-printing processes. Higher shear thinning is usually desired for two reasons: (1) the polymer extruded through the nozzle (high shear rate) should have high

flowability, which translates into low viscosity values; and (2) during the deposition step (low shear rate), the polymer should have high viscosity to hold its shape under gravity and under the layers on top [84], [108].

$$\eta = K \times \dot{\gamma}^{n-1} \tag{4.3}$$

4.3.2. Printing Challenges

Adhesion was the first challenge encountered when printing with HDPE and HDPE-V. At room temperature, neither of the materials adhered to the aluminum bed substrate of the AM1 Cosine. Previous studies have shown that adhesion between PE parts and the bed can be improved by (1) increasing the build temperature to prevent solidification of the first layer, or (2) by selecting an appropriate build material [94]. Some examples of build materials include polypropylene (PP) [102], ultra-high molecular weight polyethylene (UHMWPE) [109], or styrene-ethylene-butylenestyrene (SEBS) sheets [101]. As a first attempt to improve bed adhesion, the build temperature was set to 125 °C. This would ensure that the material was above the crystallization temperature, which could mitigate the shrinkage and warpage that takes place when the material cools down. Additionally, this would delay the crystallization, which could improve the polymer chain diffusion between the beads, leading to lower mechanical anisotropy in the printed parts [110]. It was decided to implement this method first due to the potential benefits this could bring to the final parts' properties. However, a high print bed temperature created a melt pool in the first two layers of the printed material due to its low viscosity. Since print quality was an issue, another approach to improve bed adhesion was utilized. The temperature of the bed was decreased to 60 °C, and a PP substrate was used. A 1/16 inch PP sheet and a Magigoo PP adhesive led to a significant increase in bed adhesion.

Additionally, a brim was added to the parts to further increase their adhesion. Incorporating a brim around the part increases the interface of the print object with the substrate. This can lower the debonding stresses and, consequently, decrease warpage. Previous studies successfully reduced warpage when using a brim with five lines [96], [111]. Additionally, Bachhar et al. showed that a 5–15-line brim did not change the warpage significantly [111]. A five-line brim was sufficient to prevent delamination of the specimens presented in this study. A comparison of the printed parts without brims is shown in Figure 4.5A, while those with brims are shown in Figure 4.5B.

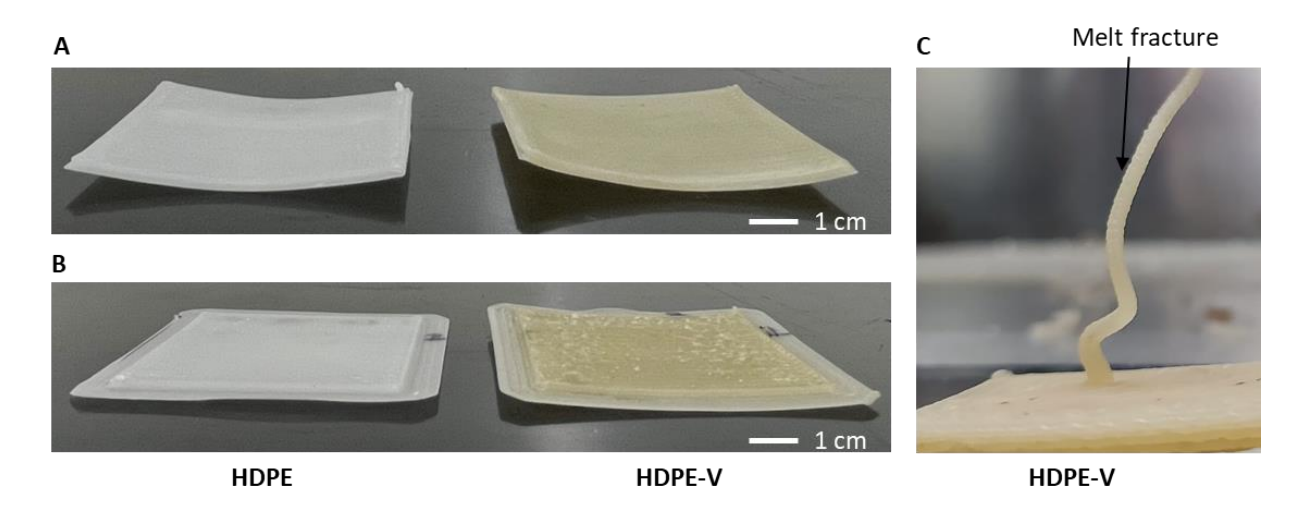


Figure 4.5. Square plates (60 mm \times 60 mm \times 3 mm) produced (**A**) without brims and (**B**) with brims. (**C**) Melt fracture observed in HDPE-V.

The second challenge observed when printing with HDPE-V was melt distortion, more commonly known as melt fracture. This can be seen as a rough surface finish in Figure 4.5C. Melt fracture is a type of flow instability that is common in extrusion operations. At low shear rates, a stable, smooth stream at the exit of the die is usually observed in polymer extrusion operations. However, at higher shear rates, the extrudate can become distorted, and this depends on the type

of polymer being extruded. Furthermore, there is an agreement that melt elasticity, which is measurable by the storage modulus (G'), plays a major role in the initiation of this type of flow instability [112], [113]. The higher G' values of HDPE-V compared to HDPE explain why melt fracture is initiated in the former material (solid lines in Figure 4.6). The melt elasticity in HDPE-V is a consequence of the crosslinked network.

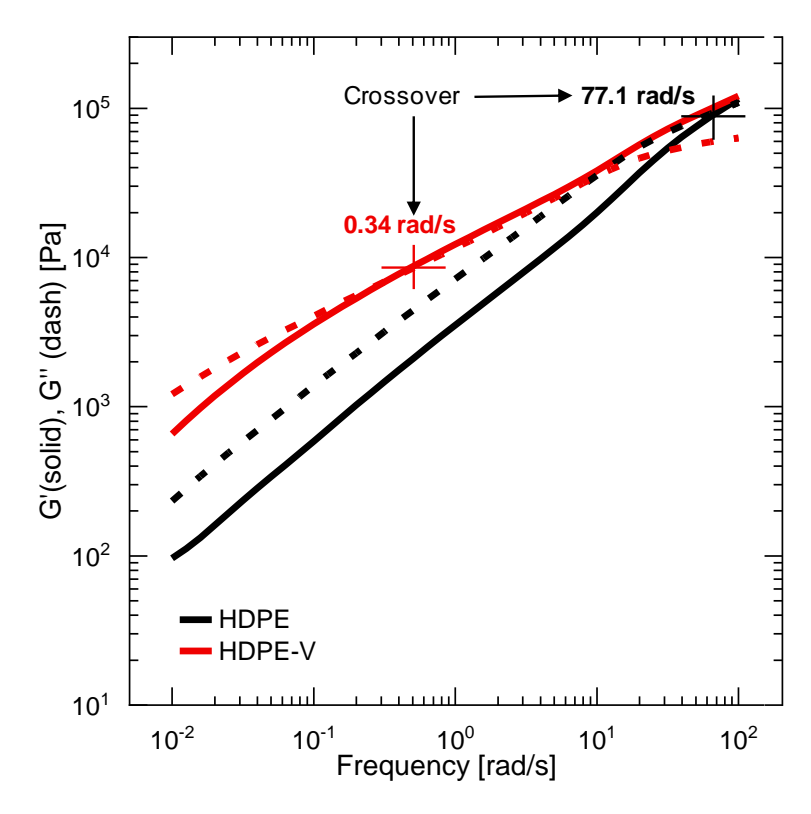


Figure 4.6. Dynamic moduli as a function of frequency for HDPE (black lines) and HDPE-V (red lines) at 220 °C. Storage modulus (G') is represented by the solid lines and viscous modulus (G'') is represented by the dashed lines.

It was important to reduce or eliminate melt fracture to avoid introducing voids between the layers. Melt fracture, usually shown as surface distortions, occurs when the polymer melt exits the die at throughput rates above a critical value. Therefore, the extrusion speed was reduced from 800 mm/min to 500 mm/min, and the multiplier was set to 1×. By decreasing the extrusion speed, the

screw rotational speed (rpm)—and, therefore, the throughput rate—was also decreased. Demonstration parts are shown in Figure 4.7A and Figure 4.7B, where an improvement in the surface finish can be seen. However, reducing the throughput led to under–extrusion, as can be observed from the gaps shown in Figure 4.7B with the red arrows. The multiplier was increased to 1.2×, which resolved this issue (Figure 4.7C). It is important to note that reducing the print speed could lead to two advantages relevant to this work: (1) it can reduce melt fracture, and (2) it can increase the weld time between beads, which can promote interlayer adhesion [87].

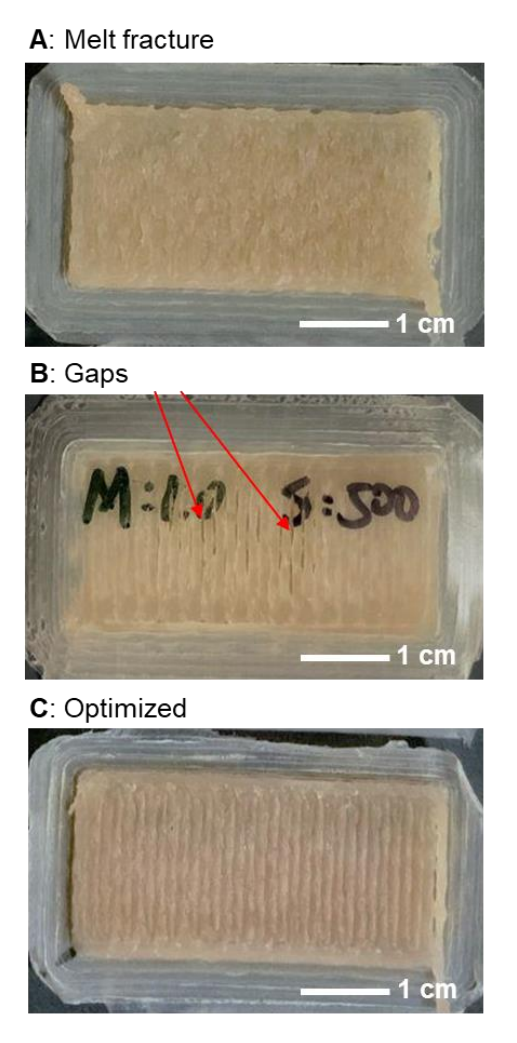


Figure 4.7. Print speed and multiplier optimization for HDPE-V to reduce melt fracture. (**A**) Speed: 800 mm/min; multiplier: 1×. (**B**) Speed: 500 mm/min; multiplier: 1×. (**C**) Speed: 500 mm/min; multiplier: 1.2×.

Since ME-AM printing parameters can affect the final parts' properties, it was essential that all 3D-printed specimens were manufactured under the same printing conditions. As previously discussed, the only parameter that required modification was the print speed. When a print speed of 800 mm/min was used, HDPE did not show any flow distortion, and the surface of the bead was smooth. However, HDPE-V exhibited flow distortions at this print speed. HDPE-V is susceptible to melt fracture due to its crosslinked network and melt elasticity [112], [113]. For this reason, the print speed was decreased until no distortion was observed. The final print speed used for all of the specimens was 500 mm/min. Finally, the optimized printing parameters used for both materials (HDPE and HDPE-V) are summarized in Table 4.2.

4.3.3. Shrinkage

During cooling, polymers experience a decrease in free volume between their macromolecular chains, which leads to shrinkage. The extent of shrinkage is greater in semicrystalline polymers such as PE due to their ability to crystallize [114]. Shrinkage can have a significant impact on the dimensional accuracy and the appearance of the final product. Any 3D-printed parts that shrink in an anisotropic manner could lead to potential issues during and after the printing process. Parts with different amounts of shrinkage in the flow and transverse flow directions can lead to part distortion. The undesirable deformation, usually referred to as warpage, is caused by residual stresses that are created during cooling [97]. Furthermore, warpage can lead to delamination during printing and, therefore, to print failures. Even if delamination could be avoided during the printing step, the dimensional accuracy of the final part would be affected. This could lead to issues during assembly or end-use application.

Shrinkage perpendicular (S_w) and parallel (S_l) to the print orientation was determined in HDPE and HDPE-V. From Table 4.3, it can be observed that HDPE-V experienced less shrinkage in both directions in comparison to HDPE. This result can be explained by the lower degree of crystallinity of HDPE-V (72.4%) compared to HDPE (77.9%). Additionally, both materials shrink in an anisotropic manner ($S_l > S_w$). This behavior could be a result of the induced molecular orientation upon shear flow during extrusion [115].

Table 4.3. Shrinkage perpendicular (S_w) and parallel (S_l) to the print orientation in the plates shown in Figure 4.2C.

Sample	S_w [%]	S_l [%]
HDPE	0.91 ± 0.13	2.62 ± 0.15
HDPE-V	0.08 ± 0.03	1.87 ± 0.12

4.3.4. Mechanical Properties

The viscoelastic behavior of untreated and annealed samples was determined using DMA under tension loading. Measurements were conducted at room temperature with the loading parallel (0°) and perpendicular (90°) to the print direction. Samples manufactured via compression molding were included for comparison purposes. Figure 4.8A and Figure 4.8B show the storage modulus (E') of HPDE and HDPE-V specimens, respectively. For all samples, E' increased with increasing frequency. This is consistent with the time-dependent behavior of polymers in response to deformation. At higher frequencies or smaller timescales, these materials behave more like solids, as characterized by higher E', whereas at lower frequencies or smaller timescales the samples behave more like fluids, as shown by lower E'.

Specimens manufactured via compression molding exhibited the highest modulus, followed by 3D-printed samples in the 0° and 90° orientations. For all samples, HDPE exhibited higher E' compared to HDPE-V. Previous research has demonstrated a linear relationship between crystallinity and stiffness [60]. Higher crystallinity in HDPE explains its higher modulus compared to HDPE-V. HDPE samples tested in the 0° orientation showed a drop of approximately 100 MPa in E' relative to compression-molded HDPE, while the 90° orientation showed a drop of around 300 MPa. HDPE-V printed with 0° and 90° orientations showed a drop of approximately 250 MPa and 350 MPa in E', respectively, relative to the compression-molded sample in the entire frequency range.

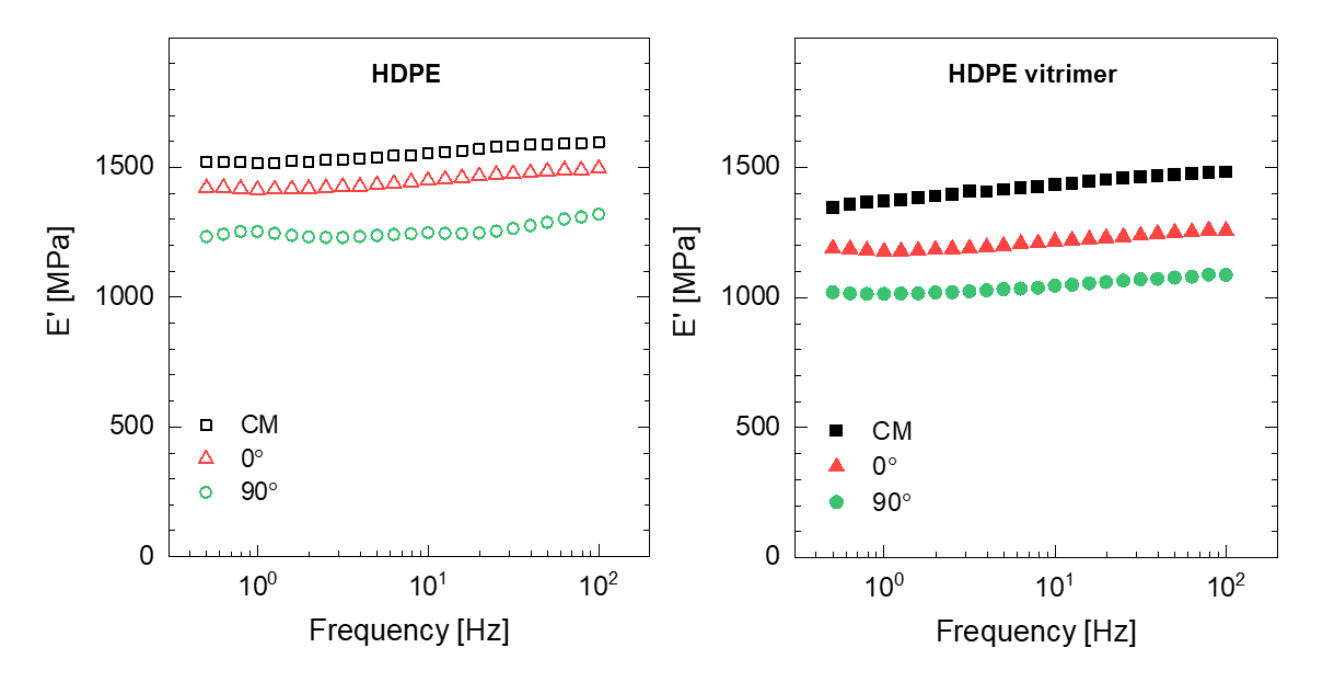


Figure 4.8. DMA frequency sweeps of compression-molded (CM) samples and 3D-printed specimens with loading parallel to the bead orientation (0°) and perpendicular to the bead orientation (90°) : (A) HDPE, and (B) HDPE-V.

Both materials displayed mechanical anisotropy consistent with material extrusion 3D printing. However, HDPE showed a lower degree of anisotropy compared to HDPE-V. This can be explained by the stronger interlayer adhesion in HDPE samples. Improved interlayer adhesion is expected if the chain interdiffusion is promoted [87]. The latter can happen if the viscous modulus (G'') of the melt dominates over the elastic modulus (G') in the terminal region. Both materials satisfied the condition of G'' > G' in the terminal region (Figure 4.6). However, the ratio of G'' to G' of HDPE and HDPE-V in the terminal region was 2.5 and 1.9, respectively. Hence, a higher interlayer adhesion is expected in HDPE.

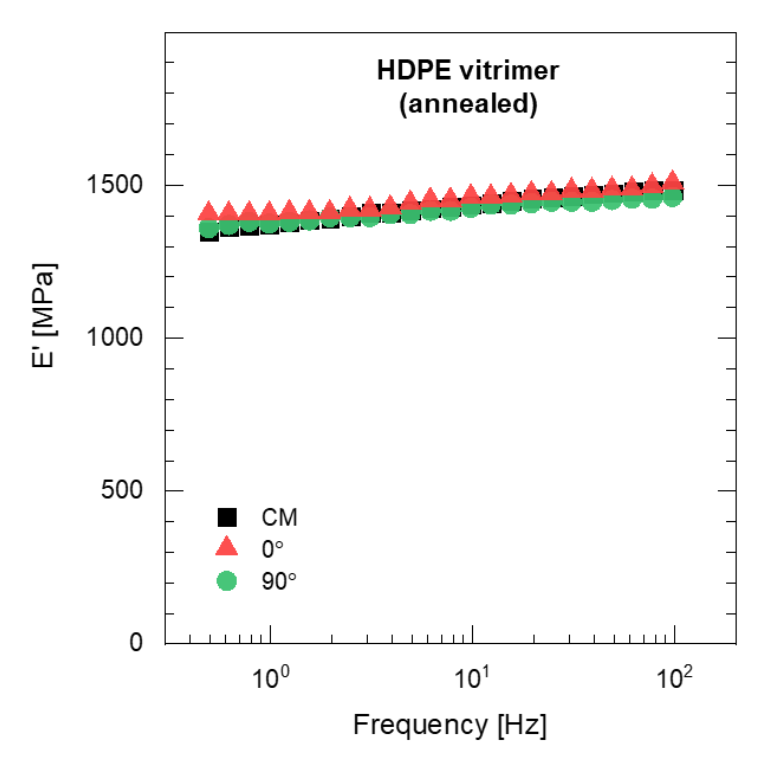


Figure 4.9. DMA frequency sweeps of compression-molded (CM) samples and 3D-printed specimens with loading parallel to the bead orientation (0°) and perpendicular to the bead orientation (90°) after an annealing process.

A thermal post-processing treatment was conducted to improve the chain interdiffusion between layers and reduce the mechanical anisotropy. In the context of Figure 4.9, lower mechanical anisotropy refers to narrowing the gap between the storage modulus (G') in the 0° and 90° orientations. A temperature closest to the end of melting of HDPE and HDPE-V was chosen

to ensure the destruction of crystallites and to enhance chain mobility. As previously observed from the DSC scans (Figure 4.3), both HDPE and HDPE-V samples were fully melted at 150 °C. When observing the samples being heated in the oven, it was revealed that the entire sample melted after 10 min. After annealing the HDPE specimens used in the DMA testing, the samples were completely deformed, while the HDPE-V specimens suffered comparatively minor changes in dimensions. A visual demonstration of the annealing process conducted in a prototype part is shown in Figure 4.10. Although in the present study the mechanical anisotropy was dramatically reduced in HDPE-V—as observed by the increase in modulus in the 0° and 90° orientations (Figure 4.9)—future studies should focus on improving the annealing methodology. An improved post-annealing dimensional accuracy will enable the usage of HDPE-V in ME-AM processes to manufacture functional isotropic parts.

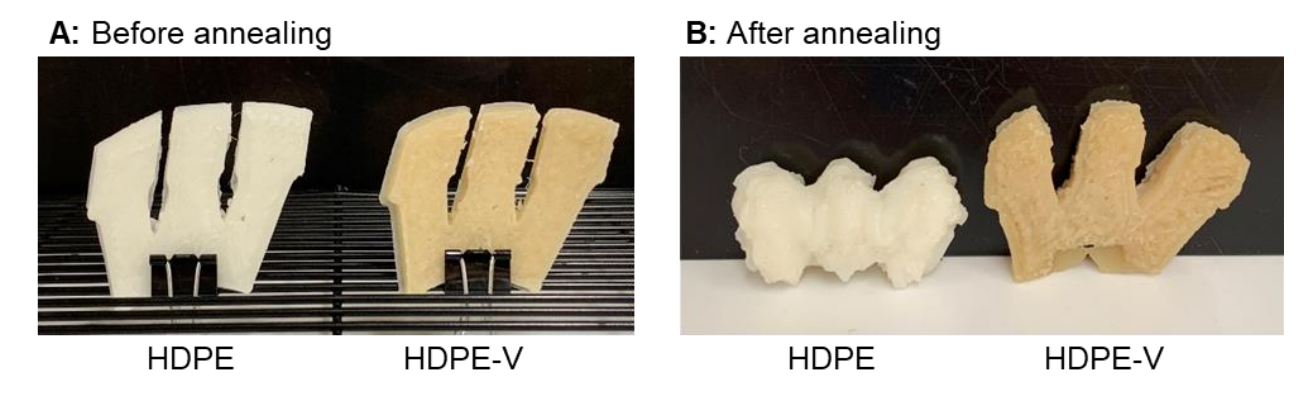


Figure 4.10. Visual demonstration of the annealing process: (**A**) before placing the parts in the oven, and (**B**) after 10 min in the oven at 150 °C.

4.3.5. Microstructures

The microstructure of the samples was observed using SEM to elucidate their interlayer adhesion and the presence of voids. Figure 4.11A–C depict the SEM micrographs of the 3D-printed samples normal to the print direction (X-Z view of the samples shown in Figure 4.2B).

Similarly, Figure 4.11D–F show the SEM micrographs of the 3D-printed samples parallel to the print direction (Y-Z view of the samples shown in Figure 4.2B). Interbead gaps characteristic of ME-AM were observed in the cross-section of HDPE and HDPE-V. Furthermore, small voids were observed in the HDPE-V samples parallel to the print direction (Figure 4.11E). These voids could have been introduced during the deposition step. This could be a result of the high viscosity of HDPE-V, which hindered the formation of a strong weld. The presence of these small voids could also contribute to the mechanical anisotropy found in HDPE-V (Figure 4.8B). Finally, after annealing, the interbead gaps were dramatically reduced and the layer adhesion was improved, as shown in Figure 4.11C.

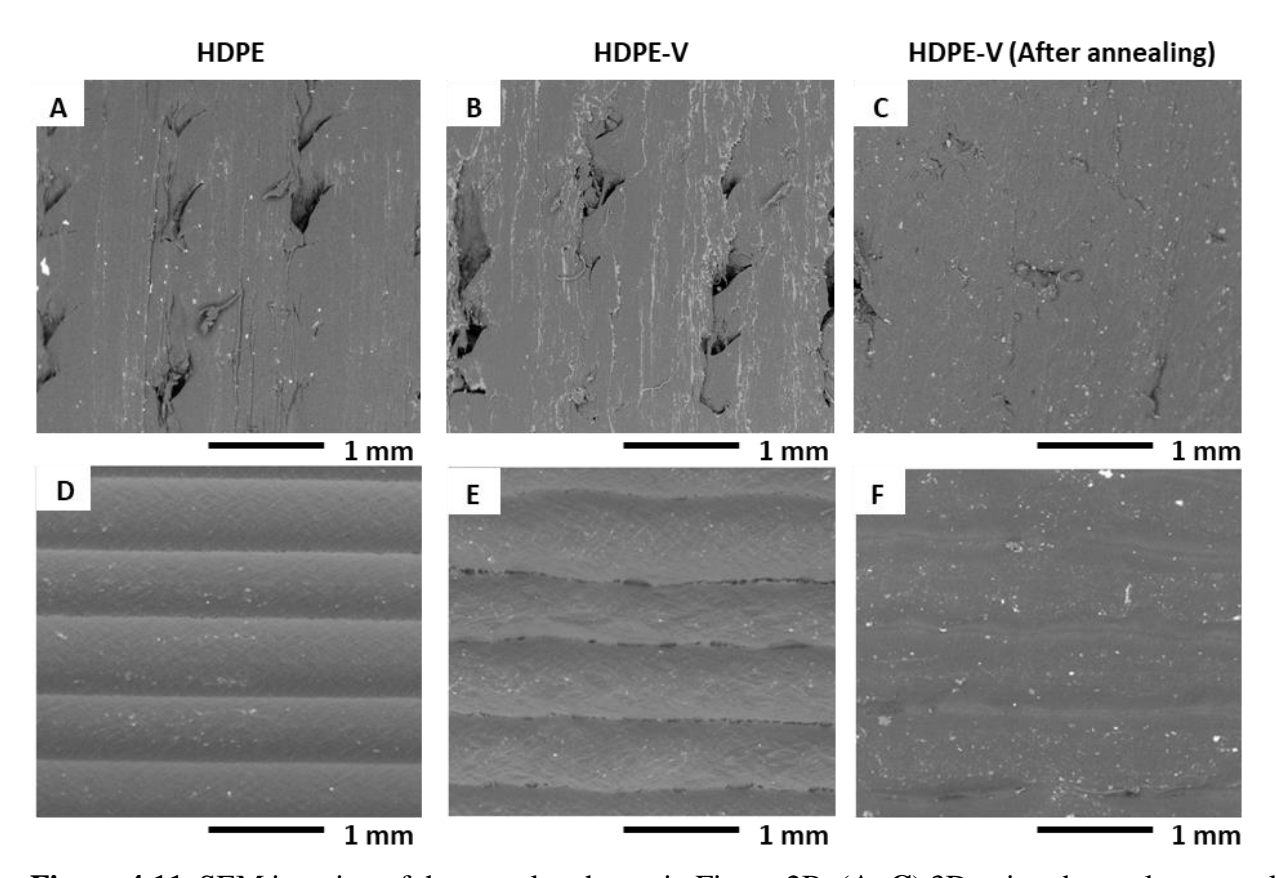


Figure 4.11. SEM imaging of the samples shown in Figure 2B: (**A**–**C**) 3D-printed samples normal to the print direction (X-Z view in Figure 2B), and (**D**–**F**) 3D-printed samples parallel to the print direction (Y-Z view in Figure 2B).

4.4. Conclusions

Material extrusion 3D printing of HDPE and HDPE vitrimers was conducted. Bed adhesion of HDPE and HDPE vitrimer parts was improved by using a PP bed substrate. Extrudate distortion (melt fracture) in HDPE vitrimers was resolved by decreasing the print speed. Rheological measurements indicated that the vitrimer has a higher shear-thinning dependency, which is usually desired in extrusion-based 3D-printing process. Thermal measurements demonstrated that HDPE vitrimers had a lower degree of crystallinity, which led to lower shrinkage during printing and increased dimensional accuracy. Viscoelastic measurements revealed the mechanical anisotropy of parts consistent with material extrusion 3D-printing processes. Interlayer adhesion was improved, and the void content was reduced in HDPE-V after a thermal post-processing step. In consequence, mechanical anisotropy was significantly reduced in HDPE-V.

5. Summary

5.1. Contributions

This dissertation presented a protocol to produce polyethylene networks with dynamic cross-links, referred to in this document as vitrimers, and a complete characterization of these materials. The study focused on three tasks: I. Developing a protocol to cross-link polyethylene vitrimers containing disulfide bonds and understand the influence on the rheological behavior of these materials, II. Determine the effect of dynamic cross-links on the thermal and mechanical properties of polyethylene vitrimers, and III. Demonstrate that polyethylene vitrimers can be successfully used in a 3D printing process to reduce mechanical anisotropy.

Chapter 2 showed that the synthesis of polyethylene vitrimer was possible in a one-step protocol via melt reactive blending in an internal batch mixer. The network formation in polyethylene vitrimer was achieved within two minutes of mixing maleic anhydride-grafted-linear low-density polyethylene (LLDPE-MAH) and 4,4° – dithiodianiline (DTA). This shows the potential to scale-up the reaction to traditional compounding equipment used for reactive extrusion operations. The presence of cross-links was confirmed with various techniques including torque rheometry, solvent swelling experiments, rotational rheometry, and dynamic mechanical analysis. Rheological characterization showed that the material became more elastic as cross-linking density was increased. The cross-links contributed to an improved dimensional stability at elevated temperatures, suggesting potential benefits of PE vitrimers in manufacturing processes requiring high melt strength. In the end, it was proven that reprocessing of polyethylene vitrimer was possible without a considerable impact on mechanical properties.

Chapter 3 proved that the presence of cross-links in polyethylene vitrimers had a significant impact on the thermal and mechanical properties of the material. The stiffness, strength, and creep performance of polyethylene vitrimers decreased in comparison to non-cross-linked polyethylene. This change in mechanical properties was attributed to a decrease in degree of crystallinity. It was proven that reprocessing of polyethylene vitrimers was possible without considerable impact on mechanical properties. The presence of cross-links improved the damping behavior and thermal stability of polyethylene vitrimers. These findings could enable using polyethylene vitrimers in applications that require flexible and damping behavior and in polymer processes that could benefit from lower levels of crystallinity. The latter is particularly of interest in 3D printing of semicrystalline materials where shrinkage and warpage are a challenge.

Chapter 4 explored the printability of polyethylene vitrimers using material extrusion additive manufacturing as an approach to reduce mechanical anisotropy and improve dimensional accuracy. It was shown that the lower degree of crystallinity of polyethylene vitrimers, previously reported in Chapter 3, contributed to lower shrinkage, and in consequence, to better dimensional accuracy than standard polyethylene. Interlayer adhesion of 3D printed parts was improved, and void content was reduced in polyethylene vitrimers after a thermal post-processing step. This thermal treatment was not possible in the non-cross-linked polyethylene due to its low dimensional stability at elevated temperatures.

5.2. Recommendations for Future Work

This dissertation demonstrated that the reaction of LLDPE-MAH and DTA led to the formation of a polyethylene vitrimer-like material. Most of the work focused on synthetizing the polyethylene vitrimer in an internal batch mixer because the residence time could be easily controlled. However,

it is important to scale-up this process to continuous processes such as single-screw extrusion and twin-screw extrusion. Since the reaction time of this polyethylene vitrimer was shown to be fast (< 2 min) there is a possibility to make it processable like traditional polyethylene. This will allow the use of polyethylene vitrimers without the need to change or modify standard polymer processing equipment.

The comprehensive material characterization performed was crucial to understand potential applications and processing methods of polyethylene vitrimer-like materials. For example, it was found that increasing cross-linking density of polyethylene vitrimers led to very elastic and viscous materials. This could introduce limitations in future processing methods. If the material is processed at high shear rates, typical in a process such as injection molding, the stress will build up until it exceeds the melt strength, leading to melt fracture. A Deborah number of less than 1, which is defined as the ratio of relaxation time over process time, is necessary to prevent melt fracture. Because of their long relation times, these materials could be limited to being an extrusion grade material.

An alternative approach could be explored to produce PE vitrimer-like materials with significantly less cross-linking density than the ones presented in this study. The objective is to find a material where the processability and mechanical properties can be exploited to the full potential. Decreasing the cross-link density can potentially decrease the disruption of the crystal formation leading to a stiffer material that may creep less. Two methods are recommended: (1) preparing a vitrimer masterbatch in a first step and blend it with a polyolefin in a second step and (2) blending functionalized polyolefin with a non-functionalized polyolefin and cross-linker in a single step. Possible challenges to address will be to fully disperse or break up the vitrimer in the polymer

matrix (a matter of dispersive mixing) and to achieve a high reaction conversion in the diluted system (a matter of distributive mixing).

5.3. Publications

The following lists detail the research products related to this dissertation:

Refereed Journal Publications

- Montoya-Ospina, M.C., Verhoogt, H., Osswald, T.A., "Processing and rheological behavior of cross-linked polyethylene containing disulfide bonds," SPE Polym. 2022, 3(1), 25
 [DOI: 10.1002/pls2.10062].
- Montoya-Ospina, M. C., Verhoogt, H., Ordner, M., Tan, X., Osswald, T. A., "Effect of cross-linking on the mechanical properties, degree of crystallinity and thermal stability of polyethylene vitrimers," SPE Polym. Eng. Sci. 2022, 62(12), 4203.

[DOI: 10.1002/pen.26178]

- Montoya-Ospina, M.C., Zeng, J.; Tan, X., Osswald, T.A., "Material Extrusion Additive Manufacturing with Polyethylene Vitrimers," *Polymers* 2023, 15(6), 1332.

[DOI: 10.3390/polym15061332]

Academic Thesis

- Lossen, A., 2022, "Characterization of Polyethylene-Glycidyl Methacrylate Vitrimers," Master Thesis, University of Wisconsin-Madison.

References

- [1] T. A. Osswald and G. Menges, *Material Science of Polymers for Engineers*. Munich: Hanser, 2012.
- [2] A. J. Peacock, *Handbook of Polyethylene: Structures, Properties, and Applications*. New York: Marcel Dekker, Inc, 2000.
- [3] M. Kutz, *Handbook of Materials Selection*. New York: Wiley, 2002.
- [4] M. Narkis, A. Tzur, and A. Vaxman, "Some Properties of Silane-Grafted Moisture-Crosslinked Polyethylene," *Polym. Eng. Sci.*, vol. 25, no. 13, pp. 857–862, 1985.
- [5] S. M. Tamboli, S. T. Mhaske, and D. D. Kale, "Crosslinked polyethylene," *Indian J. Chem. Technol.*, vol. 11, no. 6, pp. 853–864, 2004, DOI: 10.1142/9781783267170_0006.
- [6] R. B. Seymur and T. Cheng, *History of Polyolefins*. Dordrecht, Holland: D. Reidel Publishing Company, 1986.
- [7] J. Morshedian and P. M. Hosseinpour, "Polyethylene Cross-linking by Two-step Silane Method: A Review," *Iran. Polym. J.*, vol. 18, no. 2, pp. 103–128, 2009.
- [8] H. G. Scott, Cross-linking of a polyolefin with a silane, no. Patent 3,646,155. 1972.
- [9] M. Mauri, N. Tran, O. Prieto, T. Hjertberg, and C. Müller, "Crosslinking of an ethylene-glycidyl methacrylate copolymer with amine click chemistry," *Polymer*, vol. 111, pp. 27–35, 2017, DOI: 10.1016/j.polymer.2017.01.010.
- [10] M. Mauri *et al.*, "Byproduct-free curing of a highly insulating polyethylene copolymer blend: An alternative to peroxide crosslinking," *J. Mater. Chem. C*, vol. 6, no. 42, pp. 11292–11302, 2018, DOI: 10.1039/c8tc04494e.
- [11] J.-M. Lehn, "Supramolecular Chemistry -Scope and Perspectives Molecules, Supermolecules, and Molecular Devices (Nobel Lecture)," *Angew. Chemie Int. Ed. English*, vol. 27, no. 1, pp. 89–112, 1998, [Online]. Available: http://onlinelibrary.wiley.com/doi/10.1002/anie.198201553/abstract
- [12] J. -M Lehn, "Perspectives in Supramolecular Chemistry—From Molecular Recognition towards Molecular Information Processing and Self-Organization," *Angew. Chemie Int. Ed. English*, vol. 29, no. 11, pp. 1304–1319, 1990, DOI: 10.1002/anie.199013041.
- [13] M. Hayashi, "Implantation of recyclability and healability into cross-linked commercial polymers by applying the vitrimer concept," *Polymers.*, vol. 12, no. 6, 2020, DOI: 10.3390/POLYM12061322.
- [14] N. J. Van Zee and R. Nicolaÿ, "Vitrimers: Permanently crosslinked polymers with dynamic network topology," *Prog. Polym. Sci.*, vol. 104, p. 101233, 2020, DOI: 10.1016/j.progpolymsci.2020.101233.
- [15] C. N. Bowman and C. J. Kloxin, "Covalent adaptable networks: Reversible bond structures incorporated in polymer networks," *Angew. Chemie Int. Ed.*, vol. 51, no. 18,

- pp. 4272–4274, 2012, DOI: 10.1002/anie.201200708.
- [16] V. K. Thakur and M. R. Kessler, "Self-healing polymer nanocomposite materials: A review," *Polymer*, vol. 69, pp. 369–383, 2015, DOI: 10.1016/j.polymer.2015.04.086.
- [17] X. Chen *et al.*, "A thermally re-mendable cross-linked polymeric material," *Science*, vol. 295, no. 5560, pp. 1698–1702, 2002, DOI: 10.1126/science.1065879.
- [18] T. F. Scott, A. D. Schneider, W. D. Cook, and C. N. Bowman, "Chemistry: Photoinduced plasticity in cross-linked polymers," *Science*, vol. 308, no. 5728, pp. 1615–1617, 2005, DOI: 10.1126/science.1110505.
- [19] D. Montarnal, M. Capelot, F. Tournilhac, and L. Leibler, "Silica-like malleable materials from permanent organic networks," *Science*, vol. 334, no. 6058, pp. 965–968, 2011, DOI: 10.1126/science.1212648.
- [20] W. Denissen, J. M. Winne, and F. E. Du Prez, "Vitrimers: Permanent organic networks with glass-like fluidity," *Chem. Sci.*, vol. 7, no. 1, pp. 30–38, 2016, DOI: 10.1039/c5sc02223a.
- [21] J. C. Dyre, "Colloquium: The glass transition and elastic models of glass-forming liquids," *Rev. Mod. Phys.*, vol. 78, no. 3, pp. 953–972, 2006, DOI: 10.1103/RevModPhys.78.953.
- [22] M. Capelot, M. M. Unterlass, F. Tournilhac, and L. Leibler, "Catalytic control of the vitrimer glass transition," *ACS Macro Lett.*, vol. 1, no. 7, pp. 789–792, 2012, DOI: 10.1021/mz300239f.
- [23] M. Guerre, C. Taplan, J. M. Winne, and F. E. Du Prez, "Vitrimers: directing chemical reactivity to control material properties," *Chem. Sci.*, vol. 11, no. 19, pp. 4855–4870, 2020, DOI: 10.1039/d0sc01069c.
- [24] W. Denissen, G. Rivero, R. Nicolaÿ, L. Leibler, J. M. Winne, and F. E. Du Prez, "Vinylogous urethane vitrimers," *Adv. Funct. Mater.*, vol. 25, no. 16, pp. 2451–2457, 2015, DOI: 10.1002/adfm.201404553.
- [25] J. Tellers, R. Pinalli, M. Soliman, J. Vachon, and E. Dalcanale, "Reprocessable vinylogous urethane cross-linked polyethylene: Via reactive extrusion," *Polym. Chem.*, vol. 10, no. 40, pp. 5534–5542, 2019, DOI: 10.1039/c9py01194c.
- [26] R. L. Snyder, D. J. Fortman, G. X. De Hoe, M. A. Hillmyer, and W. R. Dichtel, "Reprocessable Acid-Degradable Polycarbonate Vitrimers," *Macromolecules*, vol. 51, no. 2, pp. 389–397, 2018, DOI: 10.1021/acs.macromol.7b02299.
- [27] M. M. Obadia, B. P. Mudraboyina, A. Serghei, D. Montarnal, and E. Drockenmuller, "Reprocessing and Recycling of Highly Cross-Linked Ion-Conducting Networks through Transalkylation Exchanges of C-N Bonds," *J. Am. Chem. Soc.*, vol. 137, no. 18, pp. 6078–6083, 2015, DOI: 10.1021/jacs.5b02653.
- [28] P. Taynton, K. Yu, R. K. Shoemaker, Y. Jin, H. J. Qi, and W. Zhang, "Heat- or water-driven malleability in a highly recyclable covalent network polymer," *Adv. Mater.*, vol. 26, no. 23, pp. 3938–3942, 2014, DOI: 10.1002/adma.201400317.

- [29] Y. Nishimura, J. Chung, H. Muradyan, and Z. Guan, "Silyl Ether as a Robust and Thermally Stable Dynamic Covalent Motif for Malleable Polymer Design," *J. Am. Chem. Soc.*, vol. 139, no. 42, pp. 14881–14884, 2017, DOI: 10.1021/jacs.7b08826.
- [30] A. Zych, R. Pinalli, M. Soliman, J. Vachon, and E. Dalcanale, "Polyethylene vitrimers via silyl ether exchange reaction," *Polymer*, vol. 199, p. 122567, 2020, DOI: 10.1016/j.polymer.2020.122567.
- [31] Y. X. Lu, F. Tournilhac, L. Leibler, and Z. Guan, "Making insoluble polymer networks malleable via olefin metathesis," *J. Am. Chem. Soc.*, vol. 134, no. 20, pp. 8424–8427, 2012, DOI: 10.1021/ja303356z.
- [32] M. Röttger, T. Domenech, R. Van Der Weegen, A. Breuillac, R. Nicolaÿ, and L. Leibler, "High-performance vitrimers from commodity thermoplastics through dioxaborolane metathesis," *Science*, vol. 356, no. 6333, pp. 62–65, 2017, DOI: 10.1126/science.aah5281.
- [33] R. G. Ricarte, F. Tournilhac, and L. Leibler, "Phase Separation and Self-Assembly in Vitrimers: Hierarchical Morphology of Molten and Semicrystalline Polyethylene/Dioxaborolane Maleimide Systems," *Macromolecules*, vol. 52, no. 2, pp. 432–443, 2019, DOI: 10.1021/acs.macromol.8b02144.
- [34] R. G. Ricarte, F. Tournilhac, M. Cloître, and L. Leibler, "Linear viscoelasticity and flow of self-assembled vitrimers: the case of a polyethylene/dioxaborolane system," *Macromolecules*, vol. 53, no. 5, 2020, DOI: 10.26434/chemrxiv.10315427.v3.
- [35] O. R. Cromwell, J. Chung, and Z. Guan, "Malleable and Self-Healing Covalent Polymer Networks through Tunable Dynamic Boronic Ester Bonds," *J. Am. Chem. Soc.*, vol. 137, no. 20, pp. 6492–6495, 2015, DOI: 10.1021/jacs.5b03551.
- [36] L. Zhou, G. Zhang, Y. Feng, H. Zhang, J. Li, and X. Shi, "Design of a self-healing and flame-retardant cyclotriphosphazene-based epoxy vitrimer," *J. Mater. Sci.*, vol. 53, no. 9, pp. 7030–7047, 2018, DOI: 10.1007/s10853-018-2015-z.
- [37] L. Imbernon, E. K. Oikonomou, S. Norvez, and L. Leibler, "Chemically crosslinked yet reprocessable epoxidized natural rubber via thermo-activated disulfide rearrangements," *Polym. Chem.*, vol. 6, no. 23, pp. 4271–4278, 2015, DOI: 10.1039/c5py00459d.
- [38] B. T. Michal, C. A. Jaye, E. J. Spencer, and S. J. Rowan, "Inherently photohealable and thermal shape-memory polydisulfide networks," *ACS Macro Lett.*, vol. 2, no. 8, pp. 694–699, 2013, DOI: 10.1021/mz400318m.
- [39] X. Zheng, H. Yang, Y. Sun, Y. Zhang, and Y. Guo, "A molecular dynamics simulation on self-healing behavior based on disulfide bond exchange reactions," *Polymer*, vol. 212, no. May 2020, p. 123111, 2021, DOI: 10.1016/j.polymer.2020.123111.
- [40] H. Si *et al.*, "Rapidly reprocessable, degradable epoxy vitrimer and recyclable carbon fiber reinforced thermoset composites relied on high contents of exchangeable aromatic disulfide crosslinks," *Compos. Part B Eng.*, vol. 199, no. June, p. 108278, 2020, DOI: 10.1016/j.compositesb.2020.108278.
- [41] A. Ruiz De Luzuriaga *et al.*, "Epoxy resin with exchangeable disulfide crosslinks to obtain reprocessable, repairable and recyclable fiber-reinforced thermoset composites," *Mater*.

- Horizons, vol. 3, no. 3, pp. 241–247, 2016, DOI: 10.1039/c6mh00029k.
- [42] B. Krishnakumar *et al.*, "Disulfide exchange assisted self-healing epoxy/PDMS/graphene oxide nanocomposites," *Nanoscale Adv.*, vol. 2, no. 7, pp. 2726–2730, 2020, DOI: 10.1039/d0na00282h.
- [43] F. Ji *et al.*, "Reprocessable and Recyclable Crosslinked Polyethylene with Triple Shape Memory Effect," *Macromol. Mater. Eng.*, vol. 304, no. 3, p. 1800528, 2018, DOI: 10.1002/mame.201800528.
- [44] M. Maaz, A. Riba-Bremerch, C. Guibert, N. J. Van Zee, and R. Nicolaÿ, "Synthesis of Polyethylene Vitrimers in a Single Step: Consequences of Graft Structure, Reactive Extrusion Conditions, and Processing Aids," *Macromolecules*, vol. 54, no. 5, pp. 2213–2225, 2021, DOI: 10.1021/acs.macromol.0c02649.
- [45] G. P. Kar, M. O. Saed, and E. M. Terentjev, "Scalable upcycling of thermoplastic polyolefins into vitrimers through transesterification," *J. Mater. Chem. A*, vol. 8, no. 45, pp. 24137–24147, 2020, DOI: 10.1039/d0ta07339c.
- [46] A. Demongeot, R. Groote, H. Goossens, T. Hoeks, F. Tournilhac, and L. Leibler, "Cross-Linking of Poly(butylene terephthalate) by Reactive Extrusion Using Zn(II) Epoxy-Vitrimer Chemistry," *Macromolecules*, vol. 50, no. 16, pp. 6117–6127, 2017, DOI: 10.1021/acs.macromol.7b01141.
- [47] Y. Zhou, J. G. P. Goossens, R. P. Sijbesma, and J. P. A. Heuts, "Poly(butylene terephthalate)/Glycerol-based Vitrimers via Solid-State Polymerization," *Macromolecules*, vol. 50, no. 17, pp. 6742–6751, 2017, DOI: 10.1021/acs.macromol.7b01142.
- [48] M. Chen, L. Zhou, Y. Wu, X. Zhao, and Y. Zhang, "Rapid Stress Relaxation and Moderate Temperature of Malleability Enabled by the Synergy of Disulfide Metathesis and Carboxylate Transesterification in Epoxy Vitrimers," *ACS Macro Lett.*, vol. 8, no. 3, pp. 255–260, 2019, DOI: 10.1021/acsmacrolett.9b00015.
- [49] A. Rekondo, R. Martin, A. Ruiz De Luzuriaga, G. Cabañero, H. J. Grande, and I. Odriozola, "Catalyst-free room-temperature self-healing elastomers based on aromatic disulfide metathesis," *Mater. Horizons*, vol. 1, no. 2, pp. 237–240, 2014, DOI: 10.1039/c3mh00061c.
- [50] J. P. Brutman, P. A. Delgado, and M. A. Hillmyer, "Polylactide vitrimers," *ACS Macro Lett.*, vol. 3, no. 7, pp. 607–610, 2014, DOI: 10.1021/mz500269w.
- [51] M. C. Montoya-Ospina, H. Verhoogt, and T. A. Osswald, "Processing and rheological behavior of cross-linked polyethylene containing disulfide bonds," *SPE Polym.*, vol. 3, no. 1, pp. 25–40, 2022, DOI: 10.1002/pls2.10062.
- [52] L. Imbernon, S. Norvez, and L. Leibler, "Stress Relaxation and Self-Adhesion of Rubbers with Exchangeable Links," *Macromolecules*, vol. 49, no. 6, pp. 2172–2178, 2016, DOI: 10.1021/acs.macromol.5b02751.
- [53] F. Caffy and R. Nicolaÿ, "Transformation of polyethylene into a vitrimer by nitroxide radical coupling of a bis-dioxaborolane," *Polym. Chem.*, vol. 10, no. 23, pp. 3107–3115,

- 2019, DOI: 10.1039/c9py00253g.
- [54] J. D. Menczel and R. B. Prime, *Thermal Analysis of Polymers: Fundamentals and Applications*. Hoboken: Wiley, 2009.
- [55] ASTM D2765, Standard Test Methods for Determination of Gel Content and Swell Ratio of. 2016. DOI: 10.1520/D2765-16.not.
- [56] M. T. Shaw and M. T. Shaw, "On estimating the zero-shear-rate viscosity: Tests with PIB and PDMS On Estimating The Zero-Shear-Rate Viscosity: Tests With PIB And PDMS," vol. 070011, 2017, DOI: 10.1063/1.4965543.
- [57] ASTM D638, Standard Test Method for Tensile Properties of Plastics. 2014. DOI: 10.1520/D0638-14.1.
- [58] M. Van-der-Mee, "Thermoreversible cross-linking of elastomers: a comparative study between ionic interactions, hydrogen bonding and covalent cross-links," Eindhoven University, 2007. DOI: 10.6100/IR629600.
- [59] F. Chambon and H. H. Winter, "Stopping of crosslinking reaction in a PDMS polymer at the gel point," *Polym. Bull.*, vol. 13, no. 6, pp. 499–503, 1985, DOI: 10.1007/BF00263470.
- [60] M. C. Montoya-Ospina, H. Verhoogt, M. Ordner, X. Tan, and T. A. Osswald, "Effect of cross-linking on the mechanical properties, degree of crystallinity and thermal stability of polyethylene vitrimers," *Polym. Eng. Sci.*, vol. 62, no. 12, pp. 4203–4213, 2022, DOI: 10.1002/pen.26178.
- [61] H. Ahmad and D. Rodrigue, "Crosslinked polyethylene: A review on the crosslinking techniques, manufacturing methods, applications, and recycling," *Polym. Eng. Sci.*, vol. 62, no. 8, pp. 2376–2401, 2022, DOI: 10.1002/pen.26049.
- [62] S. J. Zack, N. T. Herrold, and K. Wakabayashi, "Mechanochemical modification of crosslinked low-density polyethylene: Effect of solid-state shear pulverization on crosslinks, branches, and chain lengths," *SPE Polym.*, vol. 3, no. 3, pp. 1–11, 2022, DOI: 10.1002/pls2.10077.
- [63] I. Chodák, "Properties of crosslinked polyolefin-based materials," *Prog. Polym. Sci.*, vol. 20, no. 6, pp. 1165–1199, 1995, DOI: 10.1016/0079-6700(95)98859-N.
- [64] J. Tellers, S. Canossa, R. Pinalli, M. Soliman, J. Vachon, and E. Dalcanale, "Dynamic Cross-Linking of Polyethylene via Sextuple Hydrogen Bonding Array," *Macromolecules*, vol. 51, no. 19, pp. 7680–7691, 2018, DOI: 10.1021/acs.macromol.8b01715.
- [65] O. Drzyzga and A. Prieto, "Plastic waste management, a matter for the 'community," *Microb. Biotechnol.*, vol. 12, no. 1, pp. 66–68, 2019, DOI: 10.1111/1751-7915.13328.
- [66] A. Chitalia, "Why polyolefins are the polymers to watch," Wood Mackenzie, 2020.
- [67] M. Mehrabzadeh, M. R. Kamal, and G. Quintanar, "Maleic anhydride grafting onto HDPE by in situ reactive extrusion and its effect on intercalation and mechanical properties of HDPE/clay nanocomposites," *Iran. Polym. J.*, vol. 18, no. 10, pp. 833–842, 2009.

- [68] G. Samay, T. Nagy, and J. L. White, "Grafting maleic anhydride and comonomers onto polyethylene," *J. Appl. Polym. Sci.*, vol. 56, no. 11, pp. 1423–1433, 1995, DOI: 10.1002/app.1995.070561105.
- [69] L. Yang, F. Zhang, T. Endo, and T. Hirotsu, "Structural characterization of maleic anhydride grafted polyethylene by 13C NMR spectroscopy," *Polymer*, vol. 43, no. 8, pp. 2591–2594, 2002, DOI: 10.1016/S0032-3861(01)00802-3.
- [70] Y. Wang *et al.*, "Crystallization, structures, and properties of different polyolefins with similar grafting degree of maleic anhydride," *Polymers.*, vol. 12, no. 3, 2020, DOI: 10.3390/polym12030675.
- [71] A. Paajanen, J. Vaari, and T. Verho, "Crystallization of cross-linked polyethylene by molecular dynamics simulation," *Polymer*, vol. 171, pp. 80–86, 2019, DOI: 10.1016/j.polymer.2019.03.040.
- [72] J.-W. Huang, W.-C. Lu, M.-Y. Yeh, C.-H. Lin, and I.-S. Tsai, "Unusual Thermal Degradation of Maleic Anhydride Grafted Polyethylene," *Polym. Eng. Sci.*, vol. 48, no. 8, pp. 1550–1554, 2008, DOI: https://doi.org/10.1002/pen.21129.
- [73] H. G. H. Melick, *Deformation and failure of polymer classes*. 2002. DOI: 10.6100/IR555099.
- [74] R. Lakes, Viscoelastic Materials. New York: Cambridge University Press, 2009.
- [75] H. A. Flocke, "Ein Beitrag zum mechanischen Relaxationsverhalten von Polyäthylen, Polypropylen, Gemischen aus diesen und Mischpolymerisaten aus Propylen und äthylen," *Kolloid-Zeitschrift Zeitschrift für Polym.*, vol. 180, 1962, DOI: 10.1007/BF01499639.
- [76] K. Maeda, K. Yamada, K. Yamada, M. Kotaki, and H. Nishimura, "Effect of Molecular Weight and Molecular Distribution on Skin Structure and Shear Strength Distribution near the Surface of Thin-Wall Injection Molded Polypropylene," *Open J. Org. Polym. Mater.*, vol. 6, no. 1, pp. 1–10, 2016, DOI: 10.4236/ojopm.2016.61001.
- [77] M. C. Montoya-Ospina, J. Zeng, X. Tan, and T. A. Osswald, "Material Extrusion Additive Manufacturing with Polyethylene Vitrimers," *Polymers.*, vol. 15, no. 6, p. 1332, 2023, DOI: 10.3390/polym15061332.
- [78] "ASTM 52900: Standard Terminology for Additive Manufacturing General Principles Terminology," *ASTM International*, vol. i. ASTM International, West Conshohocken, pp. 1–9, 2015. [Online]. Available: http://compass.astm.org/EDIT/html_annot.cgi?ISOASTM52900+15
- [79] L. Love, B. Post, M. Noakes, A. Nycz, and V. Kunc, "There's plenty of room at the top," *Addit. Manuf.*, vol. 39, p. 101727, 2021, DOI: https://doi.org/10.1016/j.addma.2020.101727.
- [80] Z. Jiang, B. Diggle, M. L. Tan, J. Viktorova, C. W. Bennett, and L. A. Connal, "Extrusion 3D Printing of Polymeric Materials with Advanced Properties," *Adv. Sci.*, vol. 7, no. 17, pp. 1–32, 2020, DOI: 10.1002/advs.202001379.
- [81] H. T. Black, M. C. Celina, and J. R. Mcelhanon, "Additive Manufacturing of Polymers:

- Materials Opportunities and Emerging Applications," no. April. Sandia National Labotatories, 2016.
- [82] E. Sanchez-Rexach, T. G. Johnston, C. Jehanno, H. Sardon, and A. Nelson, "Sustainable Materials and Chemical Processes for Additive Manufacturing," *Chem. Mater.*, vol. 32, no. 17, pp. 7105–7119, 2020, DOI: 10.1021/acs.chemmater.0c02008.
- [83] T. D. Ngo, A. Kashani, G. Imbalzano, K. T. Q. Nguyen, and D. Hui, "Additive manufacturing (3D printing): A review of materials, methods, applications and challenges," *Compos. Part B Eng.*, vol. 143, no. December 2017, pp. 172–196, 2018, DOI: 10.1016/j.compositesb.2018.02.012.
- [84] R. Arrigo and A. Frache, "FDM Printability of PLA Based-Materials: The Key Role of the Rheological Behavior," *Polymers.*, vol. 14, no. 9, p. 1754, 2022, DOI: 10.3390/polym14091754.
- [85] X. Gao, S. Qi, X. Kuang, Y. Su, J. Li, and D. Wang, "Fused filament fabrication of polymer materials: A review of interlayer bond," *Addit. Manuf.*, vol. 37, no. 2, p. 101658, Jan. 2021, DOI: 10.1016/j.addma.2020.101658.
- [86] J. L. Colón Quintana *et al.*, "Viscoelastic properties of fused filament fabrication parts," *Addit. Manuf.*, vol. 28, pp. 704–710, Aug. 2019, DOI: 10.1016/j.addma.2019.06.003.
- [87] J. E. Seppala, S. Hoon Han, K. E. Hillgartner, C. S. Davis, and K. B. Migler, "Weld formation during material extrusion additive manufacturing," *Soft Matter*, vol. 13, no. 38, pp. 6761–6769, 2017, DOI: 10.1039/C7SM00950J.
- [88] V. Kishore *et al.*, "Infrared preheating to improve interlayer strength of big area additive manufacturing (BAAM) components," *Addit. Manuf.*, vol. 14, no. May 2020, pp. 7–12, Mar. 2017, DOI: 10.1016/j.addma.2016.11.008.
- [89] N. P. Levenhagen and M. D. Dadmun, "Reactive Processing in Extrusion-Based 3D Printing to Improve Isotropy and Mechanical Properties," *Macromolecules*, vol. 52, no. 17, pp. 6495–6501, Sep. 2019, DOI: 10.1021/acs.macromol.9b01178.
- [90] L. Chen *et al.*, "3D printable robust shape memory PET copolyesters with fire safety: Via π-stacking and synergistic crosslinking," *J. Mater. Chem. A*, vol. 7, no. 28, pp. 17037–17045, 2019, DOI: 10.1039/c9ta04187g.
- [91] K. Yang *et al.*, "Diels–Alder Reversible Thermoset 3D Printing: Isotropic Thermoset Polymers via Fused Filament Fabrication," *Adv. Funct. Mater.*, vol. 27, no. 24, pp. 1–11, 2017, DOI: 10.1002/adfm.201700318.
- [92] A. Abbott *et al.*, "Melt extrusion and additive manufacturing of a thermosetting polyimide," *Addit. Manuf.*, vol. 37, no. July, p. 101636, Jan. 2021, DOI: 10.1016/j.addma.2020.101636.
- [93] S. Kim *et al.*, "Analysis on part distortion and residual stress in big area additive manufacturing with carbon fiber-reinforced thermoplastic using dehomogenization technique," in *CAMX 2019 Composites and Advanced Materials Expo*, 2019, pp. 1–14.
- [94] M. Jin, R. Giesa, C. Neuber, and H. W. Schmidt, "Filament Materials Screening for FDM

- 3D Printing by Means of Injection-Molded Short Rods," *Macromol. Mater. Eng.*, vol. 303, no. 12, pp. 1–7, 2018, DOI: 10.1002/mame.201800507.
- [95] A. Koffi *et al.*, "Extrusion-based 3D printing with high-density polyethylene Birch-fiber composites," *J. Appl. Polym. Sci.*, vol. 139, no. 15, p. 51937, Apr. 2022, DOI: 10.1002/app.51937.
- [96] A. Gudadhe, N. Bachhar, A. Kumar, P. Andrade, and G. Kumaraswamy, "Three-dimensional printing with waste high-density polyethylene," *ACS Appl. Polym. Mater.*, vol. 1, no. 11, pp. 3157–3164, 2019, DOI: 10.1021/acsapm.9b00813.
- [97] M. Spoerk, C. Holzer, and J. Gonzalez-Gutierrez, "Material extrusion-based additive manufacturing of polypropylene: A review on how to improve dimensional inaccuracy and warpage," *J. Appl. Polym. Sci.*, vol. 137, no. 12, pp. 1–16, 2020, DOI: 10.1002/app.48545.
- [98] W. Zou, J. Dong, Y. Luo, Q. Zhao, and T. Xie, "Dynamic Covalent Polymer Networks: from Old Chemistry to Modern Day Innovations," *Adv. Mater.*, vol. 29, no. 14, p. 1606100, Apr. 2017, DOI: 10.1002/adma.201606100.
- [99] N. E. Zander, Recycled Polymer Feedstock for Material Extrusion Additive Manufacturing. In Polymer-Based Additive Manufacturing: Recent Developments, 1 st. in ACS Symposium Series. Washington, DC: American Chemical Society, 2019. DOI: 10.1021/bk-2019-1315.
- [100] C. Baechler, M. Devuono, and J. M. Pearce, "Distributed recycling of waste polymer into RepRap feedstock," *Rapid Prototyp. J.*, vol. 19, no. 2, pp. 118–125, 2013, DOI: 10.1108/13552541311302978.
- [101] C. G. Schirmeister, T. Hees, E. H. Licht, and R. Mülhaupt, "3D printing of high density polyethylene by fused filament fabrication," *Addit. Manuf.*, vol. 28, no. April, pp. 152–159, 2019, DOI: 10.1016/j.addma.2019.05.003.
- [102] S. Chong, G. T. Pan, M. Khalid, T. C. K. Yang, S. T. Hung, and C. M. Huang, "Physical Characterization and Pre-assessment of Recycled High-Density Polyethylene as 3D Printing Material," *J. Polym. Environ.*, vol. 25, no. 2, pp. 136–145, 2017, DOI: 10.1007/s10924-016-0793-4.
- [103] J. M. Justino Netto, H. T. Idogava, L. E. Frezzatto Santos, Z. de C. Silveira, P. Romio, and J. L. Alves, "Screw-assisted 3D printing with granulated materials: a systematic review," *Int. J. Adv. Manuf. Technol.*, vol. 115, no. 9–10, pp. 2711–2727, 2021, DOI: 10.1007/s00170-021-07365-z.
- [104] H. A. Little, N. G. Tanikella, M. J. Reich, M. J. Fiedler, S. L. Snabes, and J. M. Pearce, "Towards distributed recycling with additive manufacturing of PET flake feedstocks," *Materials (Basel).*, vol. 13, no. 19, 2020, DOI: 10.3390/MA13194273.
- [105] G. A. M. Capote *et al.*, "Compounding a High-Permittivity Thermoplastic Material and Its Applicability in Manufacturing of Microwave Photonic Crystals," *Materials (Basel).*, vol. 15, no. 7, 2022, DOI: 10.3390/ma15072492.
- [106] Z. de C. Silveira, M. S. de Freitas, P. I. Neto, P. Y. Noritomi, and J. V. L. da Silva,

- "Design development and functional validation of an interchangeable head based on mini screw extrusion applied in an experimental desktop 3-D printer," *Int. J. Rapid Manuf.*, vol. 4, no. 1, p. 49, 2014, DOI: 10.1504/ijrapidm.2014.062037.
- [107] "ASTM D955: Standard Test Method of Measuring Shrinkage from Mold Dimensions of Thermoplastics." ASTM International, West Conshohocken, pp. 1–8, 2021. DOI: 10.1520/D0955-21.
- [108] T. Jain *et al.*, "Synthesis, Rheology, and Assessment of 3D Printability of Multifunctional Polyesters for Extrusion-Based Direct-Write 3D Printing," *ACS Appl. Polym. Mater.*, vol. 3, no. 12, pp. 6618–6631, 2021, DOI: 10.1021/acsapm.1c01275.
- [109] M. Spoerk *et al.*, "Optimisation of the adhesion of polypropylene-based materials during extrusion-based additive manufacturing," *Polymers.*, vol. 10, no. 5, 2018, DOI: 10.3390/polym10050490.
- [110] Y. Shang *et al.*, "Slowing crystallization to enhance interlayer strength of 3D printed poly (ether ether ketone) parts by molecular design," *Addit. Manuf.*, vol. 59, no. PA, p. 103104, 2022, DOI: 10.1016/j.addma.2022.103104.
- [111] N. Bachhar, A. Gudadhe, A. Kumar, P. Andrade, and G. Kumaraswamy, "3D printing of semicrystalline polypropylene: towards eliminating warpage of printed objects," *Bull. Mater. Sci.*, vol. 43, no. 1, pp. 1–8, 2020, DOI: 10.1007/s12034-020-02097-4.
- [112] L. Blyler and A. C. Hart, "Capillary flow instability of ethylene polymer melts," vol. 10, no. 4, 1970.
- [113] Y. C. Kim and K. S. Yang, "Effect of peroxide modification on melt fracture of linear low density polyethylene during extrusion," *Polym. J.*, vol. 31, no. 7, pp. 579–584, 1999, DOI: 10.1295/polymj.31.579.
- [114] D. Vaes and P. Van Puyvelde, "Semi-crystalline feedstock for filament-based 3D printing of polymers," *Prog. Polym. Sci.*, vol. 118, p. 101411, 2021, DOI: 10.1016/j.progpolymsci.2021.101411.
- [115] F. Liu *et al.*, "Structural Evolution of PCL during Melt Extrusion 3D Printing," *Macromol. Mater. Eng.*, vol. 303, no. 2, pp. 1–6, 2018, DOI: 10.1002/mame.201700494.

Appendix

A.1. FTIR

The MAH conversion was determined by measuring the wt.% of MAH (peak at 1789 cm⁻¹) in the samples before (Figure A.1A) and after the reaction (Figure A.1B).

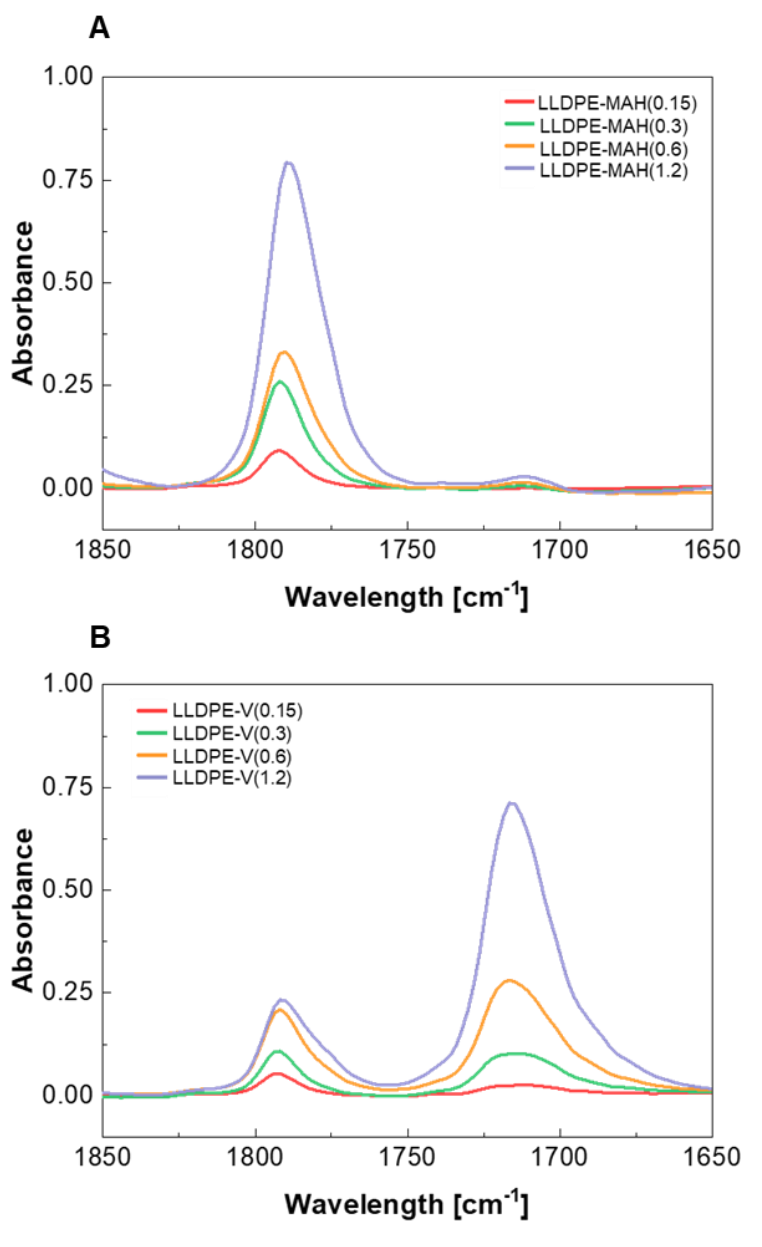


Figure A.1. FTIR spectral curves of: **(A)** LLDPE-MAH and **(B)** LLDPE-V with different initial MAH content (0.15, 0.3, 0.6 and 1.2 wt.%). Zoom-in in (1850-1650) cm⁻¹ region.

A calibration was performed using 5 standards with known concentration of MAH (0-2.6 wt.%). The composition of the calibration samples was determined with titration. The MAH measured by titration was used for correlation with the IR-signal (Figure A.2). The equation used in this study to calculate the wt.% of MAH was:

$$Y = 2.7763X - 0.1865 \tag{A.1}$$

Where Y is the peak area ratio of MAH/PE at (1804 -1766)/(4364 - 4295) cm⁻¹ and X is the wt.% of MAH in the sample. The polyethylene peak at 4322 cm⁻¹ is used as reference peak for correction of differences in film thickness.

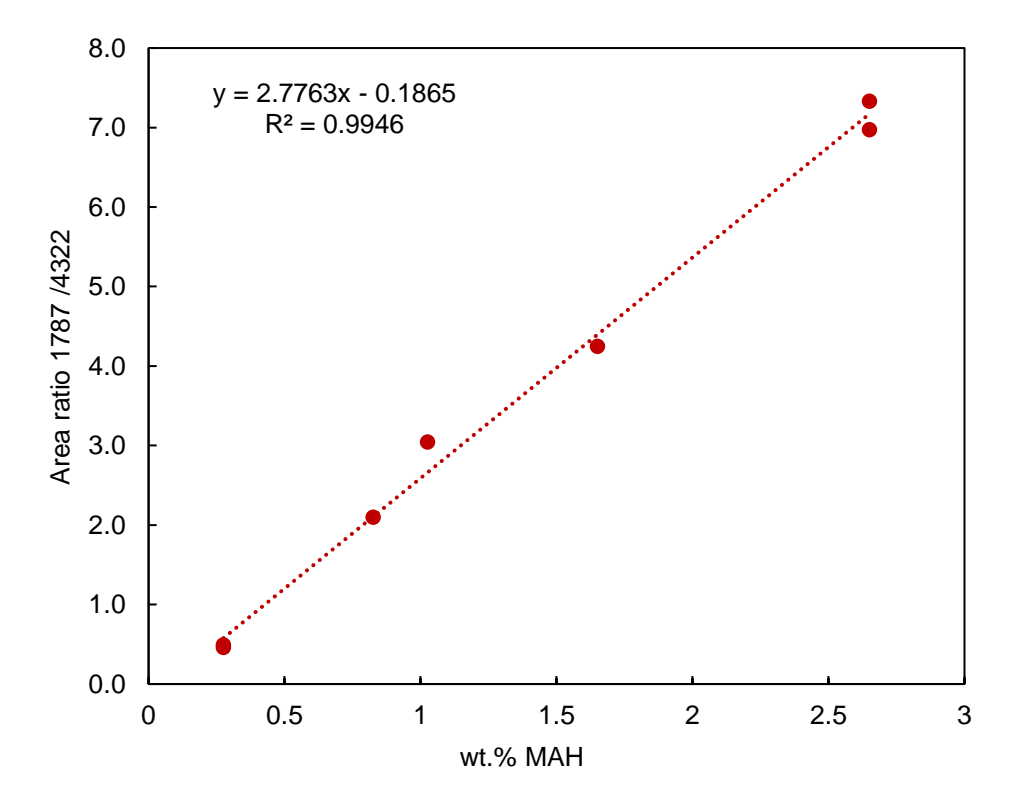


Figure A.2. Calibration line used to calculate the wt.% of MAH in the samples using FTIR.

A.2. Rheology models

Table A.1. Cross model fitting parameters for LLDPE, LLDPE-MAH and LLDPE-V

Materials	η ₀ [Pa*s]	λ [s]	n [-]	\mathbb{R}^2	RSS
LLDPE	2365.13	0.0239	0.41	0.99987	0.0001303
LLDPE-MAH(0.15)	2666.92	0.0498	0.49	0.99893	0.0014426
LLDPE-MAH(0.3)	2052.32	0.0463	0.51	0.99897	0.001209
LLDPE-MAH(0.6)	1975.66	0.0587	0.54	0.99875	0.0014997
LLDPE-MAH(1.2)	4368.44	0.3072	0.53	0.99892	0.0024172
LLDPE-V(0.15)	7820.80	0.6561	0.53	0.99854	0.0040905
LLDPE-V(0.3)	2.62E+05	1.93E+02	0.45	0.99992	0.0005346
LLDPE-V(0.6)	5.56E+09	6.45E+06	0.27	0.99977	0.0038594
LLDPE-V(1.2)	1.64E+10	8.67E+05	0.15	0.99927	0.0160648

 Table A.2. Carreau model fitting parameters for LLDPE and LLDPE-MAH.

Materials	η ₀ [Pa*s]	λ [s]	n [-]	\mathbb{R}^2	RSS
LLDPE	2174.2156	0.1548451	0.649327	0.988792	0.0128
LLDPE-MAH(0.15)	2351.5386	0.3282847	0.679765	0.984108	0.0213
LLDPE-MAH(0.3)	1803.4819	0.3709669	0.707962	0.983949	0.0188
LLDPE-MAH(0.6)	1708.2101	0.4768178	0.718934	0.983585	0.0196
LLDPE-MAH(1.2)	3457.6257	1.0917574	0.662724	0.988332	0.026

Materials	η ₀ [Pa*s]	λ [s]	a [-]	\mathbb{R}^2	RSS
LLDPE	2469.7498	0.0028201	2.236053	0.999744	0.0003
LLDPE-MAH(0.15)	2922.6643	0.0018706	2.85028	0.999967	4E-05
LLDPE-MAH(0.3)	2250.0245	0.0011642	3.020427	0.999954	5E-05
LLDPE-MAH(0.6)	2210.3853	0.0008739	3.282613	0.999903	0.0001
LLDPE-MAH(1.2)	5945.1007	0.0018306	4.075927	0.999976	5E-05

Table A.3. Adams-Crane model fitting parameters for LLDPE and LLDPE-MAH.

A.3. Determination of cross-linking density

Dynamic mechanical thermal analysis (DMTA) was performed on a GABO EPLEXOR[®] from NETZSCH. Rectangular samples (45 x 10 x 3 mm) were used in tensile mode to perform a temperature sweep (35 °C - 220°C, 3°C/min) at frequency of 10 Hz and a strain of 0.1%. The results are shown in Figure A1. The cross-linking density (ν) was determined using Equation A.2 using the storage modulus (E') at 180 °C and the results are summarized in Table A.4.

$$\nu = \frac{E'(T)}{3RT} \tag{A.2}$$

Where (E') is the storage modulus, R is the universal gas constant $(8.3145 \text{ J mol}^{-1} \text{ K}^{-1})$ and T refers to the absolute temperature in the rubbery region (453.15 K).

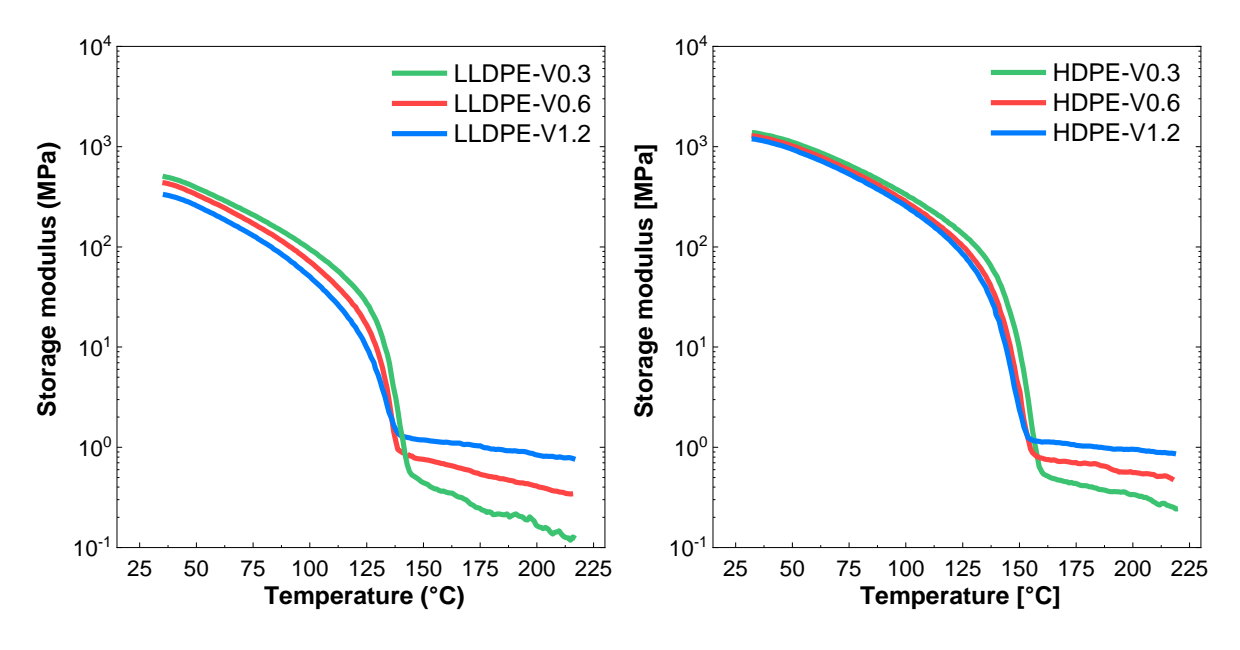


Figure A.3. Storage modulus of LLDPE and HDPE vitrimer based materials with varying cross-linking content. Data acquired from tension DMTA (35 °C - 220°C, 3°C/min, 10 Hz and 0.1% strain)

Table A.4. Cross-linking density of LLDPE and HDPE vitrimer based materials obtained from DMTA characterization.

Material	E' at 453.15 K [MPa]	Cross-linking density, $\nu \times 10^{-5}$ [mol/cm ³]
LLDPE-V0.3	0.21	1.86
LLDPE-V0.6	0.51	4.51
LLDPE-V1.2	0.96	8.50
HDPE-V0.3	0.40	3.54
HDPE-V0.6	0.68	6.02
HDPE-V1.2	1.03	9.12